



Supplement of

Future projections of Siberian wildfire and aerosol emissions

Reza Kusuma Nurrohman et al.

Correspondence to: Tomomichi Kato (tkato@agr.hokudai.ac.jp)

The copyright of individual parts of the supplement might differ from the article licence.

1 S2.2.1. Burned area calculation input variables

2 Mean fire area can be calculated as equation S4 as fires tend to take on an elliptical reform and spread at varying
3 speeds both with and against the direction of the wind (Albini, 1976; Forestry Canada Fire Danger Group, 1992).

$$\bar{a}f = \frac{\pi}{4 \times L_B} \times (Dt)^2 \quad (S4)$$

4 Dt is the length of major axis (m), in SEIB-DGVM we use the resolution of establishment site for woody PFTs
5 (Dived) variable. L_B is the length-to-breadth ratio of the elliptical form of fires (Forestry Canada Fire Danger
6 Group, 1992) and calculated PFTs specific, for woody and grass PFTs. L_B can be estimated as a weighted average
7 of $L_{B,tree}$ and $L_{B,grass}$.

$$L_{B,tree} = 1.0 + 8.729 \times (1 - e^{-0.03 \times U_{forward}})^{2.155} \quad (S5)$$

$$L_{B,grass} = 1.1 + (U_{forward})^{0.464} \quad (S6)$$

8 Ignition event $E(n_{ig})$ is the sum of independent calculations of lightning-caused (n_{il}) and human-caused (n_{ih}) fire
9 ignition events, ignoring stochastic variations (Thonicke et al., 2010).

$$E(n_{ig}) = n_{ih} + n_{il} \quad (S7)$$

10

11 S2.2.2. Ignition events

12 The LIS/OTD High-Resolution Full Climatology (HRFC) V2.3.2015 (Cecil, 2001) data provided frequency of
13 lightning-caused ignition events (n_{il}), actual unit is count $\text{km}^{-2} \text{year}^{-1}$ then converted into count $\text{ha}^{-1} \text{year}^{-1}$, and
14 gives the annual frequency of total lightning flash rates. Human-caused ignition events (n_{ih}) used population
15 density data obtained from Gridded Population of the World (GPWv4) (CIESIN, 2018), as the default unit is
16 person km^{-2} , we converted it into person/ha.

17 The population density and lightning flash data detailed information are shown in Table S1 in the Supplement. As
18 the first improvement step, we modified the data format, the GPWv4 (netCDF) and LIS/OTD HRFC (hdf5) data
19 are gridded into 1° grid mesh (360×180) as the SEIB-DGVM requirements for land property (land_prop.txt)
20 input, then converted into text format (.txt), and make sure that the sequence is N90W180, N90W179, ...,
21 N89W180, ..., S90E180, each line corresponds to one grid mesh, so the data structure will be 1 column and 64800
22 rows, text format files.

23 The SEIB-DGVM fire module improvement workflow was shown in Figure 3 in the main article, and the orange
24 color inside the dashed box indicates the new input and there is absolute certainty to add another new input that
25 might be considered in the further improvement of SEIB-DGVM. Interestingly, we found a novel discovery in
26 this model improvement process that there will be a huge possibility improvement of SEIB-DGVM in the near
27 future for many research areas because SEIB-DGVM is able to accept any new input as long as it meets the input
28 data requirements and able to process well and can be integrated with the variables in it, so we believed that SEIB-
29 DGVM has a high potential to be a rapid-growing model for analyzing and simulating global vegetation dynamics
30 from many perspectives, needs, and scientific focus areas.

31 To ensure that the data can be read and processed well by SEIB-DGVM, we visualize it on a global scale and in
32 Siberia, according to the research area as shown in Figure S1, prepared the data in (netCDF) format in 0.5° spatial
33 resolution to be able to compare with the output results of the data in SEIB-DGVM (as the data output from SEIB-
34 DGVM is in 0.5° spatial resolution).

35 Figure S2 shows the SEIB-DGVM output of Lightning flash rate and Population density and it's the comparison
36 with the original input GPWv4 and LIS/OTD HRFC data. Based on the comparison results we get the high value
37 of coefficients determination (R^2) and correlation coefficients (R) for both data comparison, the value of lightning
38 flash rate comparison is $R^2=0.97$, $R=0.99$, and for population density data is $R^2=0.93$, $R=0.97$. Although it doesn't
39 produce 100% comparison results, but 97% and 93%, followed by 0.99 and 0.97 correlation coefficients, for

40 lightning flash rate and population density data comparison shows a strong relationship between the input and
41 output, and these results proved that the SEIB-DGVM was able to read and process the new input well.

42 Further explanation of the input-output comparison is: the input data has different formats and spatial resolutions,
43 then the first thing we did is data transformation, transformed the data format and regridding the data to 1° grid
44 for SEIB-DGVM input and to 0.5° grid for output comparison, this process we used the Climate Data Operator
45 (CDO) software (Schulzweida, 2019) remapcon operators, first-order conservative remapping that remaps all
46 fields conservatively to a Gaussian N32 grid. We know that the process of remapping or regridding data will
47 produce a bias, moreover multiple-time regridding the same data, and the size of the bias depends on the technique
48 and method used. The method we used in this study is the best method for regridding compared to other methods,
49 as the first- and second-order conservative methods provide an accurate and conservative machine accuracy,
50 completely general, weights can be computed for any type of grid on a sphere, enabling component model
51 developers to use any grid that is suitable for a specific component without being restricted by compatibility with
52 other component model grids in a connected model environment (Jones, 1999).

53 After the new input is confirmed able to be read and processed properly by SEIB-DGVM, we implement the
54 complete ignition events equation from SPITFIRE (Thonicke et al., 2010) with some model configuration
55 adjustments and environmental factor parameters.

$$N_{il} = I_p \times \text{Lightning Flash Rate} \quad (\text{S8})$$

56 Latham and Williams, (2001) stated that 0.20 of these are cloud-to-ground flashes (CG), and under ideal
57 conditions for igniting fires, their effectiveness is 0.04 (Latham and Schlieter, 1989; Latham and Williams, 2001).
58 I_p is an ignition parameter (0.0 – 1.0), and in this study, we used 1.0 because lightning strikes are the primary
59 source of wildfire ignition in Siberia (Sofronov et al., 1998; Ivanova and Ivanov, 2005; Kharuk et al., 2016), with
60 continued regional warming, the role of lightning as a source of wildfire ignition is likely to increase both because
61 of the increased availability of dry fuel as well as from a direct increase in lightning frequency (Kharuk et al.,
62 2022). Research in areas with similar environmental conditions about lightning strikes in the continental USA
63 projects that an increase in air temperature by 1°C leads to an increase in lightning frequency of ~12% (Romps et
64 al., 2014), and for Alaska and northern Canada, lightning ignition was estimated to increase by 90–230% by the
65 end of this century (Hessilt et al., 2021).

66 Regarding the lightning input dataset on the module, we used one-year and annual data of LIS/OTD HRFC as
67 interannual variability in lightning is generally small (Thonicke et al., 2010).

$$N_{ih} = P_D \times k(P_D) \times \frac{a(N_D)}{100} \quad (\text{S9})$$

$$k(P_D) = 30.0 \times e^{-0.5 \times \sqrt{P_D}} \quad (\text{S10})$$

68 After climatic sensitivity ignition, human activity grew to become a stronger factor in controlling fire regimes
69 also due to the construction of the Trans-Siberian Railway and the subsequent development of settlements in
70 remote areas (Ivanova and Ivanov, 2005). Thus, in this improvement, we considered the population density
71 ignition factor also. P_D is the population density (persons km⁻²), and $a(N_D)$ (ignitions individual⁻¹) is a parameter
72 expressing a person's probability of causing an ignition event (Thonicke et al., 2010). The function forms is
73 supported by Archibald et al., (2009) analysis, that the number of fires in southern Africa tends to rise as
74 population density rises up to roughly 10 kilometers and declines thereafter. At the global scale analysis, Knorr
75 et al., (2014) also discovered that fire frequency rises by 10 to 20% in areas with less than 0.1 persons per km²
76 compared to its value in areas with no population. In the SEIB-DGVM, $a(N_D)$ is and user-definable parameter,
77 with a scale of 0.0 – 1.0, and in this study we adjust the value to 0.7 or 70% (total of human and unknown caused
78 fire), as the recent research in eastern Siberia Xu et al., (2022), shown that fires over Yakutia, 31.4 ± 6.8% caused
79 by lightning ignitions, 51.0 ± 6.9% caused by anthropogenic ignitions, and the last 14.4% unknown cause.

80

81 **S2.2.3. Fuel moisture content**

82 Default SEIB-DGVM already has a fuel moisture content equation, and according to Thonicke et al., (2001) we
 83 made variable name adjustments as GlobFIRM to make tracking and improvement easier. The fuel moisture
 84 content calculation (m), is as follows:

$$m = \frac{\text{frac moisture litter} \times \text{pool w1 runningrecord}(1)}{\text{Depth} * \text{Wfi}} \quad (\text{S11})$$

$$m = 0.4994 \times \tilde{m} + 1.02 \quad (\text{S12})$$

85 Fuel moisture content calculation inside SEIB-DGVM (Equation S11) is based on the fuel moisture content
 86 calculation in the LPJ-DGVM (Equation S12), where *frac moisture litter* is a local parameter of the fraction of
 87 litter moisture to soil moisture at the top layer and the default value is 0.5, *pool w1 runningrecord*(1) is annual
 88 soil water content of first soil layer, *Depth* is soil depth (there are 3 soil layers and the depth of each layer is 500
 89 mm, 1000 mm, and 1500 mm, respectively) and *Wfi* is field capacity (Sato et al., 2007). Equation S13 obtained
 90 from equation 8 by Viegas et al., (1992), that used to predict the fuel load on the Moisture module inside the
 91 BEHAVE system.

92 In the fire module improvement, we added the equation of relative moisture content (ω_o) of the fuel load:

$$\omega_o = e^{-\left(\sum_{i=1}^3 \alpha_i \times \frac{wo_i}{wo}\right) \times NI} \quad (\text{S13})$$

93 The values of α_{av} ($^{\circ}\text{C}^{-2}$) are average of inverse proportion to their surface-area-to-volume ratios of each fuel classes,
 94 with $\alpha_{1h} = 1.0 \times 10^{-3}$, $\alpha_{10h} = 5.42 \times 10^{-5}$, and $\alpha_{100h} = 1.49 \times 10^{-5}$. wo_i is fuel load classification for each
 95 fuel type (leaf, trunk and root) and wo is total fuel load. We used the average value of (α_{1h} , α_{10h} , and α_{100h})
 96 because SEIB-DGVM classifies fuel load by biomass type: litter trunk, litter leaf, and root. LPJ-DGVM SPTIFIRE
 97 allocated among four fuel classes: 1-h (leaves and twigs, i.e. leaf mass plus 4.5% of the carbon stored as heartwood
 98 (HW) and the sapwood (SW), respectively), 10-h (small branches, i.e. 7.5% of HW and SW), 100-h (large
 99 branches, i.e. 21% of HW and SW) and 1000-h (boles or trunks, i.e. 67% of HW and SW) (Thonicke et al., 2010).
 100 The consumption of 1000-h fuels is not considered in the calculation of moisture content because does not
 101 influence fire spread or intensity (Pyne et al., 1996).

102 NI is an abbreviation of Nesterov Index ($^{\circ}\text{C}^2$), is a cumulative function of daily maximum temperature T_{max} and
 103 dew-point temperature T_{dew} ($^{\circ}\text{C}$):

$$NI = \sum T_{max} \times (T_{max} - T_{dew}) \quad (\text{S14})$$

$$NI = \sum T_{max} \times (T_{max} - (T_{min} - 4.0)) \quad (\text{S15})$$

104 We approximate T_{dew} by $(T_{min} - 4)$, where T_{min} is the daily minimum temperature (Running et al., 1987), same
 105 approach used by (Venevsky et al., 2002), and (Thonicke et al., 2010).

106

107 **S2.2.4. Fire Danger Index**

108 Fire Danger Index (FDI) is the probability that an ignition event will start a fire and can be calculated by combining
 109 the relative moisture content equation (ω_o) (Equation S13), the fire spread probability equation (P_{spread}) (Equation
 110 S16), and also depends on fire weather conditions as described by NI (Equation S15). Moisture extinction (m_e)
 111 is PFT-specific disturbance parameter that indicates the proportion of litter moisture extinction due to fire.

$$P_{spread} = \left\{ 1 - \frac{\omega_o}{m_e}, \omega_o \leq m_e \quad 0, \omega_o > m_e \right\} \quad (\text{S16})$$

112

$$FDI = \max\left(0, \left(1 - \frac{1}{m_e} \times e^{-((\alpha_{av} \times \text{fuel load}) \times NI)}\right)\right) \quad (S17)$$

Equation S17 will produce the Fire Danger Index (*FDI*) value if there is enough fuel load that satisfies the minimum threshold (200 g C m⁻²), and *FDI* will be zero if there is no fuel or the fuel has a high moisture content that is unable to be ignited.

116

117 **S2.2.5. Rate of spread**

The rate of Spread (ROS) is the predicted speed of the fire in the front or head of the fire, where it spreads the fastest, is known as which accounts for both crowning and spotting and can be obtained using Rothermell equations (Rothermell, 1972; Wilson, 1982; Pyne et al., 1996). We also implemented the complete rate of spread equations as SPITFIRE (Thonicke et al., 2010) as we were able to add all of the needed parameters, integrate it, and create new variables on SEIB-DGVM.

The forward and backward fire rate of spread $ROS_{f,surface}$ and $ROS_{b,surface}$ (m min⁻¹) respectively, can be obtained by:

$$ROS_{f,surface} = \frac{I_R \times \xi \times (1 + \phi_w)}{\rho_b \times \varepsilon \times Q_{ig}} \quad (S18)$$

$$ROS_{b,surface} = ROS_{f,surface} \times e^{-0.012 \times U_{forward}} \quad (S19)$$

I_R is the reaction intensity, the energy that is released per unit fire front area (kJm⁻² min⁻¹); ξ is the propagating flux ratio, the percentage of I_R that causes nearby fuel particles to heat up and ignite; ϕ_w is a multiplier that takes into consideration how wind affects the effective value of ξ ; ρ_b is the fuel bulk density (kgm⁻³), assigned by PFT-specific parameter (Table 1); ε is the effective heating number, the percentage of a fuel particle that reaches ignition temperature at the beginning of flame combustion; and Q_{ig} is the heat of pre-ignition, the heat needed to ignite a specific mass of fuel (kJ kg⁻¹). The ROS variable calculation details are explained in more detail in Appendix A.

The estimated fire duration can also be calculated based on the fire danger index, using the following equation:

$$t_{fire} = \frac{241}{1 + 240 \times e^{-11.06 \times FDI}} \quad (S20)$$

133 **S2.2.6. Fire fraction and intensity**

The surface fire intensity, $I_{surface}$ (kW m⁻¹) is the product of the forward rate of fire spread $ROS_{f,surface}$, fuel consumption FC , fuel heat content h , and area burnt fraction $A_{b,frac}$ (Byram, 1959).

$$I_{surface} = h \times \frac{\sum_{i=1}^3 FC}{1000 \times A_{b,frac}} \times \frac{ROS_{f,surface}}{60} \quad (S21)$$

$$A_{b,fraction} = \frac{A_b}{A} \quad (S22)$$

FC is fuel consumption in a surface fire (gDM m⁻²), and calculated using empirical equations as fuel moisture function of the fuel load (Peterson and Ryan, 1986), this equation has been adjusted for SEIB-DGVM as there is no fuel classification based on the length of combustion.

139

140 **S2.2.7. Fire damage to plants**

141 The SPITFIRE module is very detailed in its classification of fire spread, ranging from surface fires to crown
 142 scorch caused by surface fire. The scorch height SH of the fire can be obtained by the following equation (Peterson
 143 and Ryan, 1986; Agee, 1997; Dickinson and Johnson, 2001):

$$SH = F \times (I_{surface})^{0.667} \quad (S23)$$

144 F is PFT-specific parameter of the crown scorch equation (Table 1). Assuming a cylindrical crown, the crown
 145 scorch fraction (CK) impacted by a fire can be obtained using the following formula:

$$CK = \frac{SH - T_H + CL}{CL} \quad (S24)$$

146 T_H is the individual tree height of woody PFT, CL is crown length, and the value is provided by PFT-specific
 147 parameters (Table 1). Post-fire tree mortality is caused by the cambium damage, and crown damage is caused by
 148 bark heating. Those causes are assumed to act independently, so the total probability of mortality P_m is determined
 149 by the probability of crown damage mortality $P_m(CK)$ and cambial damage $P_m(\tau)$.

$$P_m = P_m(\tau) + P_m(CK) - (P_m(\tau) \times P_m(CK)) \quad (S25)$$

150 The probability of crown damage mortality $P_m(CK)$ is obtained by:

$$P_m(CK) = r(CK) \times CK^p \quad (S26)$$

151 $r(CK)$ is the crown damage resistance factor, and p is Woody PFTs parameter, the values of each parameter are
 152 described in Table 1 (Peterson and Ryan, 1986; Williams et al., 1998; Cochrane, 2003).

153 Probability of cambial damage mortality $P_m(\tau)$:

$$P_m(\tau) = \left\{ 0, \frac{\tau_l}{\tau_c} \leq 0.22 \ 0.563 \times \frac{\tau_l}{\tau_c} - 0.125, \frac{\tau_l}{\tau_c} > 0.22 \ 1, \frac{\tau_l}{\tau_c} \geq 2.0 \right\} \quad (S27)$$

154 τ_l is the residence time of the fire, τ_c is the critical time of cambial damage, so τ_l/τ_c is the ratio of fire residence time
 155 to the cambial damage (Peterson and Ryan, 1986). The value of τ_l is dependent on I_R , as provided by the fire spread
 156 model (Rothermell, 1972; Wilson, 1982), described in Appendix A. The critical time of cambial damage τ_c (min),
 157 depends on the bark thickness (cm) (Peterson and Ryan, 1986).

$$\tau_c = 2.9 \times BT^2 \quad (S28)$$

$$BT = par_1 \times DBH + par_2 \quad (S29)$$

158 BT calculated from the diameter at breast height, DBH (cm), and par_1 and par_2 are PFT-specific parameters (Table
 159 1). Generally, during a fire, all leaf biomass of grass, all leaf biomass of dead and surviving trees, half of the trunk
 160 biomass of dead trees, and half of the litter pool are burned (classified into surface fire and crown scorch), while
 161 the remaining biomass of dead trees is transformed into litter. In response to fire, the phenology phase of all grass
 162 PFTs changes to dormant (they reenter the growth phase as described previously in the section titled 'Phenology').
 163 If the stock resource of grass PFTs ($gmassstock$) does not satisfy the minimum value (50 g DM m⁻²) after fire,
 164 the deficit is supplemented by litter (Sato et al., 2007). The fraction of individual trees killed in a fire also depends
 165 on PFT fire resistance (M3, Table 1).

166

167

168

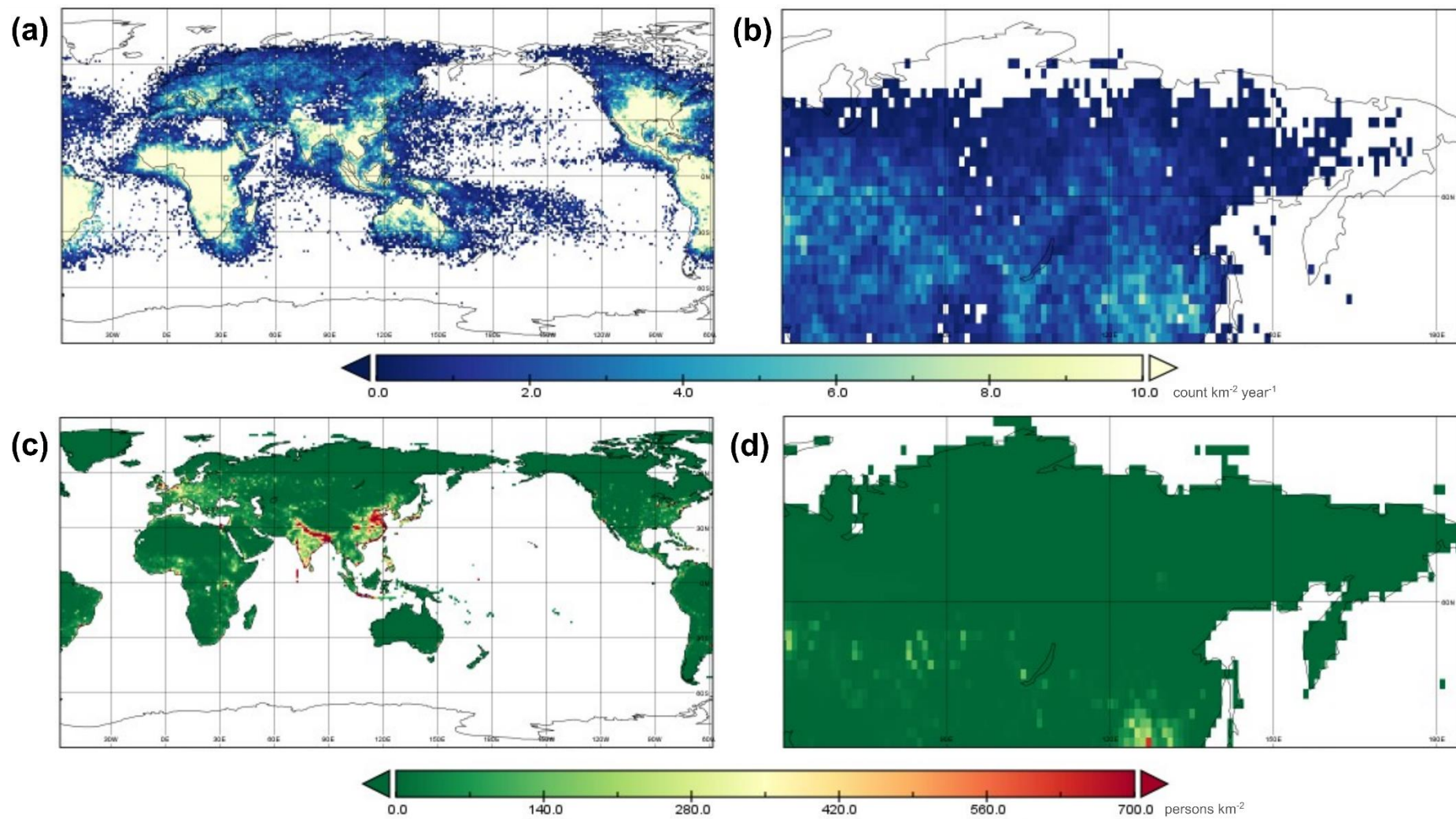


Figure S1. Spatial distribution of lightning flash rate (LIS/OTD HRFC) and population density (GPWv4) input data: (a) LIS/OTD HRFC global, (b) LIS/OTD HRFC Siberian, (c) GPWv4 global, (d) GPWv4 Siberian

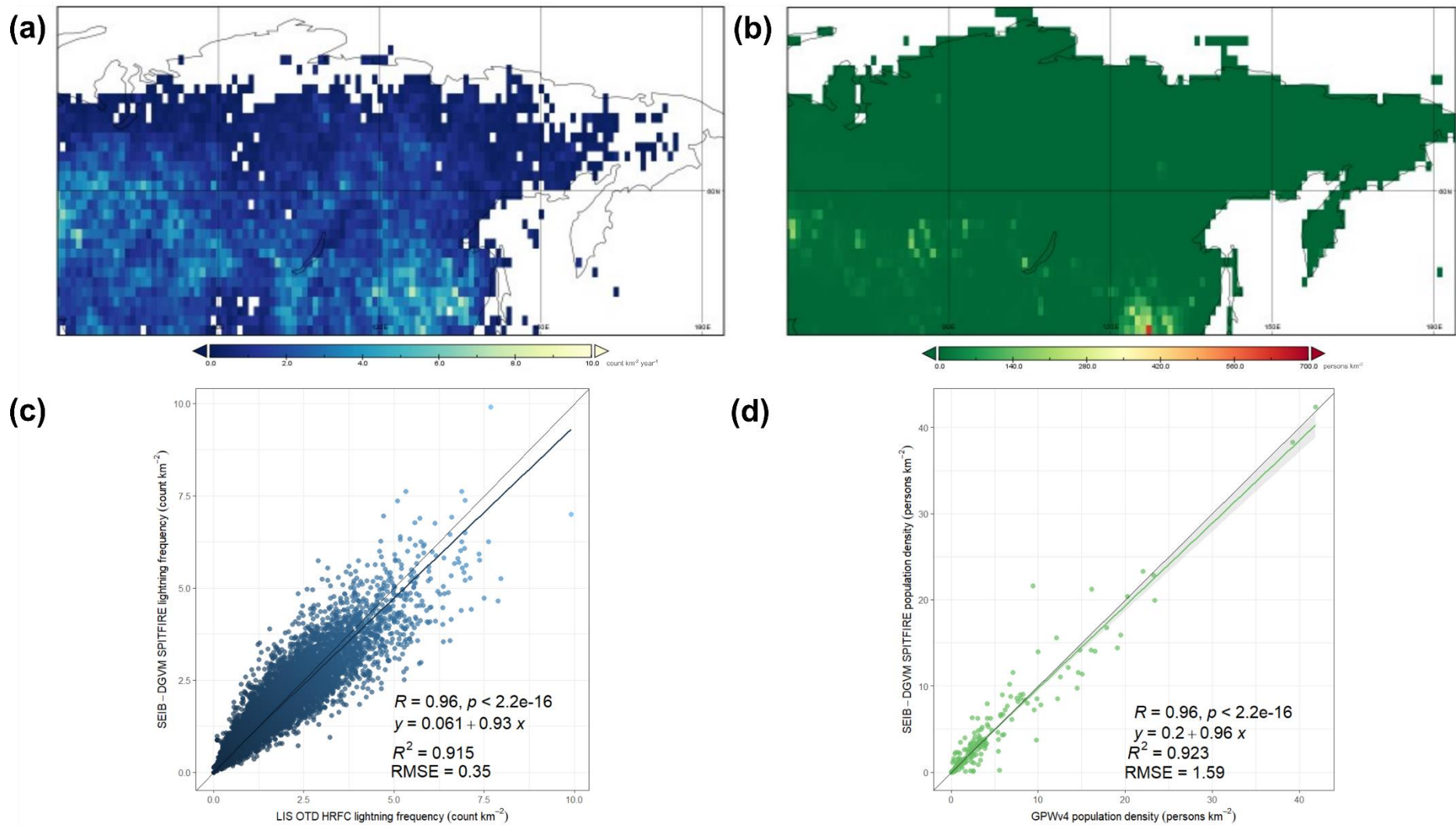


Figure S2. (a) Spatial distribution of lightning flash rate model output, (b) Spatial distribution of population density model output, (c) Comparison between simulated lightning flash rate and observational lightning flash rate (LIS/OTD HRF), (d) Comparison between simulated population density and population density (GPWv4)

Table S1. Population and lightning input data information

Variable	Unit	Product	Spatial resolution	Temporal resolution	Temporal coverage	Reference
Population density	person km ⁻²	Gridded Population of the World (GPWv4)	2.5 arc-minute	Annual	2000-2020	(CIESIN, 2018)
OTD Flash Rate	count km ⁻² year ⁻¹	LIS/OTD High Resolution Full Climatology (HRFC) V2.3.2015	0.5 degree	Annual	2015	(Cecil, 2001)

Table S2. Emission factors (g species (kg DM⁻¹)) for land cover types (LCTs) (Andreae and Merlet, 2001; Andreae, 2019)

No.	Species	PFT parameter abbreviation	Grassland/ savana	Tropical forest	Temperate forest	Boreal forest	Cropland
1	CO ₂	ES1	1647	1613	1566	1549	1421
2	CO	ES2	70	108	112	124	78
3	CH ₄	ES3	2.5	6.3	5.8	5.1	5.9
4	NHMC	ES4	5.5	7.1	14.6	5.3	5.8
5	H ₂	ES5	0.97	3.11	2.09	1.66	2.65
6	NO _x	ES6	2.58	2.55	2.9	1.69	2.67
7	N ₂ O	ES7	0.18	0.2	0.25	0.25	0.09
8	PM _{2.5}	ES8	7.5	8.3	18.1	20.2	8.5
9	TPM	ES9	8.5	10.9	18.1	15.3	11.3
10	TPC	ES10	3.4	6	8.4	10.6	5.5
11	OC	ES11	3.1	4.5	8.9	10.1	5
12	BC	ES12	0.51	0.49	0.66	0.5	0.43
13	SO ₂	ES13	0.51	0.78	0.75	0.75	0.81
14	C ₂ H ₆ (ethane)	ES14	0.42	0.94	0.71	0.9	0.76
15	CH ₃ OH (methanol)	ES15	1.48	3.15	2.13	1.53	2.63
16	C ₃ H ₈ (propane)	ES16	0.14	0.53	0.29	0.28	0.2

No.	Species	PFT parameter abbreviation	Grassland/ savana	Tropical forest	Temperate forest	Boreal forest	Cropland
17	C ₂ H ₂ (acetylene)	ES17	0.34	0.43	0.35	0.27	0.32
18	C ₂ H ₄ (ethylene)	ES18	1.01	1.11	1.22	1.49	1.14
19	C ₃ H ₆ (propylene)	ES19	0.49	0.86	0.67	0.66	0.48
20	C ₅ H ₈ (isoprene)	ES20	0.12	0.22	0.19	0.07	0.18
21	C ₁₀ H ₁₆ (terpenes)	ES21	0.1	0.15	1.07	1.53	0.03
22	C ₇ H ₈ (toluene)	ES22	0.2	0.23	0.43	0.32	0.18
23	C ₆ H ₆ (benzene)	ES23	0.34	0.38	0.46	0.52	0.31
24	C ₈ H ₁₀ (xylene)	ES24	0.09	0.09	0.17	0.1	0.09
25	CH ₂ O (formaldehyde)	ES25	1.33	2.4	2.22	1.76	1.8
26	C ₂ H ₄ O (acetaldehyde)	ES26	0.86	2.26	1.2	0.78	1.82
27	C ₃ H ₆ O (acetone)	ES27	0.47	0.63	0.7	0.61	0.61
28	C ₃ H ₆ O ₂ (hydroxyacetone)	ES28	0.52	1.13	0.85	1.48	1.74
29	C ₆ H ₅ OH (phenol)	ES29	0.37	0.23	0.33	2.96	0.5
30	NH ₃ (ammonia)	ES30	0.91	1.45	1	2.82	1.04
31	HCN (hydrogen cyanide)	ES31	0.42	0.38	0.62	0.81	0.43
32	MEK/2-butanone	ES32	0.13	0.5	0.23	0.15	0.6
33	CH ₃ CN (acetonitrile)	ES33	0.17	0.51	0.23	0.3	0.25

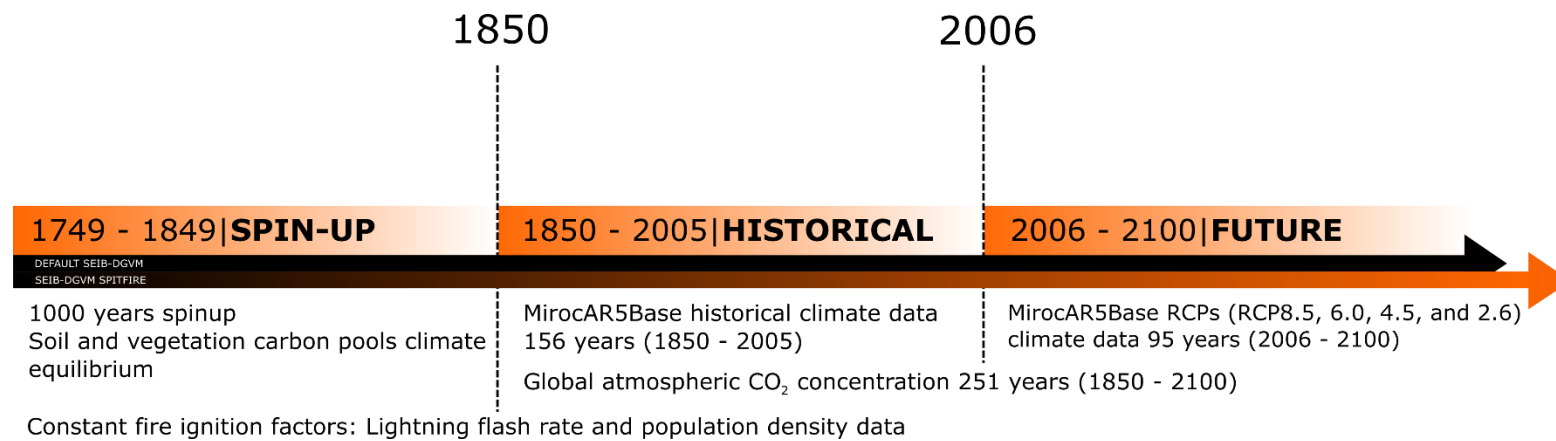


Figure S3. SEIB-DGVM SPITFIRE simulation protocols

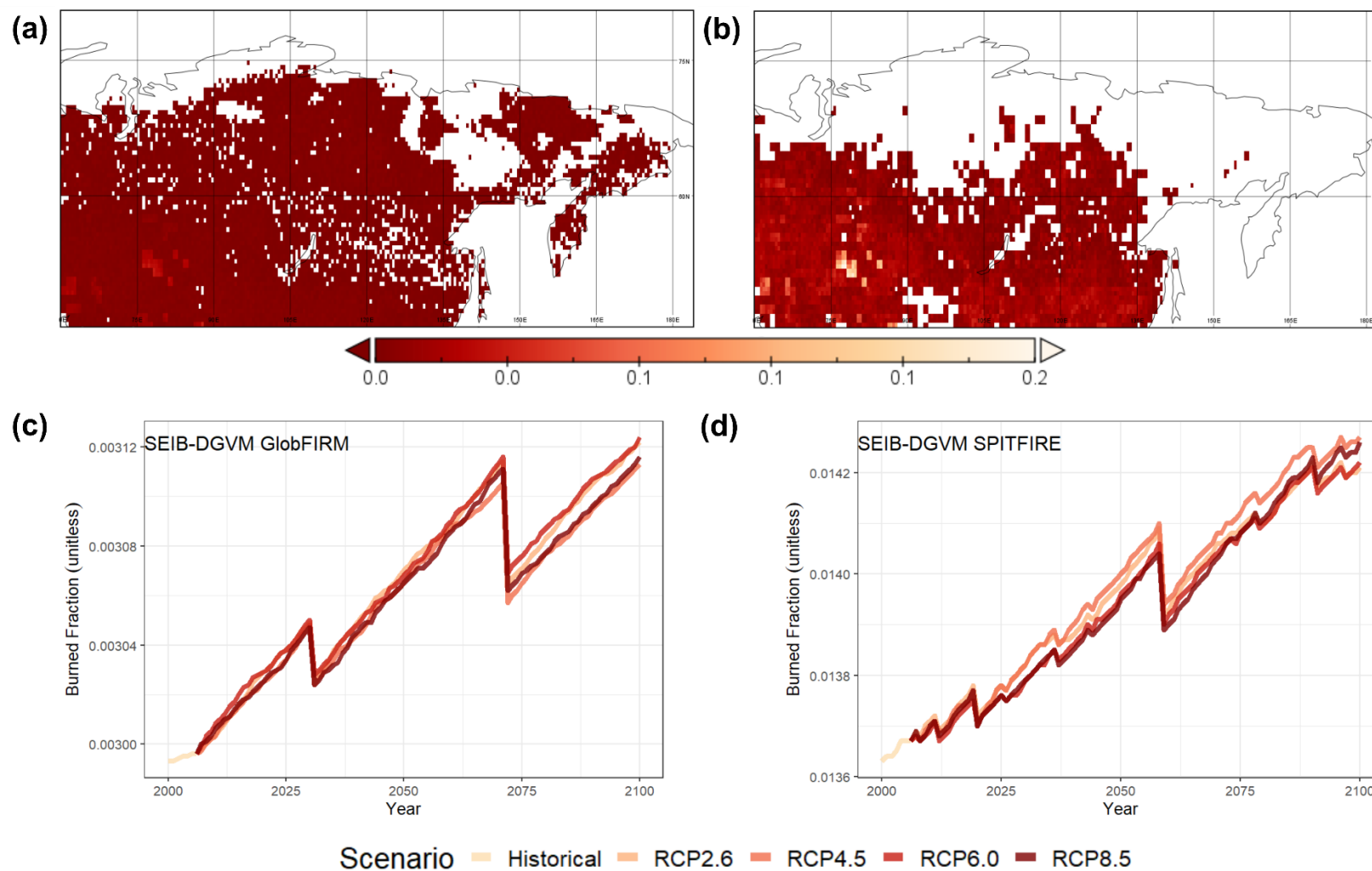


Figure S4. (a) Spatial distribution of annual averaged burned fraction of SEIB-DGVM GlobFIRM from 2006 to 2100. (b) Spatial distribution of annual averaged burned fraction of SEIB-DGVM SPITFIRE from 2006 to 2100. (c) Temporal variation of burned fraction of SEIB-DGVM GlobFIRM from 2000 to 2100. (d) Temporal variation of burned fraction of SEIB-DGVM SPITFIRE from 2000 to 2100.

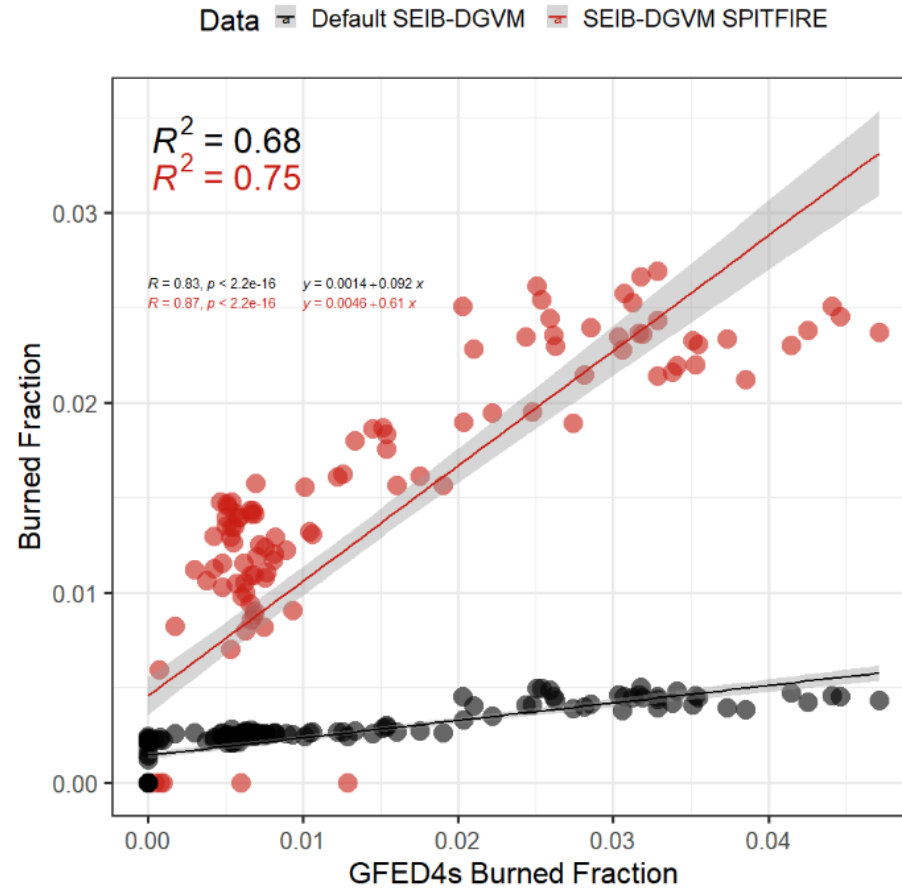


Figure S5. Comparison between annual averaged burned fraction variable of default SEIB-DGVM (GlobFIRM fire module) and SEIB-DGVM SPITFIRE with burned fraction of GFED4s from 1997 to 2016

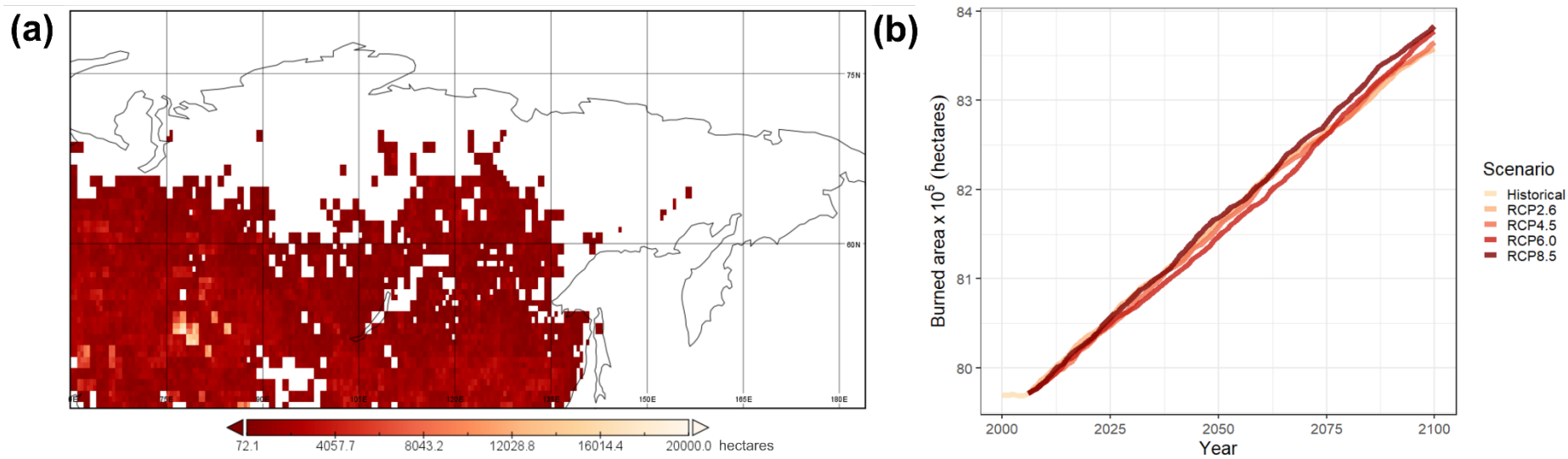


Figure S6. (a) Spatial distribution of annual averaged burned area of SEIB-DGVM SPITFIRE from 2006 to 2100. (b) Temporal variation of burned area of SEIB-DGVM SPITFIRE from 2000 to 2100.

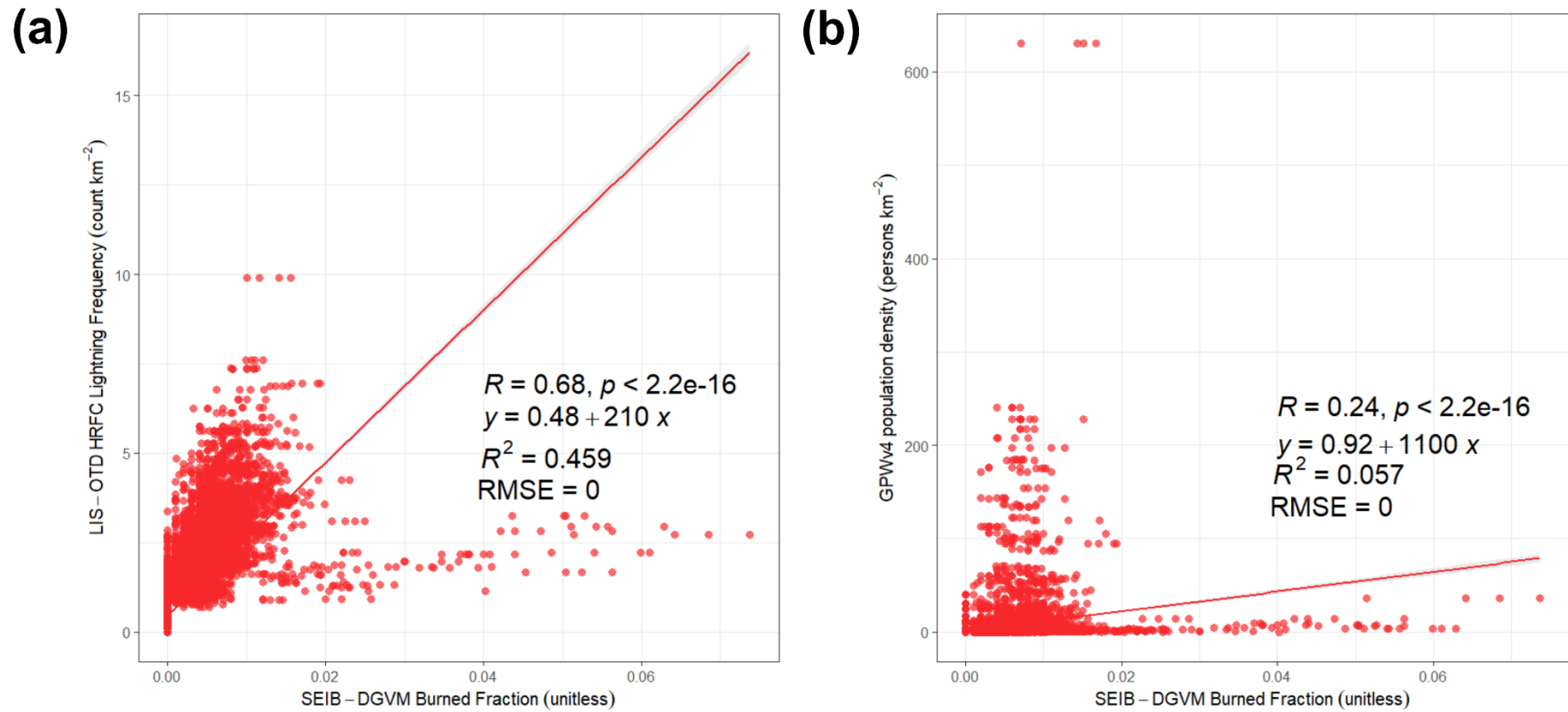


Figure S7. (a) Comparison of annual averaged LIS/OTD HRFC lightning flash rate (2000-2020) with simulated burned fraction of SEIB-DGVM SPITFIRE (1996-2005). **(b)** Comparison of annual averaged GPWv4 population density (2015) with simulated burned fraction of SEIB-DGVM SPITFIRE (1996-2005).

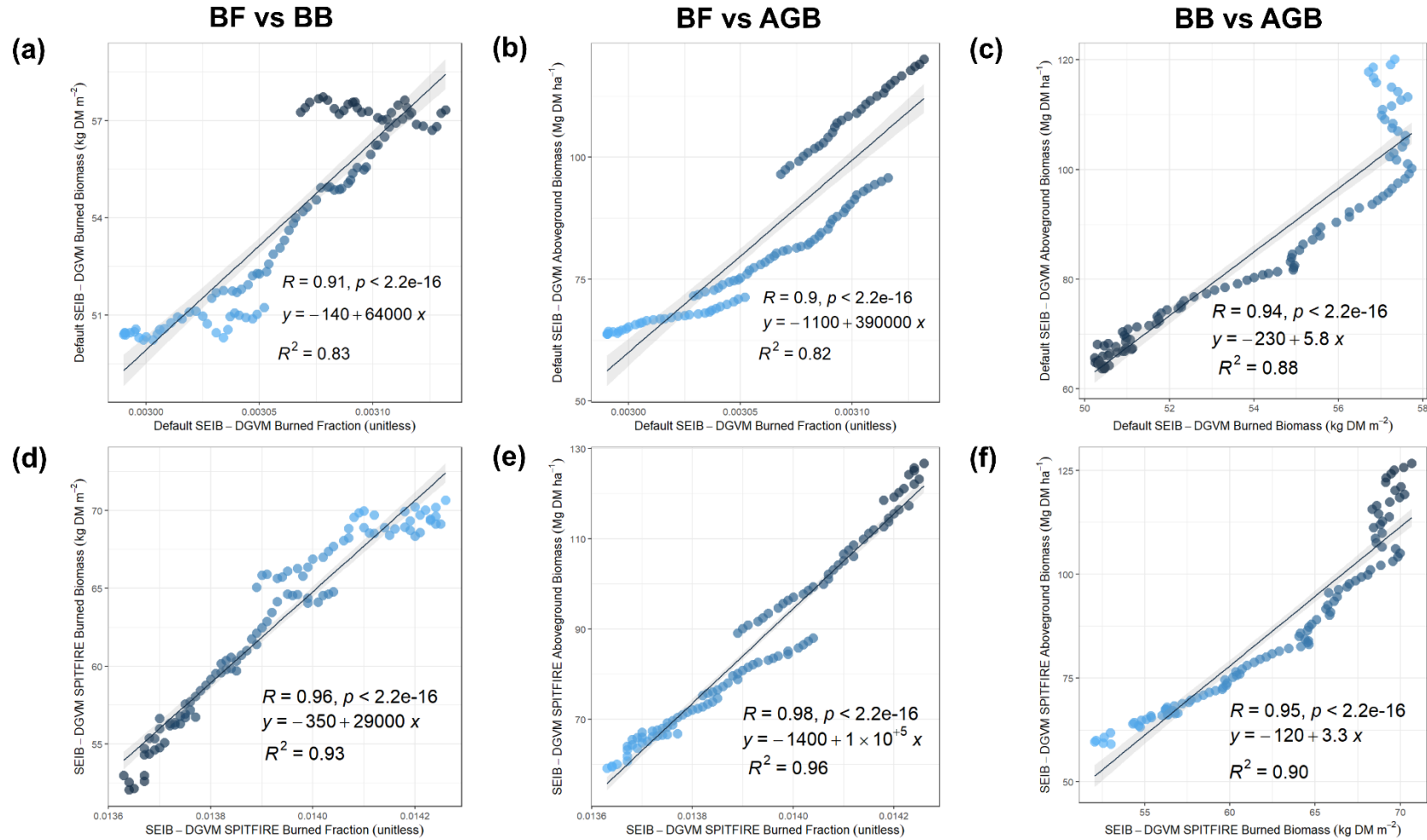


Figure S8. (a) Comparison of annual averaged burned fraction and burned biomass variables of default model (SEIB-DGVM GlobFIRM) from 2000 to 2100. (b) Comparison of annual averaged burned fraction and aboveground biomass variables of SEIB-DGVM GlobFIRM from 2000 to 2100. (c) Comparison of annual averaged burned biomass and aboveground biomass variables of SEIB-DGVM GlobFIRM from 2000 to 2100. (d) Comparison of annual averaged burned fraction and burned biomass variables of improved model (SEIB-DGVM SPITFIRE) from 2000 to 2100. (e) Comparison of annual averaged burned fraction and aboveground biomass variables of SEIB-DGVM SPITFIRE from 2000 to 2100. (f) Comparison of annual averaged burned biomass and aboveground biomass variables of SEIB-DGVM SPITFIRE from 2000 to 2100.

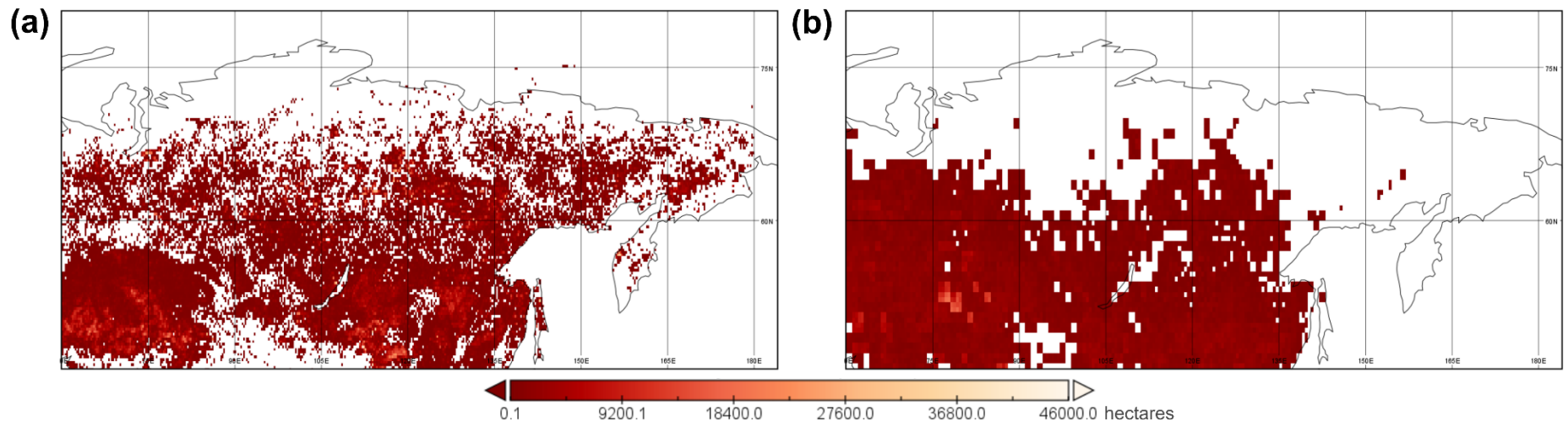


Figure S9. Spatial distribution of annual averaged (1996-2016) burned area variable of: (a) GFED4 (b) SEIB-DGVM SPITFIRE

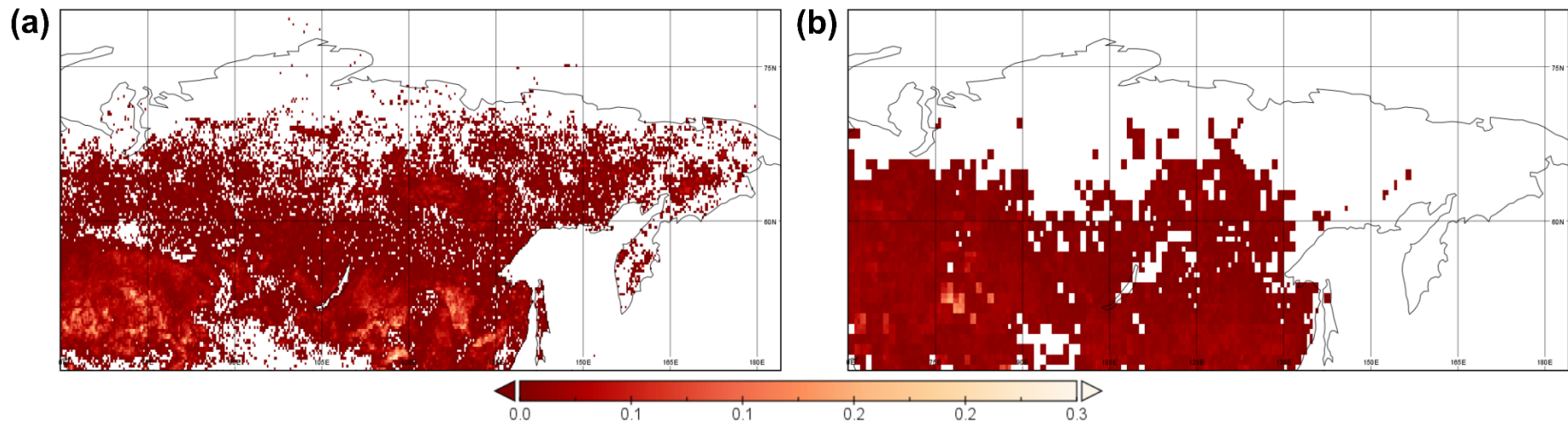


Figure S10. Spatial distribution of annual averaged (1997-2016) burned fraction variable of: (a) GFED4s (b) SEIB-DGVM SPITFIRE

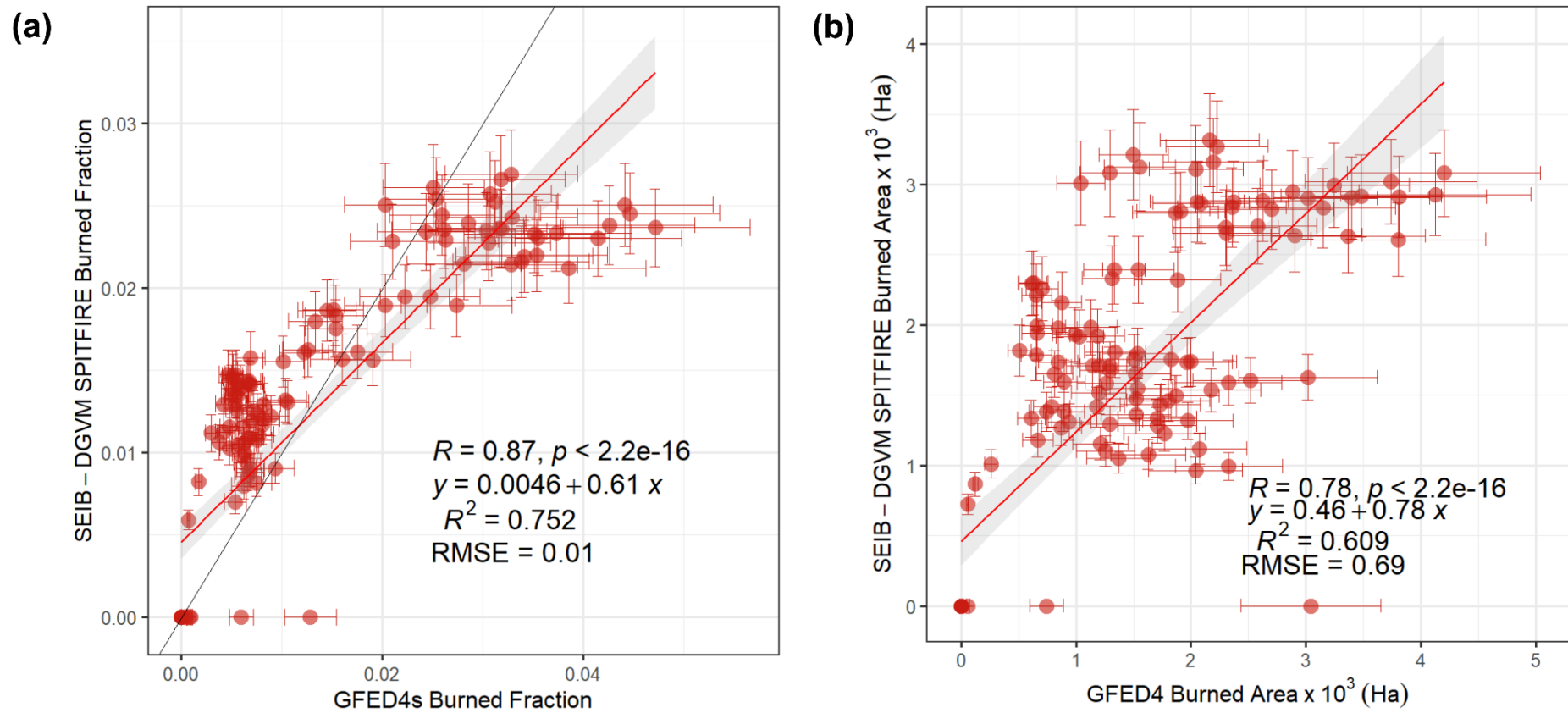


Figure S11. (a) Latitude average spatial comparison of annual averaged simulated burned fraction of SEIB-DGVM SPITFIRE and burned fraction of GFED4s from 1997 to 2016. (b) Latitude average spatial comparison of annual averaged simulated burned area of SEIB-DGVM SPITFIRE and burned area of GFED4 from 1996 to 2016.

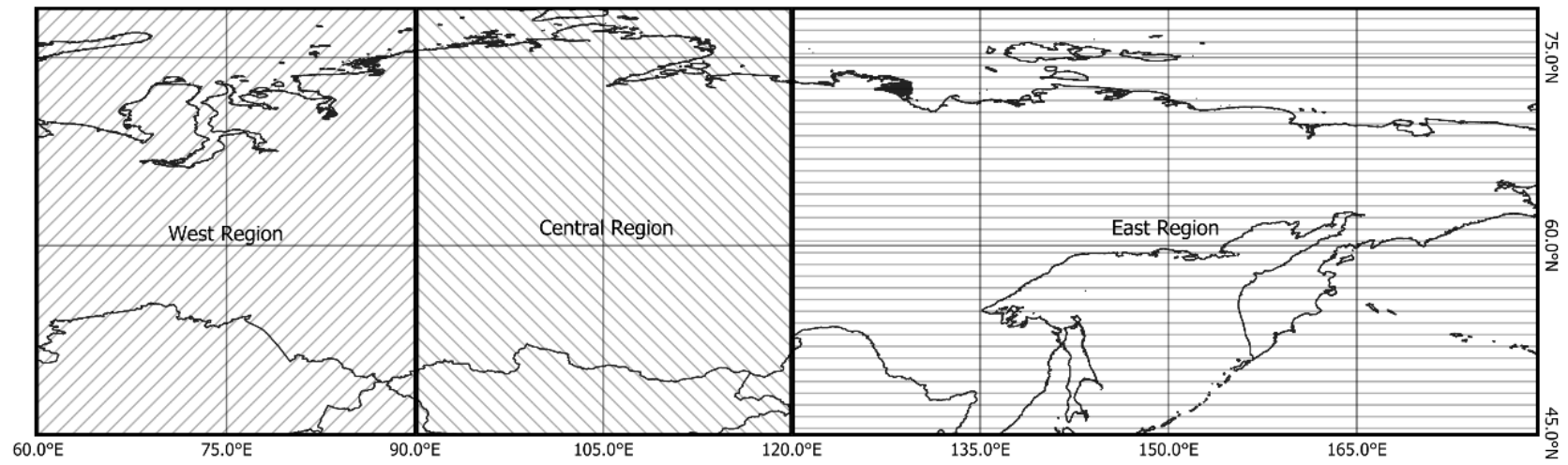


Figure S12. Division of Siberia into three regions: west region (60°-90°E and 45°-80°N), central region (90°-120°E and 45°-80°N), and east region (120°-180°E and 45°-80°N)

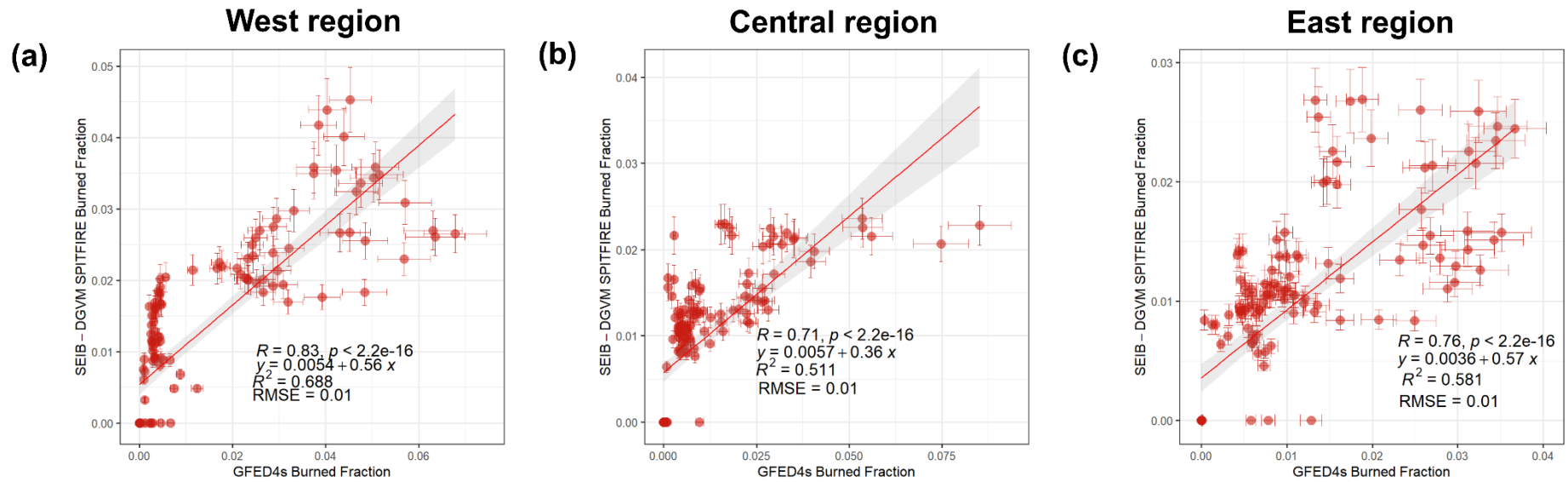


Figure S13. Latitude average spatial comparison of annual averaged (1997-2016) simulated burned fraction of SEIB-DGVM SPITFIRE and burned fraction of GFED4s in: **(a)** west region **(b)** central region, **(c)** east region

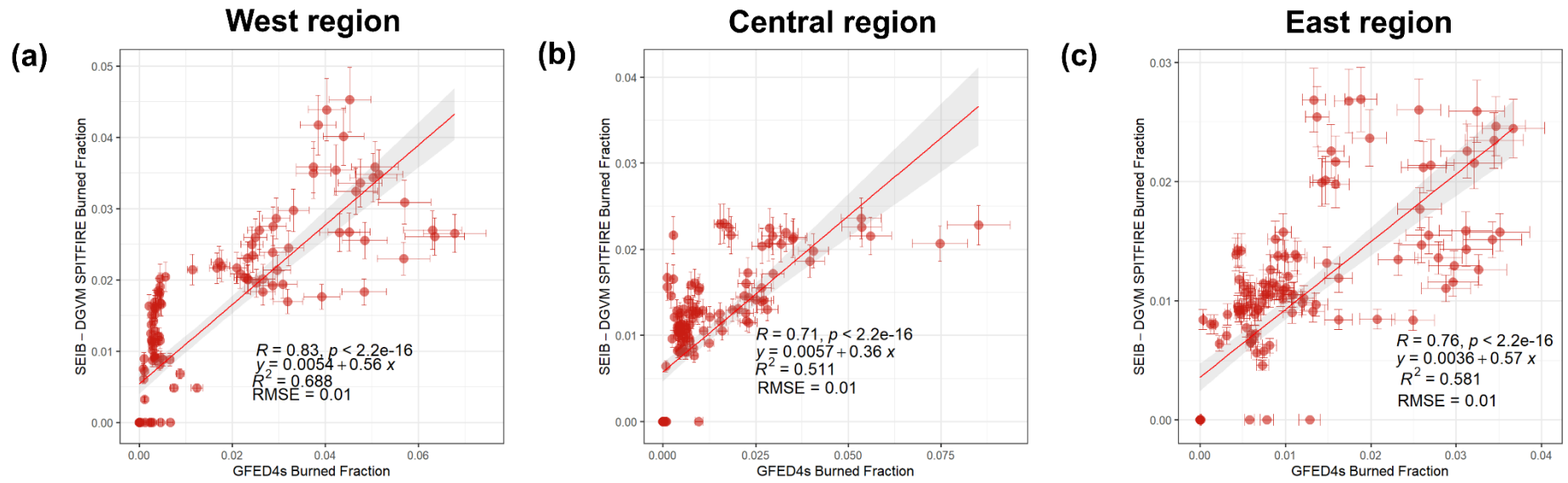


Figure S14. Latitude average spatial comparison of annual averaged (1996-2016) simulated burned area of SEIB-DGVM SPITFIRE and burned area of GFED4s in: **(a)** west region **(b)** central region, **(c)** east region

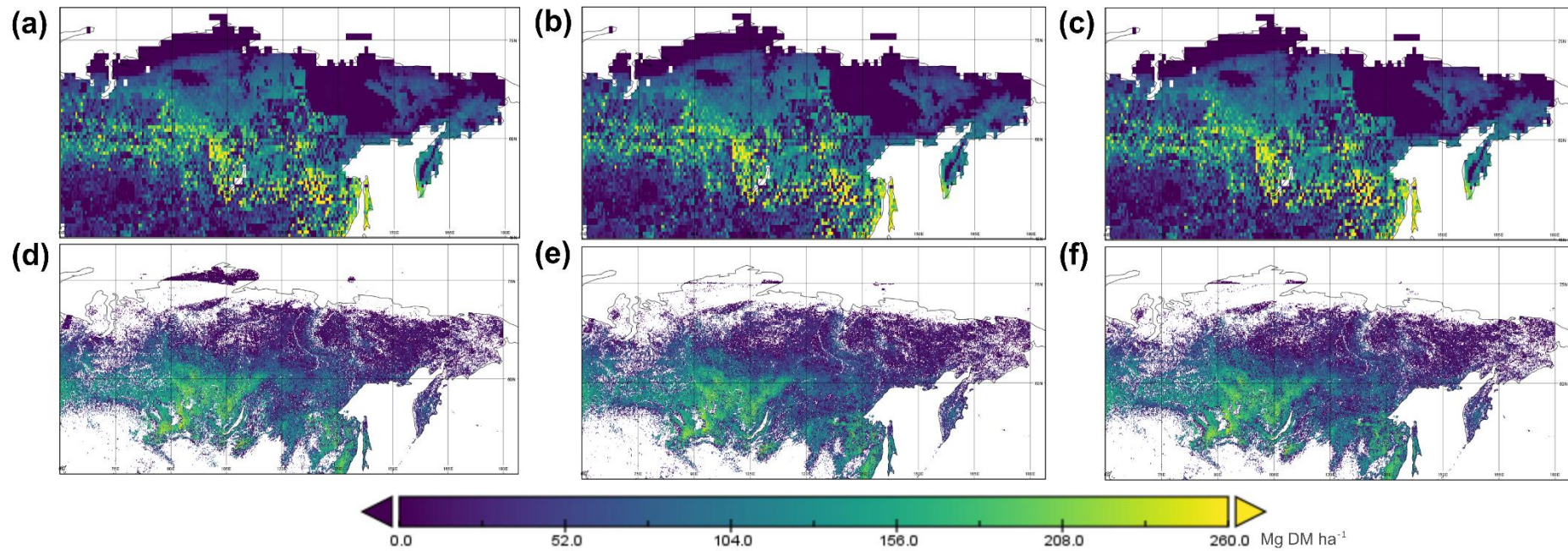


Figure S15. Spatial distribution of annual averaged aboveground biomass (AGB) of: **(a)** SEIB-DGVM SPITFIRE 2010. **(b)** SEIB-DGVM SPITFIRE 2017. **(c)** SEIB-DGVM SPITFIRE 2018. **(d)** ESA Biomass Climate Change Initiative (CCI) 2010. **(e)** ESA Biomass CCI 2017. **(f)** ESA Biomass CCI 2018.

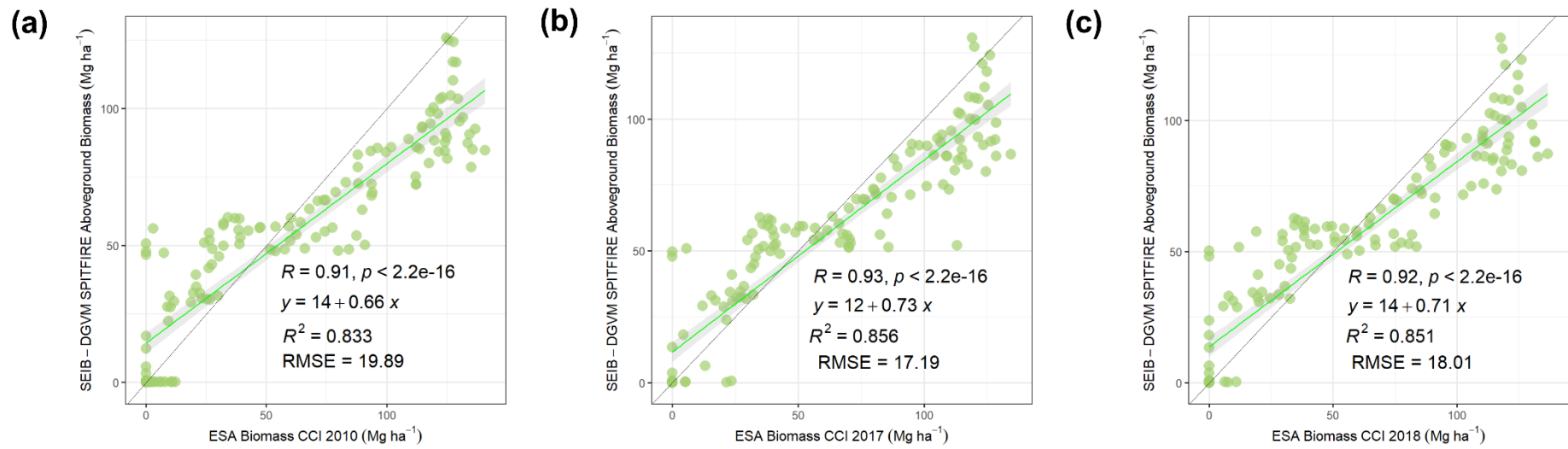
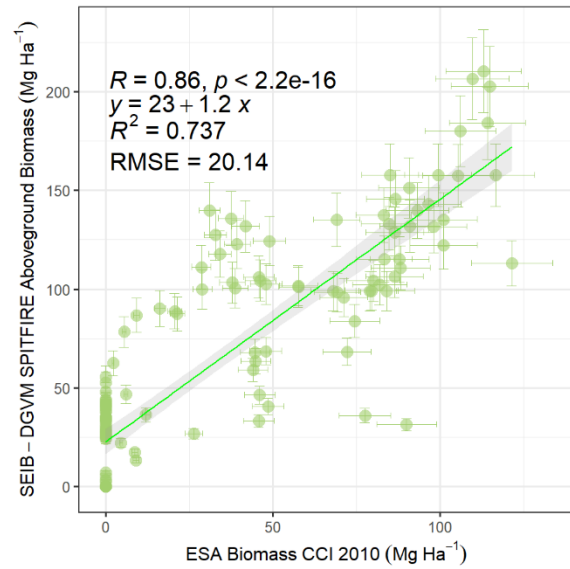
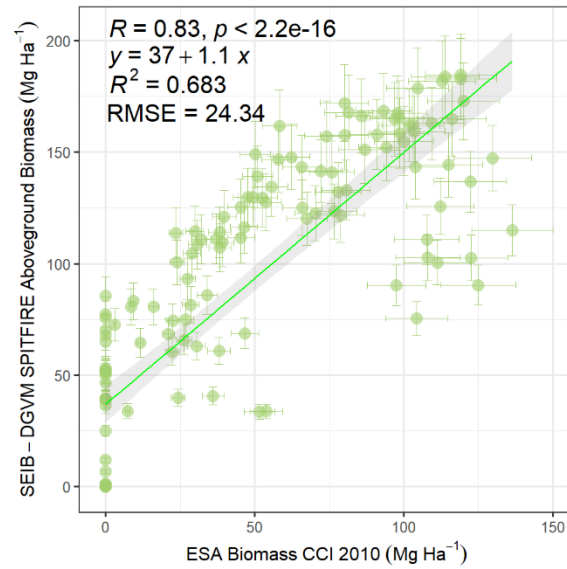


Figure S16. Latitude average spatial comparison of annual averaged simulated aboveground biomass of SEIB-DGVM SPITFIRE and aboveground biomass of ESA Biomass CCI in: **(a)** 2010. **(b)** 2017. **(c)** 2018.

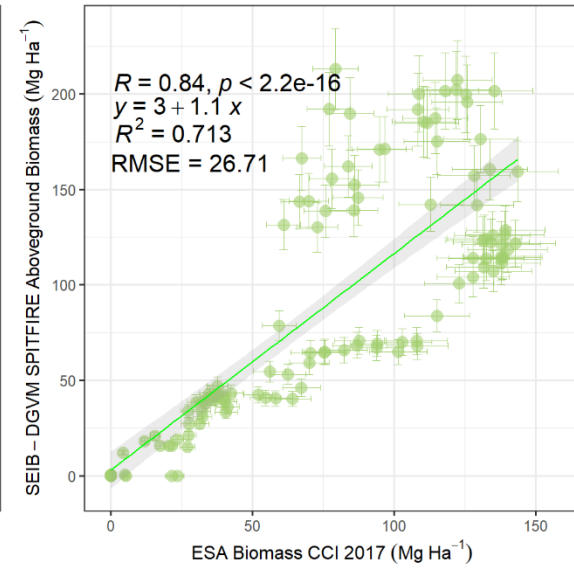
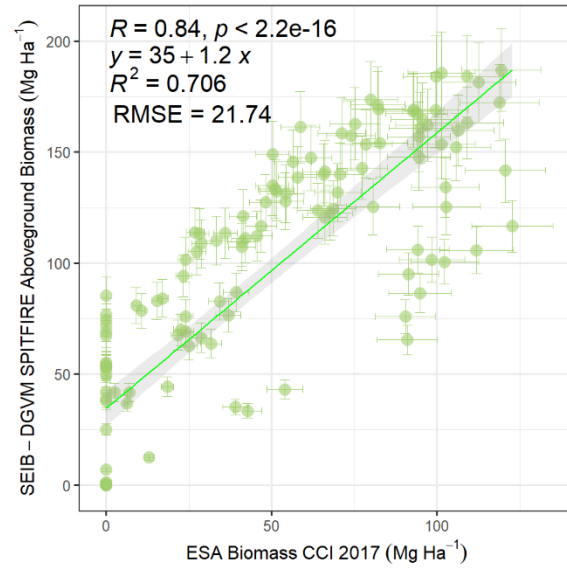
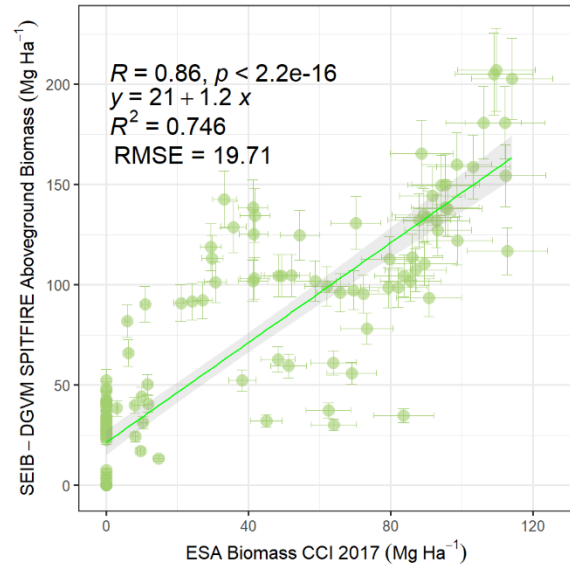
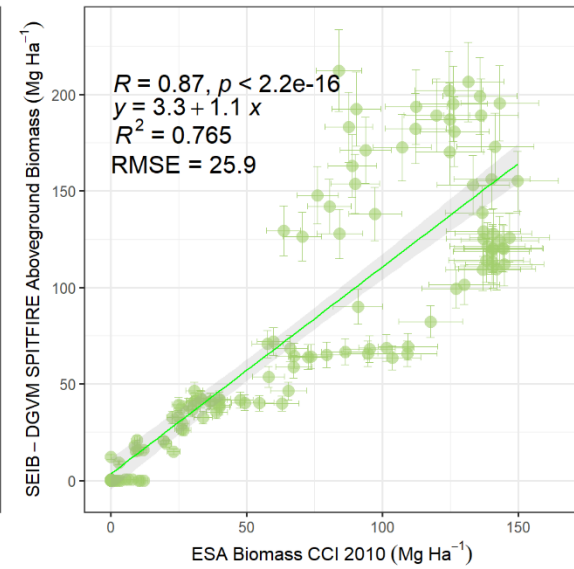
West region



Central region



East region



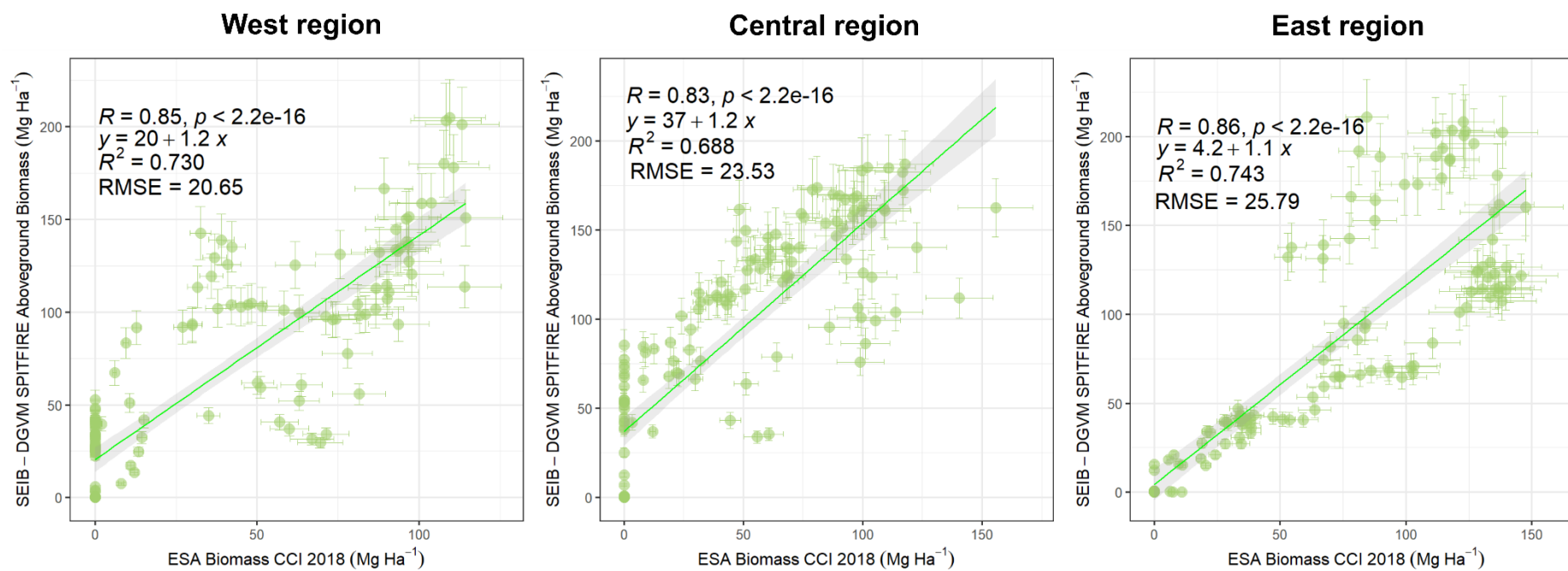


Figure S17. Latitude average spatial comparison between annual averaged (2010, 2017, 2018) simulated aboveground biomass of SEIB-DGVM SPITFIRE and aboveground biomass of ESA Biomass CCI in the classified region in Siberia

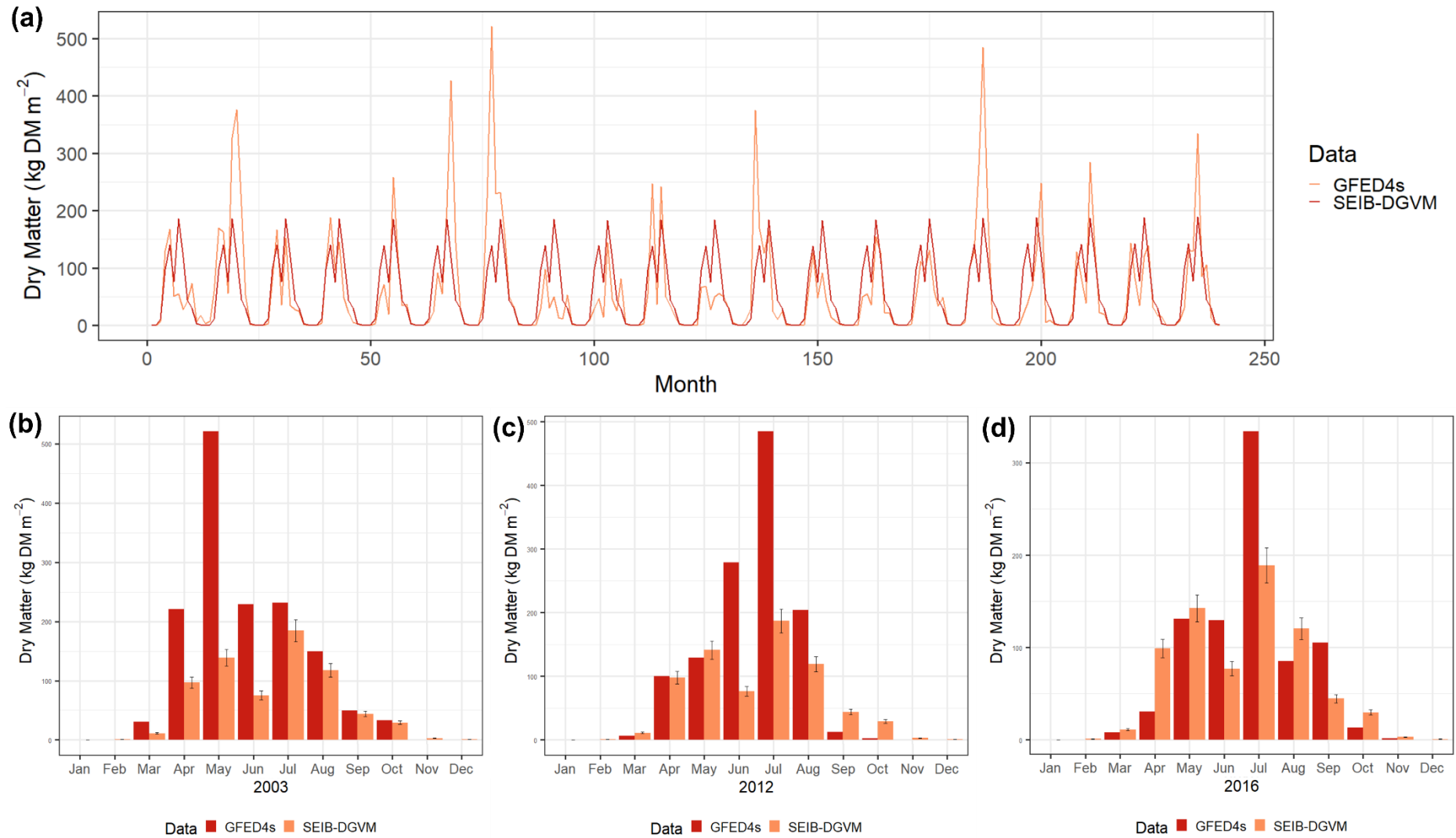


Figure S18. Temporal variation of monthly dry matter emission variable of SEIB-DGVM SPITFIRE and GFED4s. **(a)** from 1997 to 2016. **(b)** 2003. **(c)** 2012. **(d)** 2016

Table S3. Annual CO₂ emissions data from GFED4s (Siberia and BOAS), GBEI, and SEIB-DGVM SPITFIRE product (1 x 10¹³ g CO₂)

Year	Siberia		BOAS	
	GFED4s	SEIB-DGVM	GBEI	GFED4s
1997	85.9423	75.06	NA	30
1998	212.3127	75.29	NA	89
1999	78.2312	75.05	NA	32
2000	91.2028	75.07	NA	35
2001	90.7241	75.27	42.49	32
2002	146.7248	75.82	58.29	51
2003	218.6563	76.12	125.1	88
2004	42.2935	76.22	43.7	14
2005	59.1899	75.90	36.37	21
2006	101.7702	75.40	64.84	43
2007	52.6425	75.57	32.62	18
2008	139.1379	75.30	89.25	57
2009	59.2727	75.28	50.47	21
2010	69.6919	75.67	41.26	28
2011	80.1802	76.04	71.73	32
2012	181.7223	76.22	126.8	67
2013	77.3021	76.24	41.23	26
2014	110.0743	76.70	71.46	41
2015	90.7468	77.08	49.86	33
2016	124.9715	77.12	70.33	46
2017	NA	77.59	46.49	NA
2018	NA	77.59	55.51	NA
2019	NA	77.52	70.98	NA
2020	NA	77.67	60.8	NA
Average	105.64 ± 50.69	76.12 ± 0.87	62.48 ± 26.09	40.2 ± 21.12

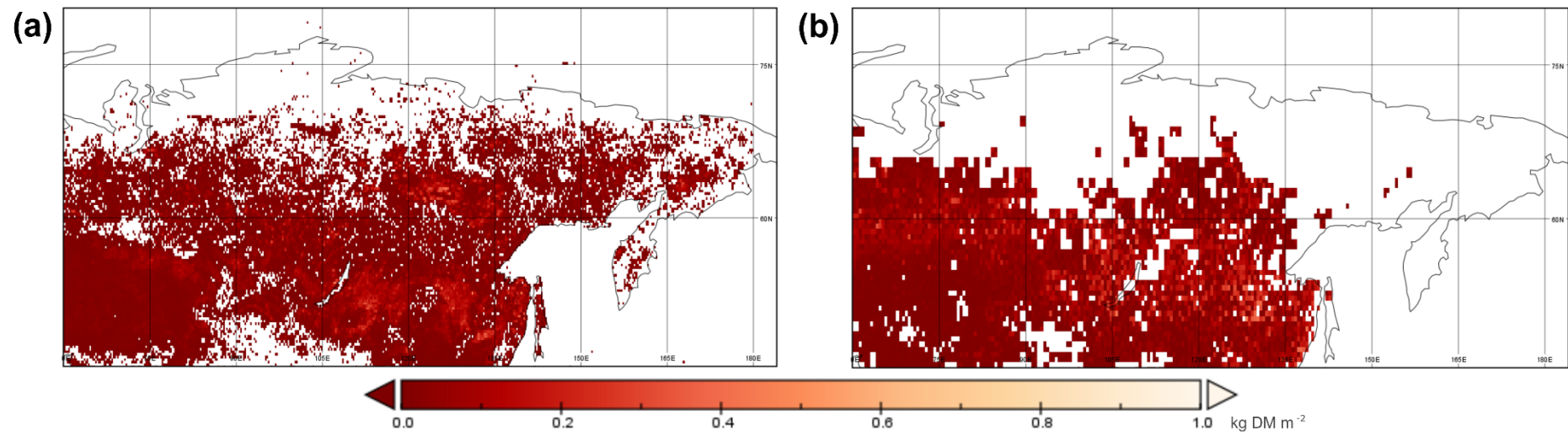


Figure S19. (a) Spatial distribution of annual averaged dry matter emissions of GFED4s from 1997-2016. (b) Spatial distribution of annual averaged dry matter emission of SEIB-DGVM SPITFIRE from 1997 to 2016

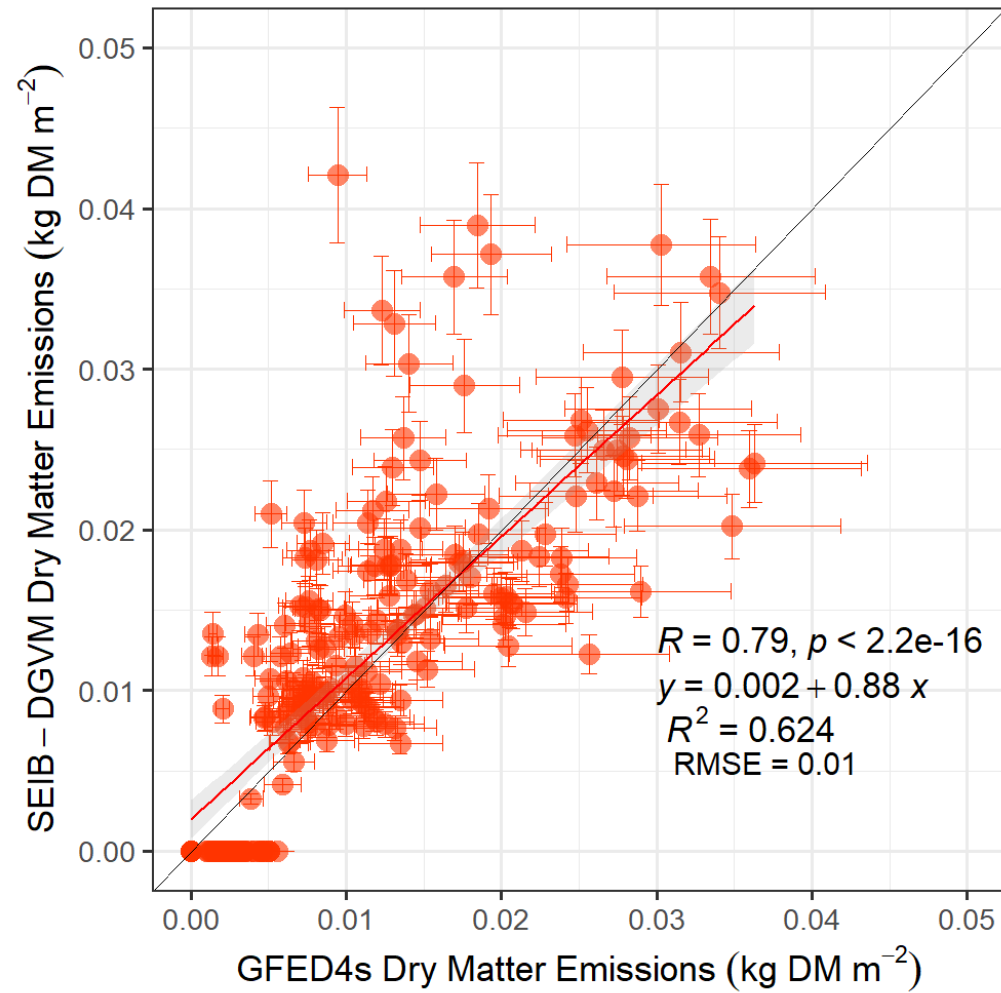


Figure S20. Latitude average spatial comparison of annual averaged simulated dry matter emission of SEIB-DGVM SPITFIRE and dry matter emission of GFED4s from 1997 to 2016.

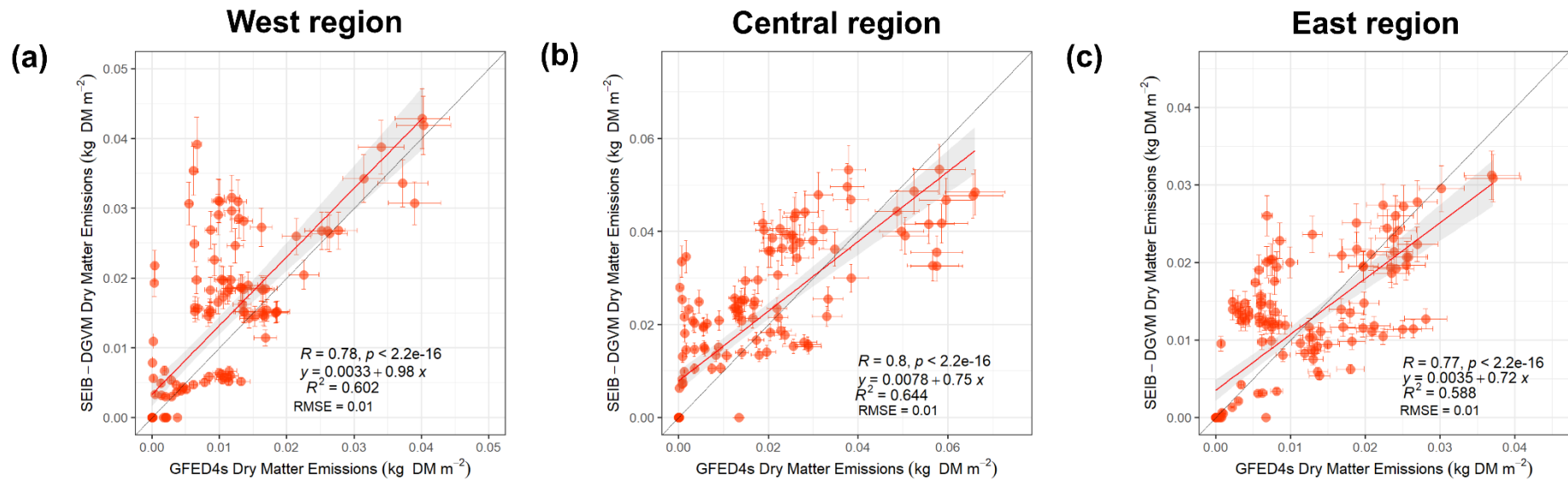


Figure S21. Latitude average spatial comparison of annual averaged (1997-2016) simulated burned fraction of SEIB-DGVM SPITFIRE and burned fraction of GFED4s in: **(a)** west region **(b)** central region, **(c)** east region

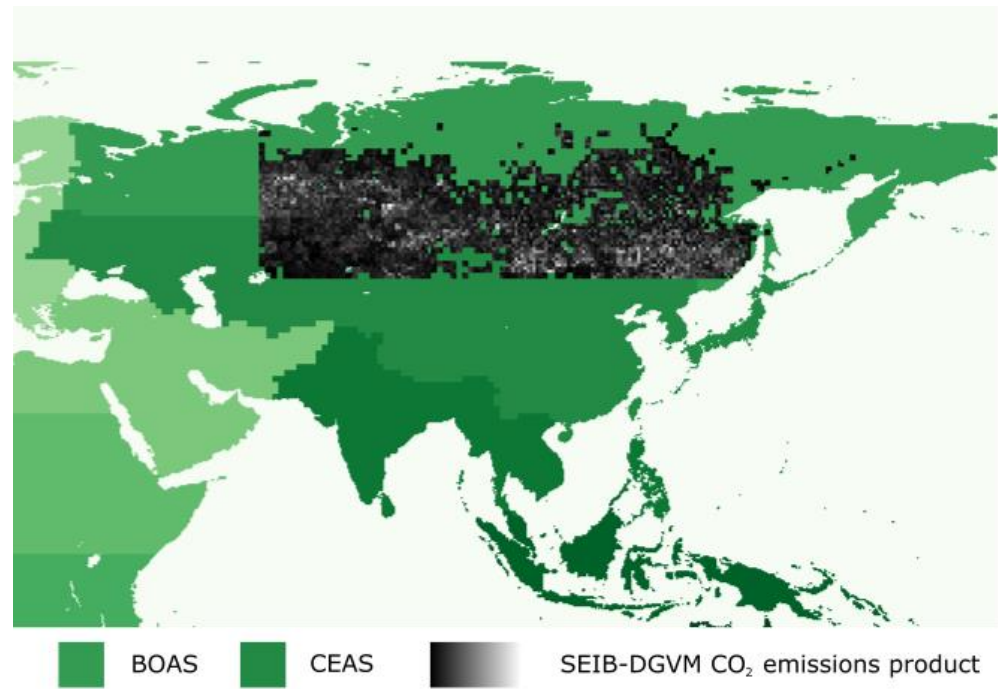


Figure S22. GFED basis region and SEIB-DGVM output area map comparison
BOAS: Boreal Asia. CEAS: Central Asia

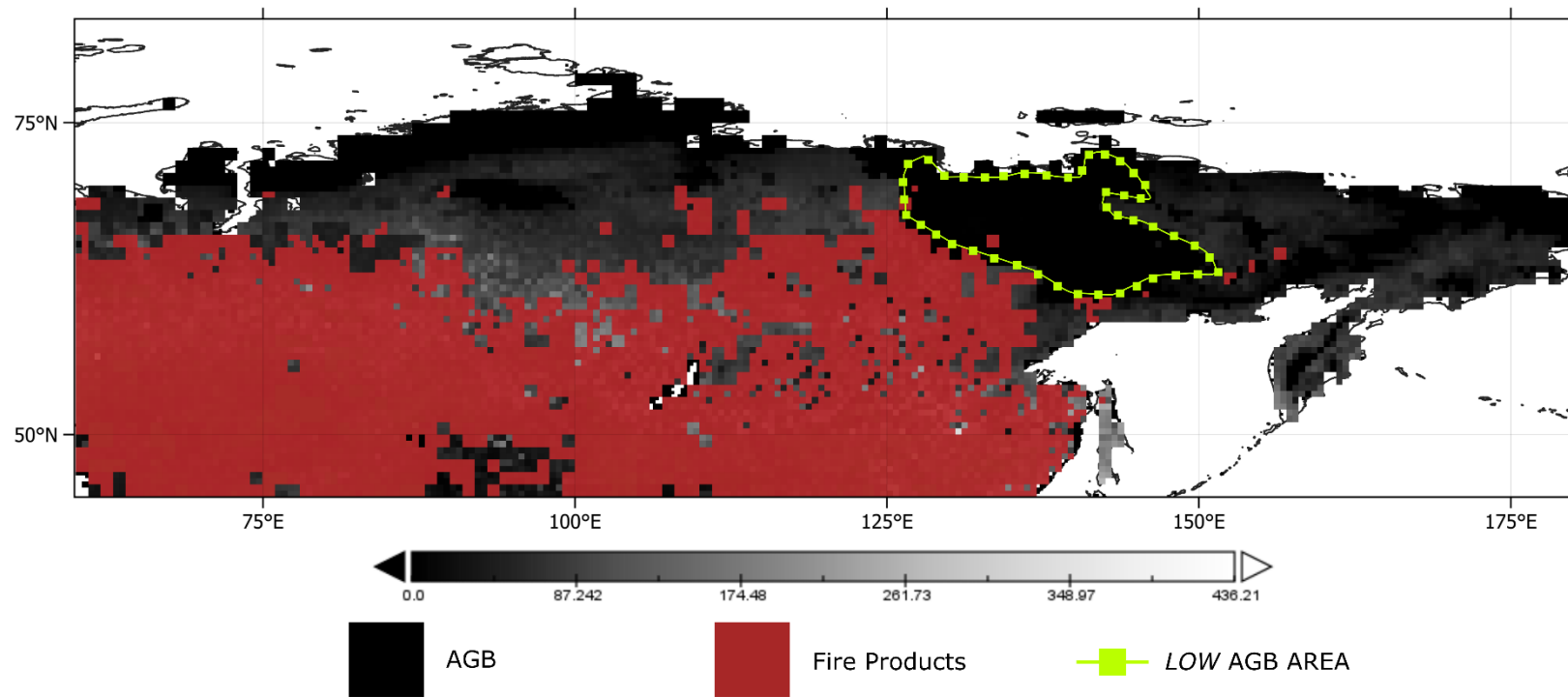


Figure S23. Spatial distribution comparison between annual averaged (1997-2016) of fire products (burned fraction, burned area, burned biomass) and aboveground biomass variable of SEIB-DGVM SPITFIRE

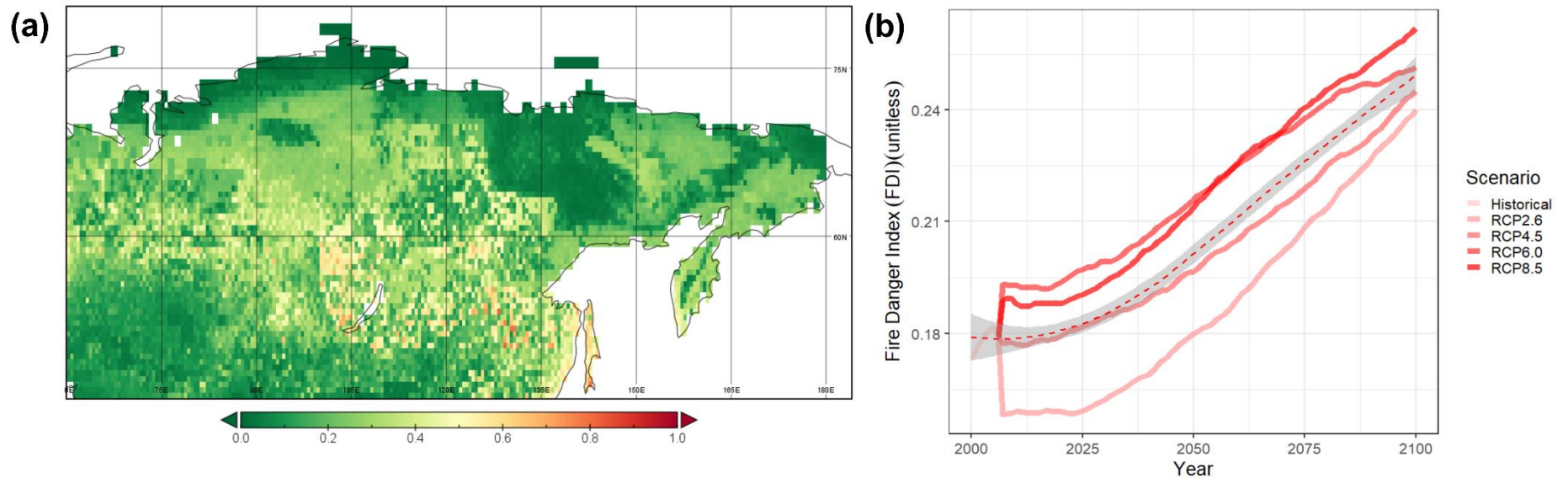


Figure S24. (a) Spatial distribution of annual averaged Fire Danger Index (FDI) of SEIB-DGVM SPITFIRE from 2000 to 2100. (b) Temporal variation of annual averaged Fire Danger Index (FDI) of SEIB-DGVM SPITFIRE from 2000 to 2100

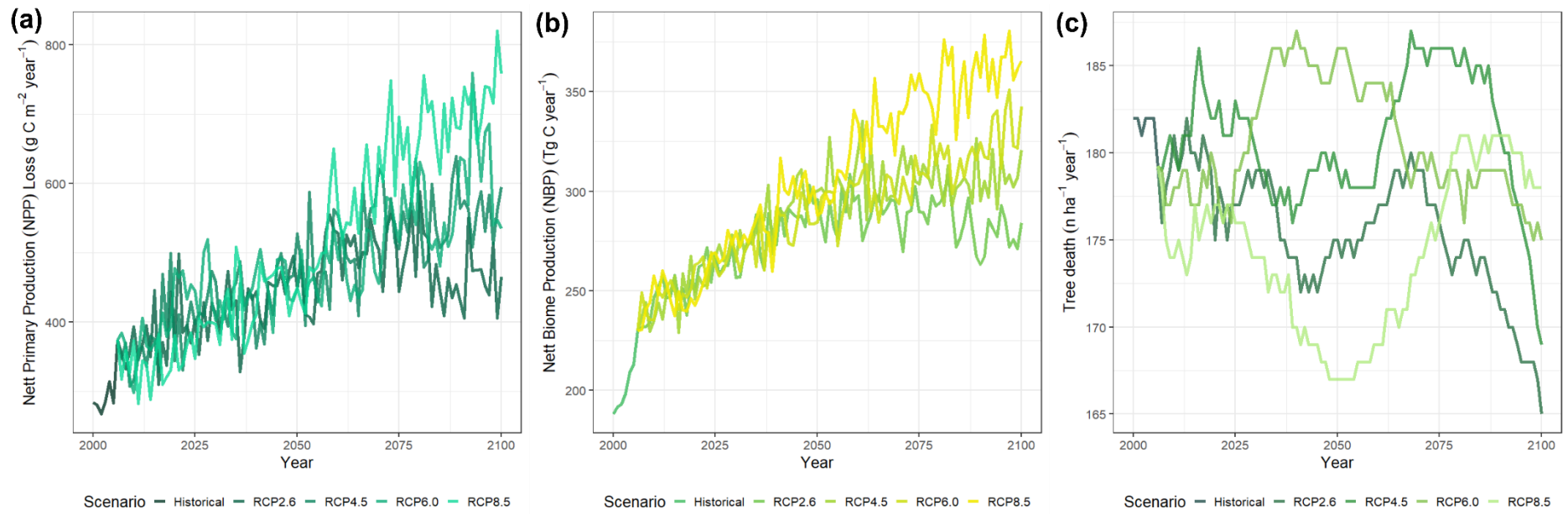


Figure S25. Temporal variation of simulated variables of SEIB-DGVM SPITFIRE in Siberia from 2000 to 2100: **(a)** NPP loss. **(b)** NBP. **(c)** Killed tree due to wildfire

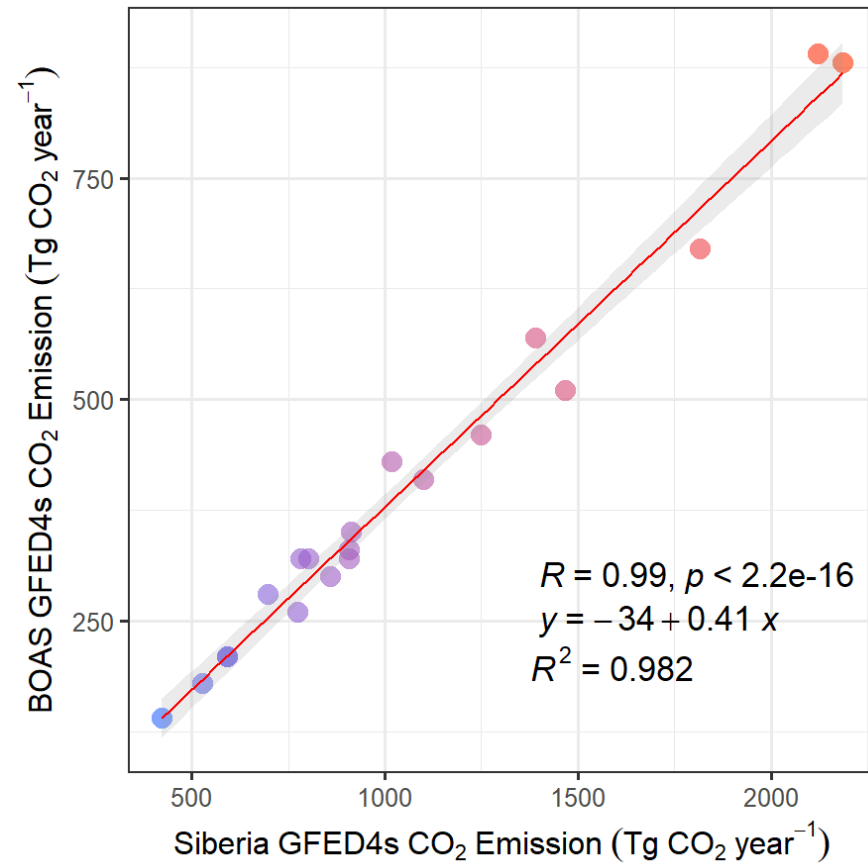


Figure S26. Comparison of annual averaged CO₂ emissions GFED4s in Siberia and Boreal Asia (BOAS) region from 1997 to 2016

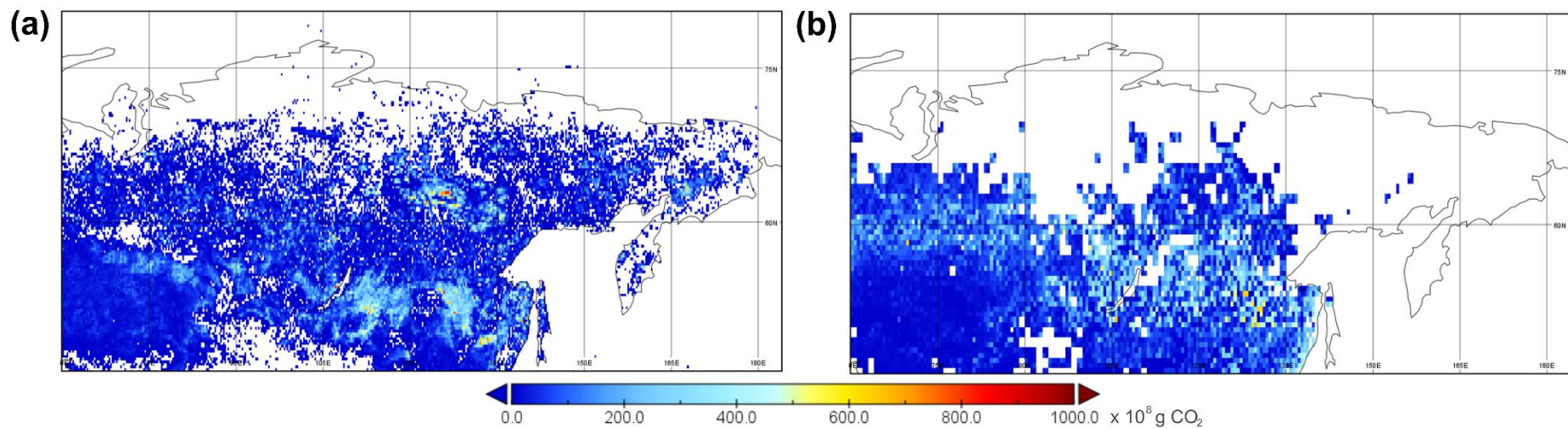


Figure S27. (a) Spatial distribution of annual averaged CO₂ emissions of GFED4s from 1997-2016. (b) Spatial distribution of annual averaged CO₂ emissions of SEIB-DGVM SPITFIRE from 1997-2016.

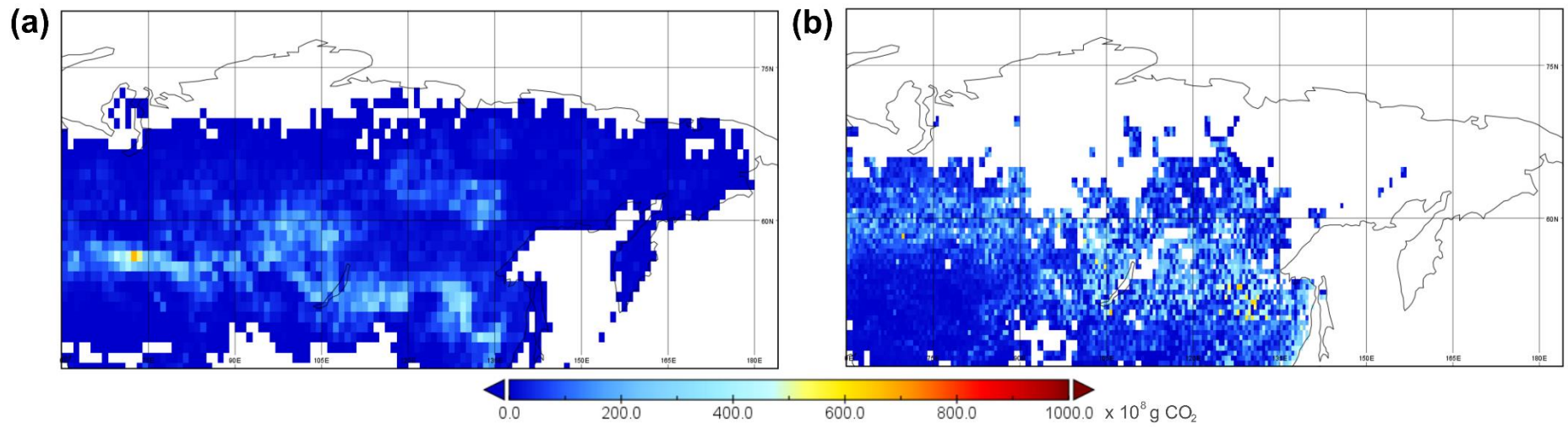


Figure S28. (a) Spatial distribution of annual averaged CO₂ emissions of GBEI from 2001 to 2020. (b) Spatial distribution of annual averaged CO₂ emissions of SEIB-DGVM SPITFIRE from 2001 to 2020.

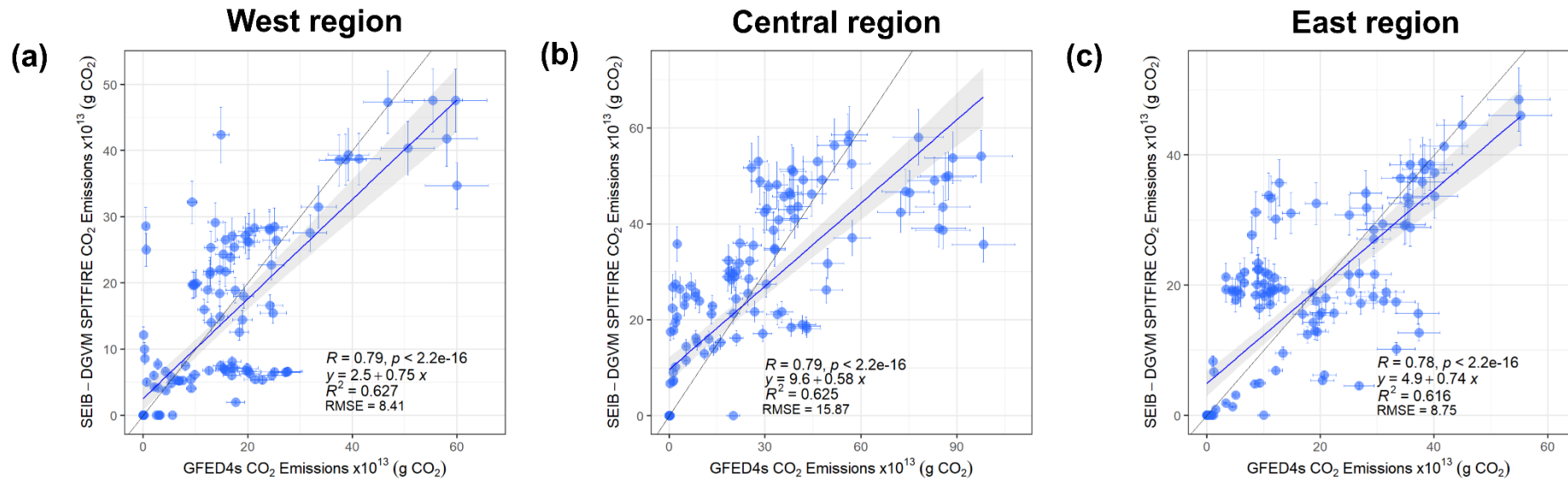


Figure S29. Latitude average spatial comparison of annual averaged (1997-2016) simulated CO₂ emissions of SEIB-DGVM SPITFIRE and CO₂ emissions of GFED4s in: **(a)** west region **(b)** central region, **(c)** east region

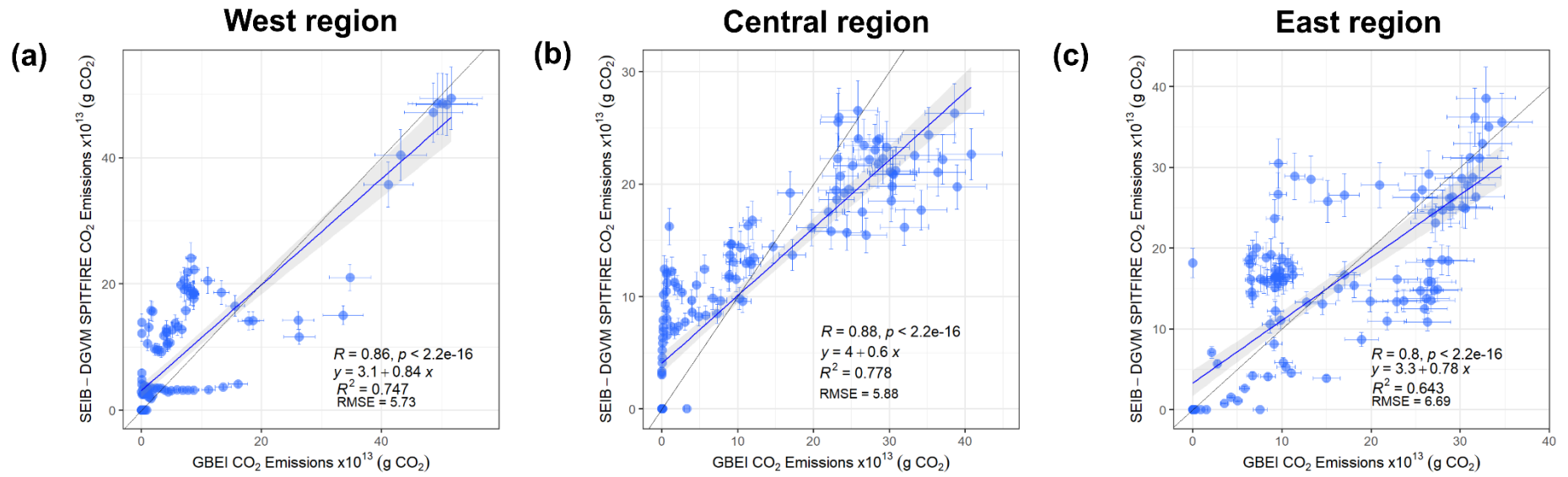


Figure S30. Latitude average spatial comparison of annual averaged (2001-2020) simulated CO₂ emissions of SEIB-DGVM SPITFIRE and CO₂ emissions of GBEI in: (a) west region (b) central region, (c) east region

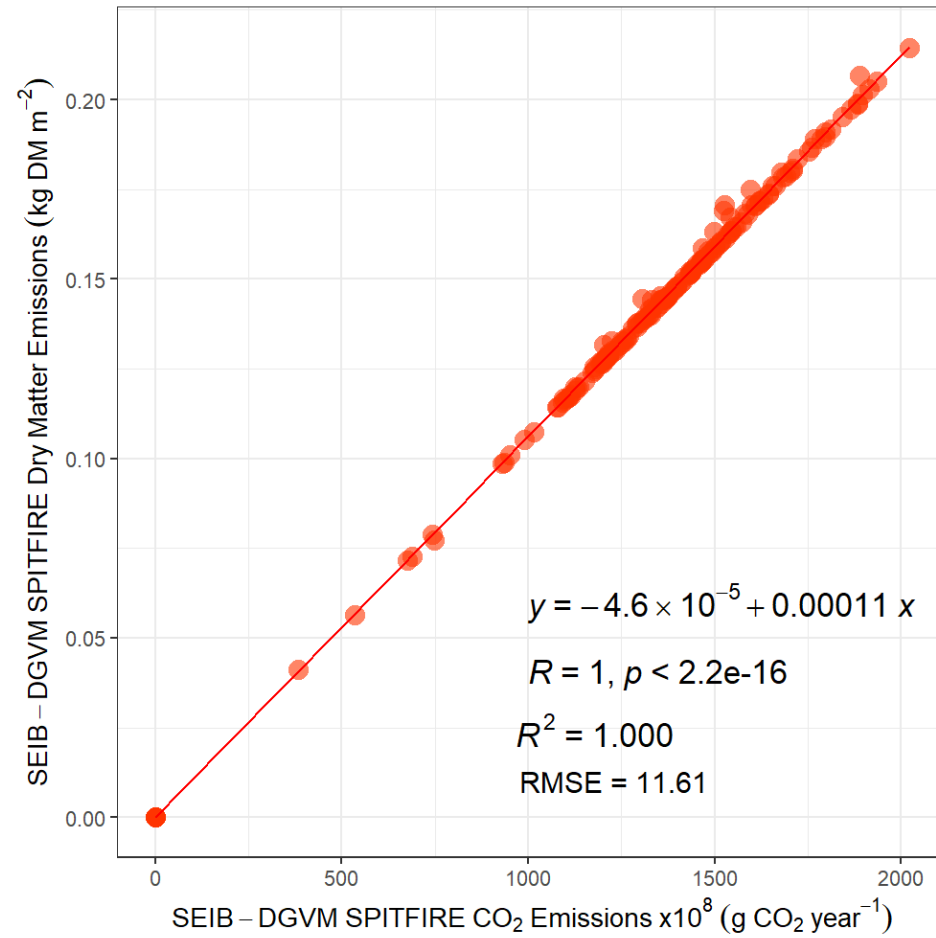


Figure S31. Comparison of annual averaged simulated dry matter and CO₂ emissions of SEIB-DGVM SPITFIRE from 1996 to 2100

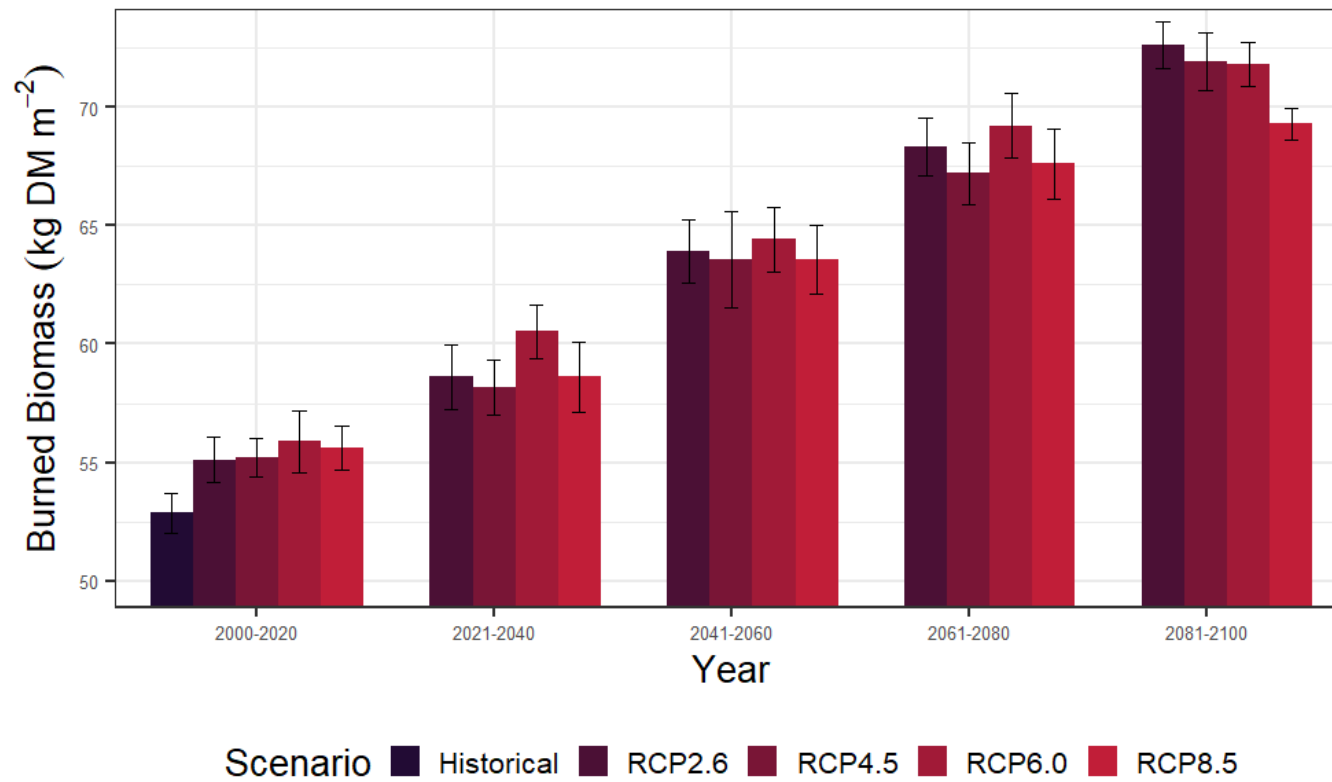


Figure S32. Temporal variation of projected burned biomass from 2000 to 2100 under different RCPs scenarios.

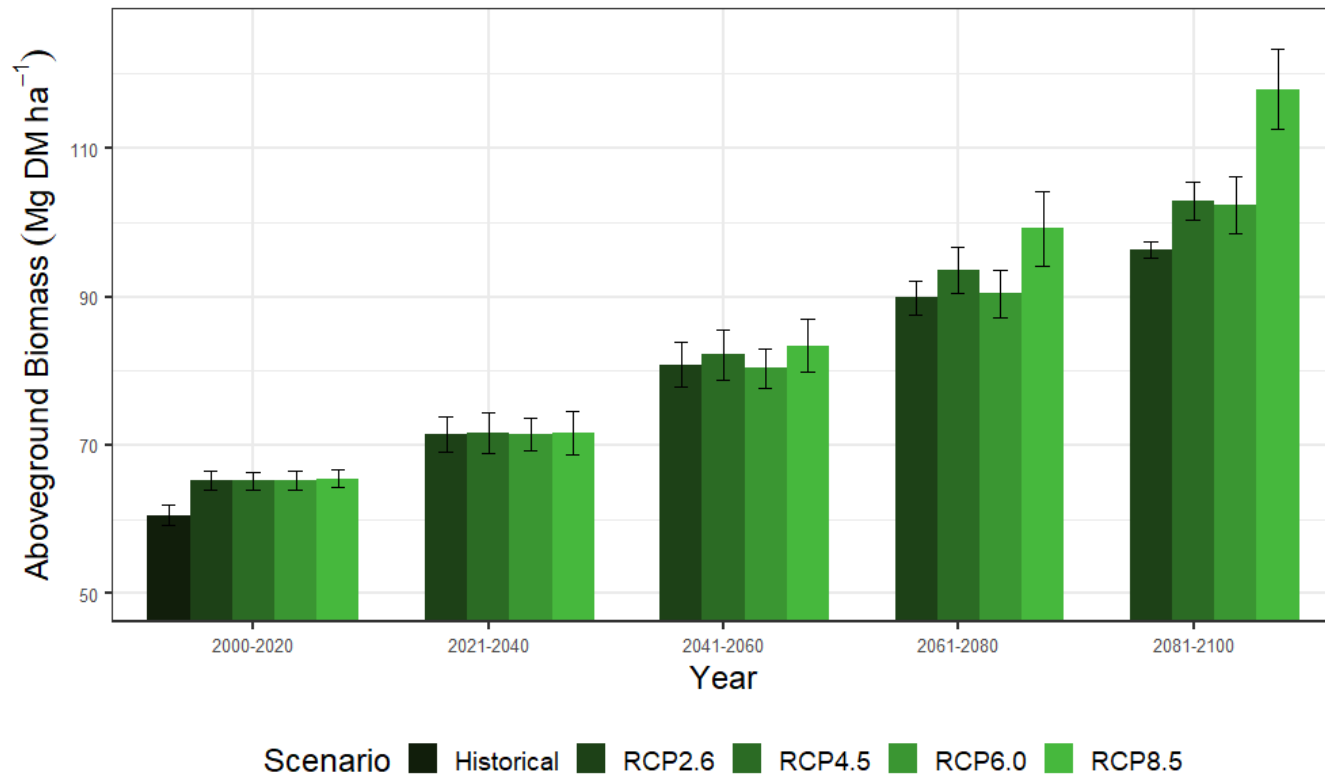


Figure S33. Temporal variation of projected aboveground biomass from 2000 to 2100 under different RCPs scenarios.

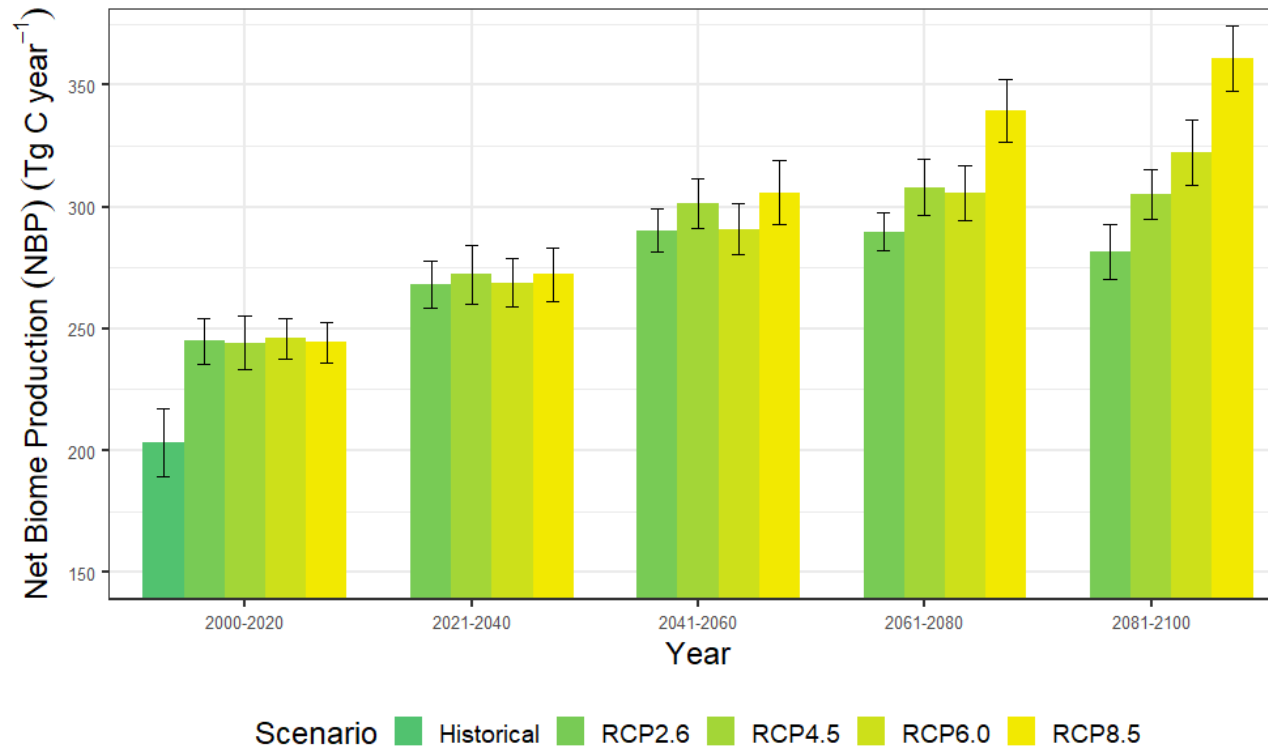


Figure S34. Temporal variation of projected Net Biome Production (NBP) from 2000 to 2100 under different RCPs scenarios. The standard deviation is obtained from the annual average data of each climate scenario.

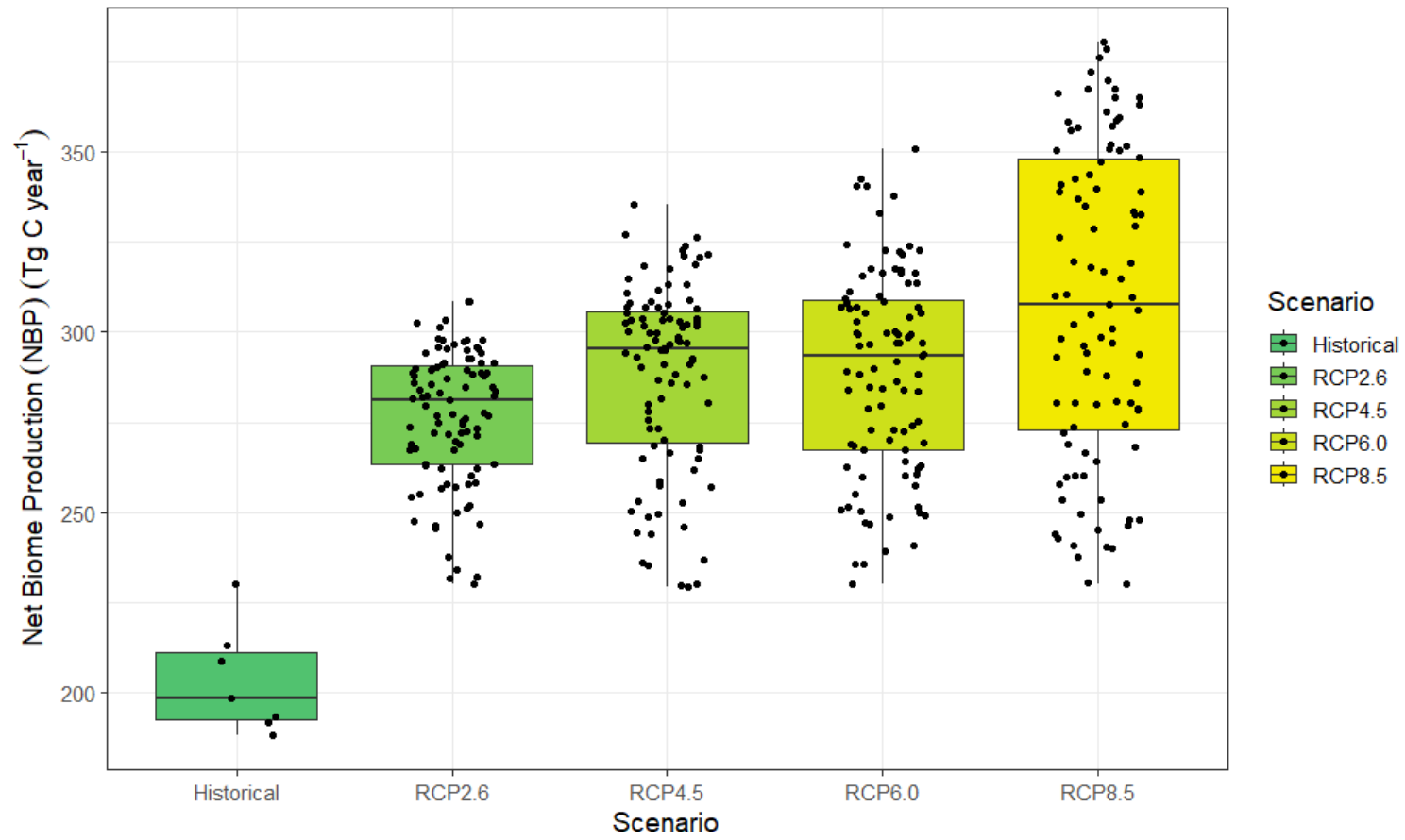


Figure S35. Comparison of annual averaged simulated NBP variables between different climate scenarios from 2000 to 2100.

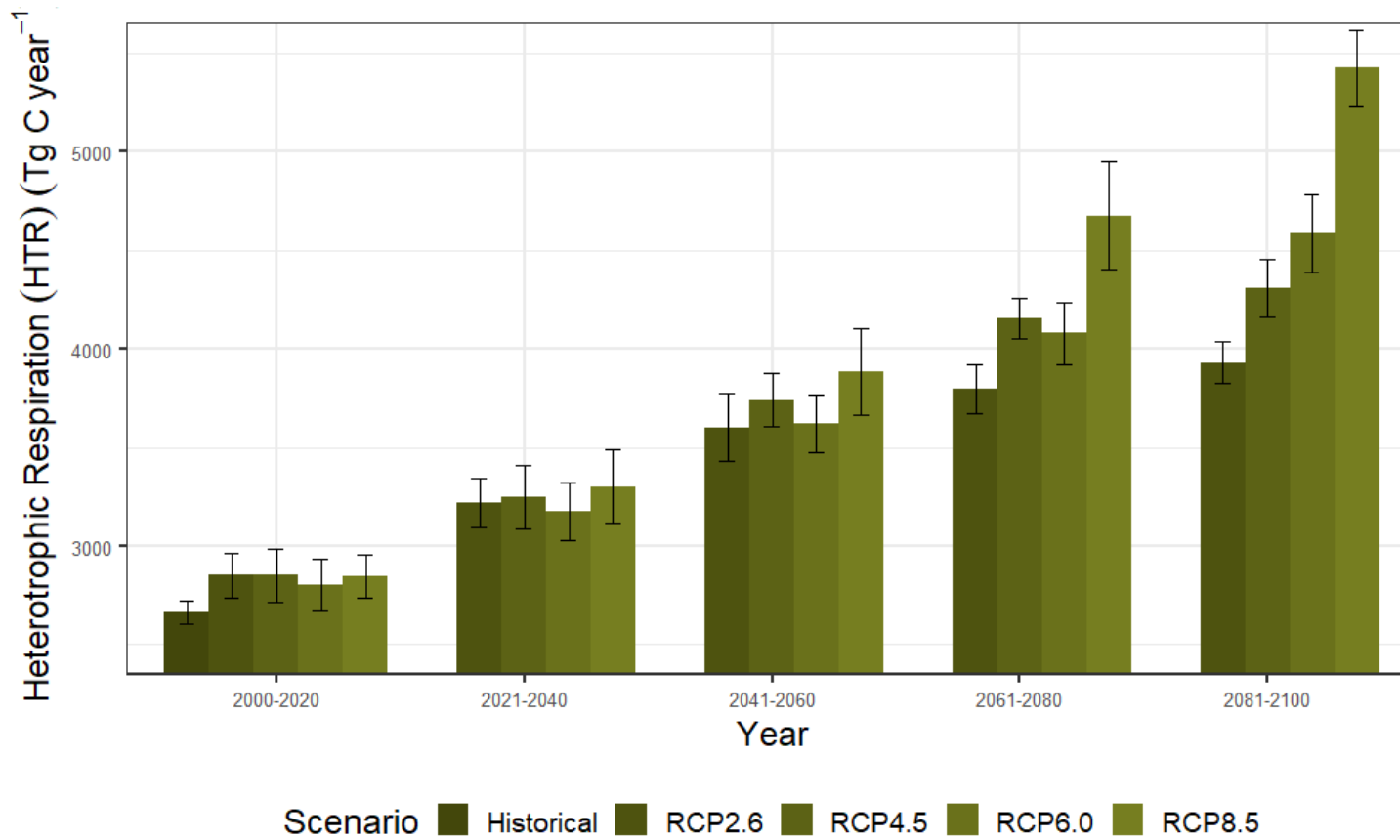


Figure S36. Temporal variation of projected Heterotrophic Respiration (HTR) from 2000 to 2100 under different RCPs scenarios. The standard deviation is obtained from the annual average data of each climate scenario.

Table S4. Twenty-year average NBP from 2000-2100 from model simulations in Siberia

Year	Historical	RCP8.5	RCP6.0	RCP4.5	RCP2.6
2000-2020	203.27 ± 13.78	244.41 ± 8.35	246.14 ± 8.31	244.17 ± 11.09	244.97 ± 9.26
2021-2040	NA	272.33 ± 10.98	268.85 ± 9.94	272.27 ± 12.06	268.23 ± 9.57
2041-2060	NA	305.86 ± 13.32	290.89 ± 10.27	301.17 ± 10.13	290.21 ± 8.80
2061-2080	NA	339.55 ± 13.00	305.65 ± 11.43	308.01 ± 11.62	289.69 ± 7.77
2081-2100	NA	360.90 ± 13.22	322.39 ± 13.27	305.22 ± 10.04	281.66 ± 11.39
Average	203.27 ± 13.78	304.61 ± 11.77	286.78 ± 10.64	286.17 ± 10.99	274.95 ± 9.36

Table S5. Twenty-year average HR from 2000-2100 from model simulations in Siberia

Year	Historical	RCP8.5	RCP6.0	RCP4.5	RCP2.6
2000-2020	2664.51 ± 59.17	2847.17 ± 111.36	2802.51 ± 130.57	2852.31 ± 135.54	2852.44 ± 114.02
2021-2040	NA	3303.00 ± 183.68	3176.25 ± 144.19	3248.85 ± 160.10	3218.30 ± 122.48
2041-2060	NA	3882.35 ± 218.50	3622.35 ± 147.67	3741.40 ± 137.27	3601.80 ± 171.54
2061-2080	NA	4674.90 ± 275.01	4078.75 ± 158.01	4154.75 ± 100.30	3796.20 ± 126.33
2081-2100	NA	5423.50 ± 191.02	4583.85 ± 196.23	4307.30 ± 147.47	3930.50 ± 106.95

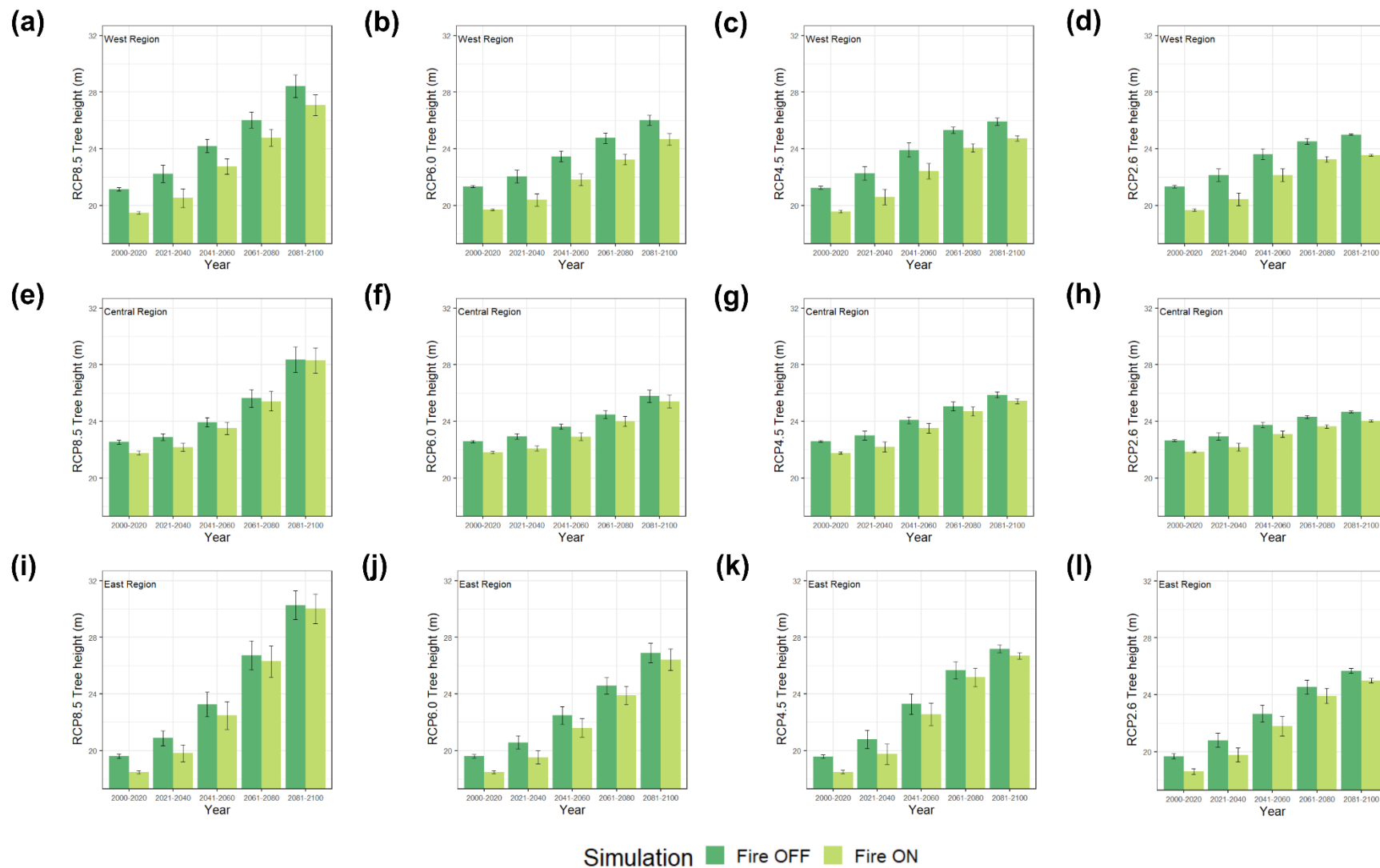


Figure S37. Twenty-year average of tree height variables under fire on and fire off simulation and under RCPs climate scenarios from 2000-2100: **(a-d)** West region, **(e-h)** Central region, dan **(i-l)** East region of Siberia

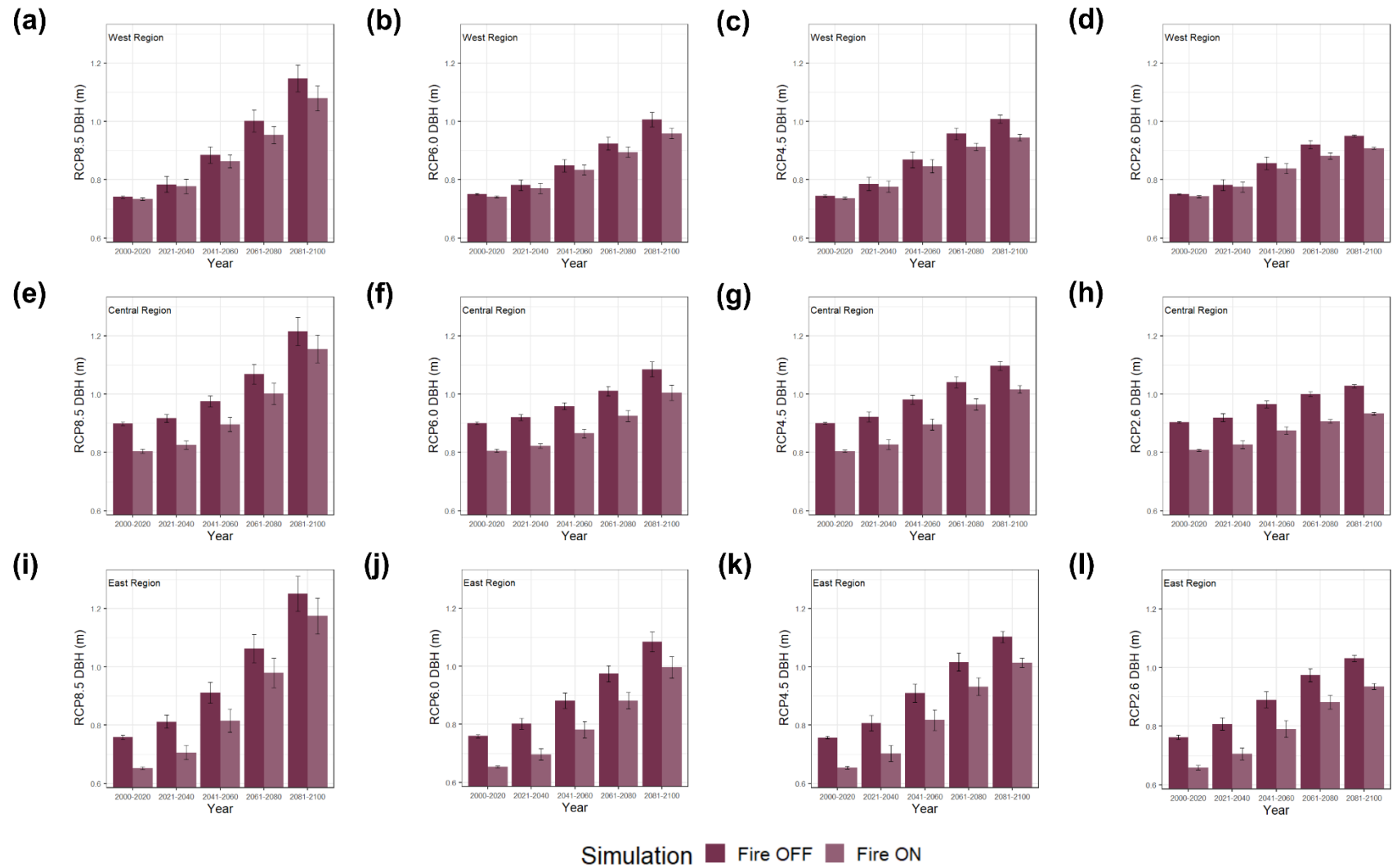


Figure S38. Twenty-year average of DBH variables under fire on and fire off simulation and under RCPs climate scenarios from 2000-2100: (a-d) West region, (e-h) Central region, dan (i-l) East region of Siberia

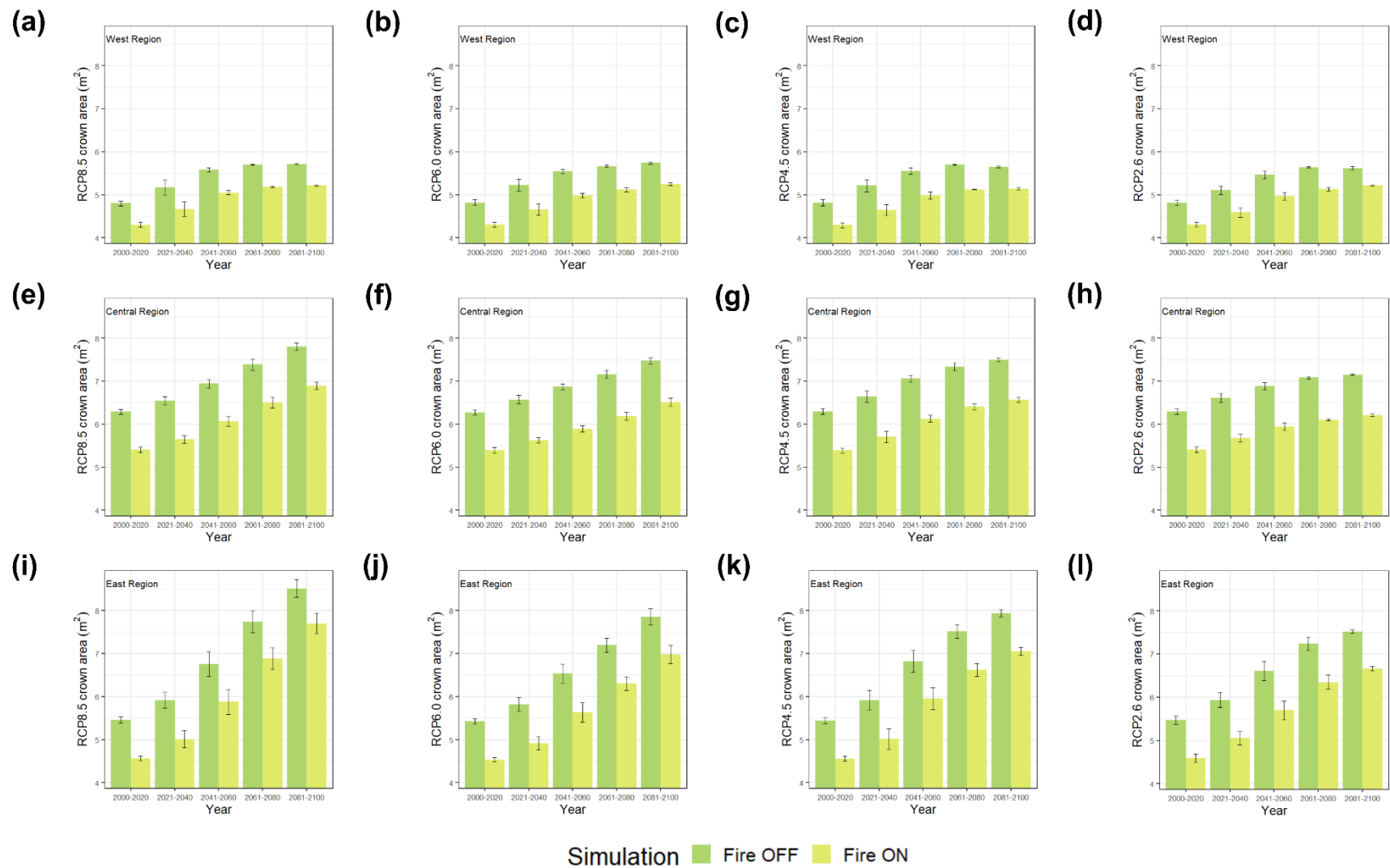


Figure S39. Twenty-year average of crown area variables under fire on and fire off simulation and under RCPs climate scenarios from 2000-2100: (a-d) West region, (e-h) Central region, dan (i-l) East region of Siberia

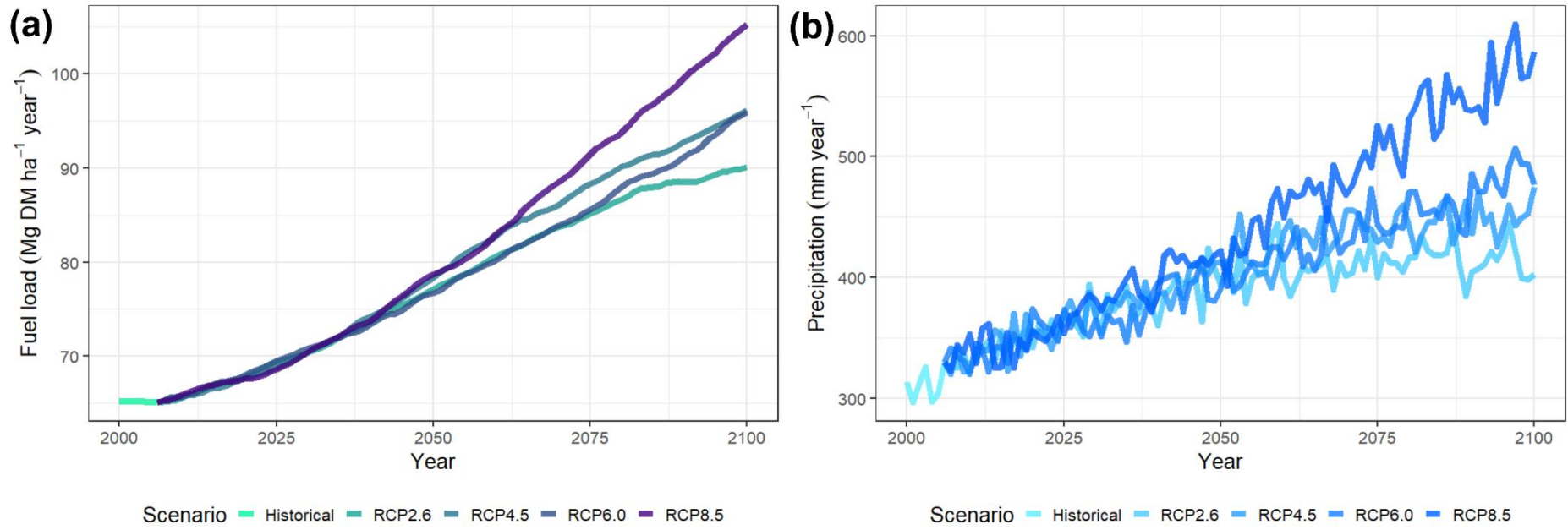


Figure S40. (a) Temporal variation of simulated SEIB-DGVM SPITFIRE fuel load in Siberia under different RCPs climate scenarios from 2000 to 2100. (b) Temporal variation of precipitation under different RCPs climate scenarios in Siberia from 2000 to 2100

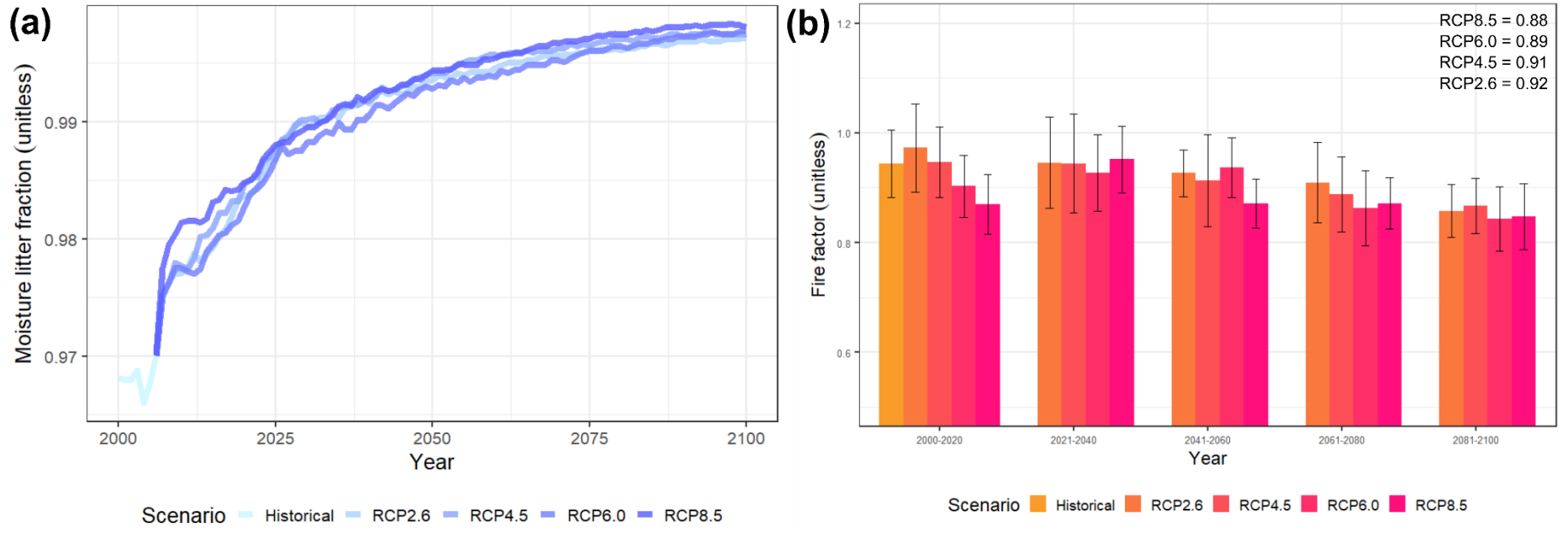


Figure S41. (a) Temporal variation of simulated SEIB-DGVM SPITFIRE moisture litter fraction in Siberia under different RCPs climate scenarios from 2000 to 2100. (b) Temporal variation of fire factor under different RCPs climate scenarios in Siberia from 2000 to 2100

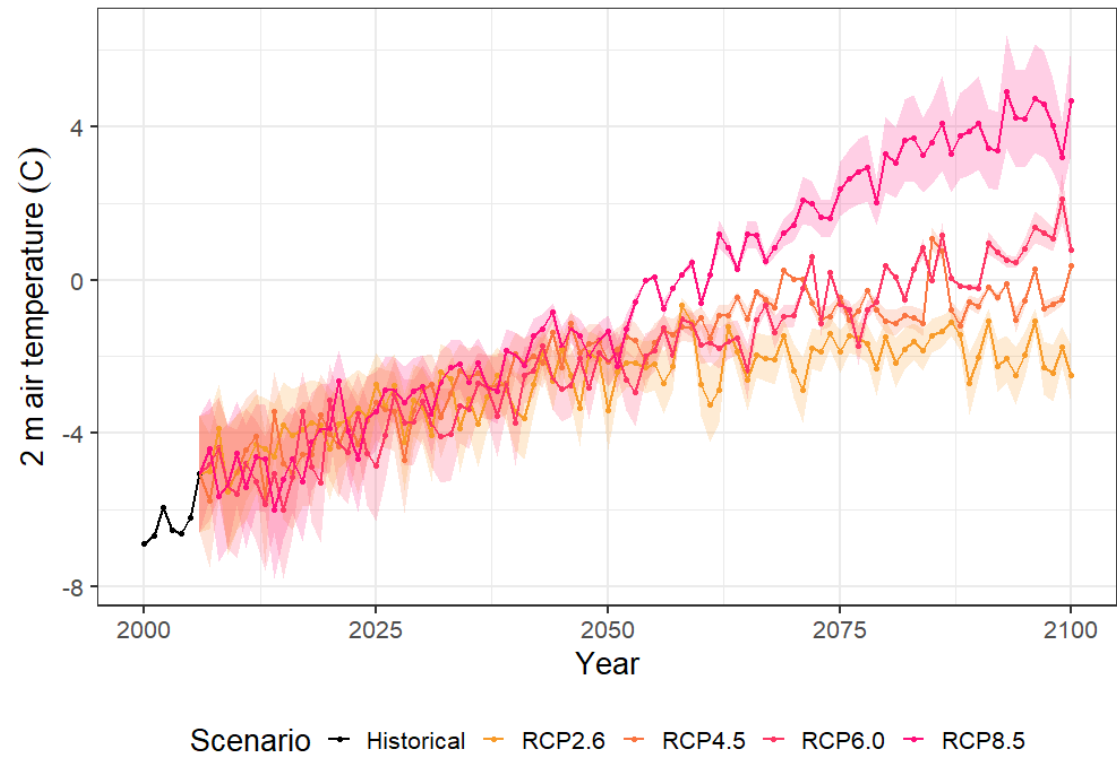
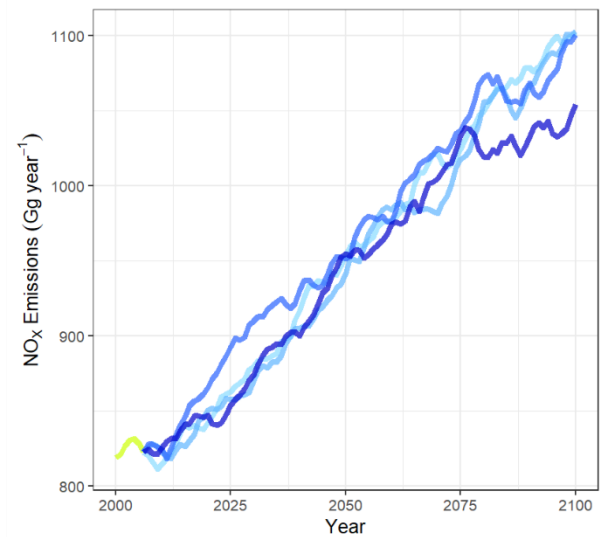
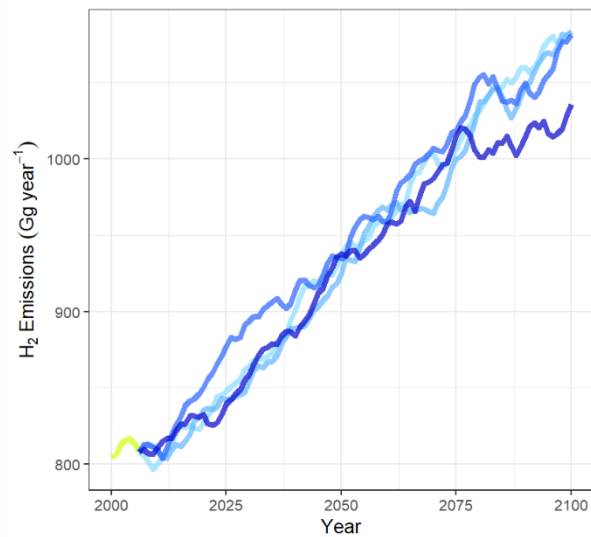
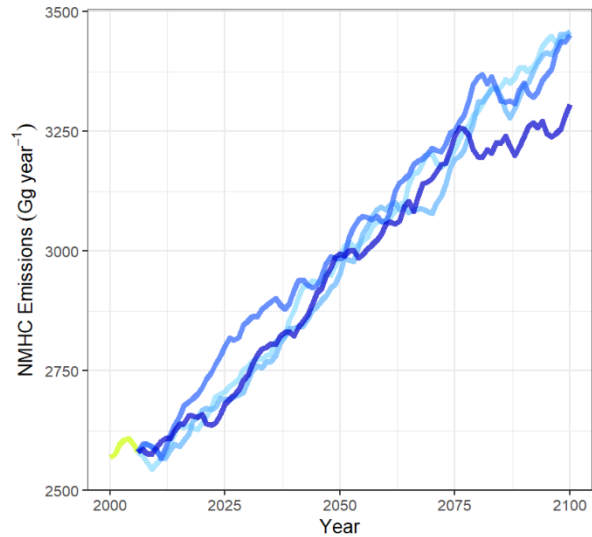
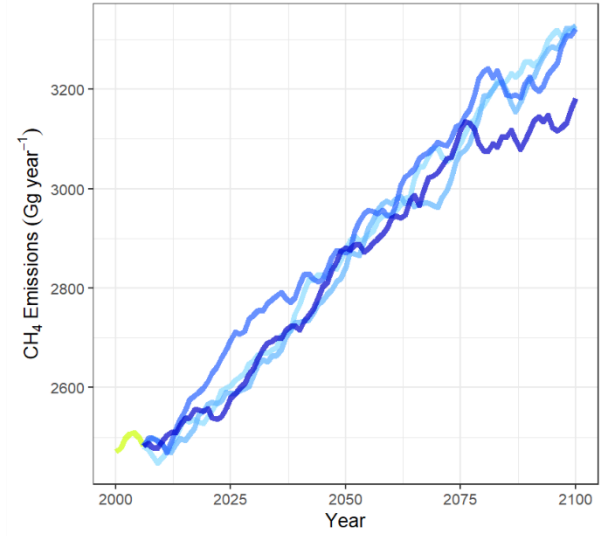
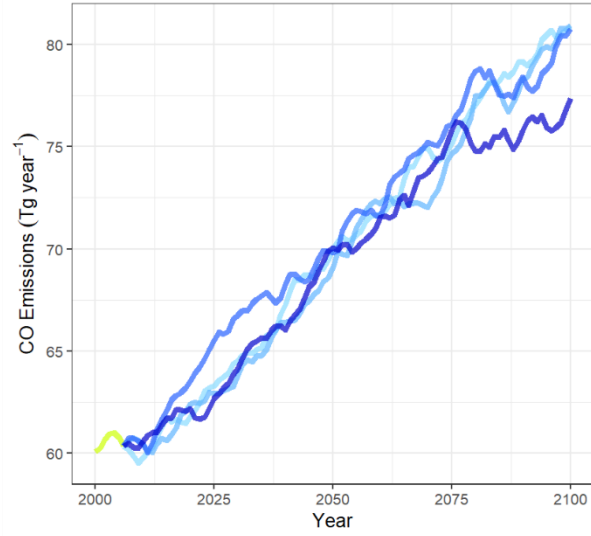
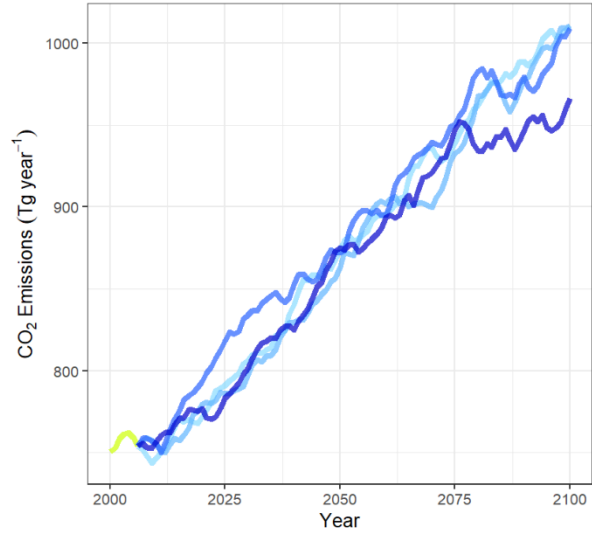
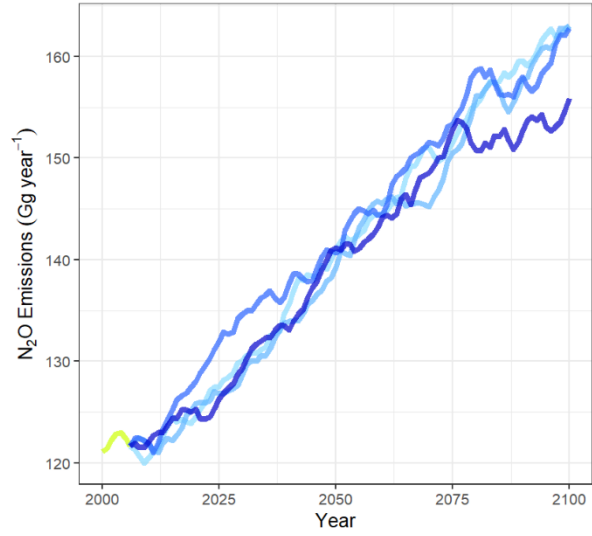
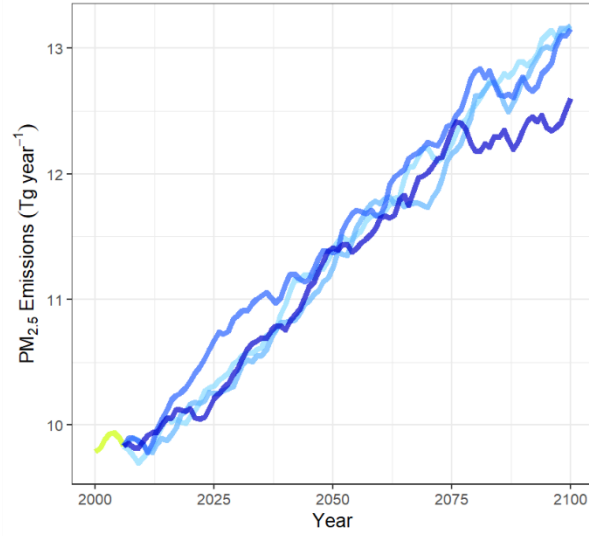


Figure S42. Temporal variation of average 2 m air temperature in Siberia under different RCPs climate scenarios from 2000 to 2100

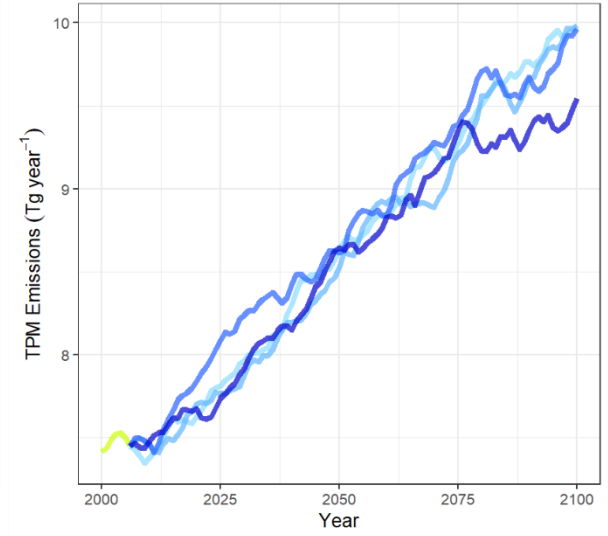




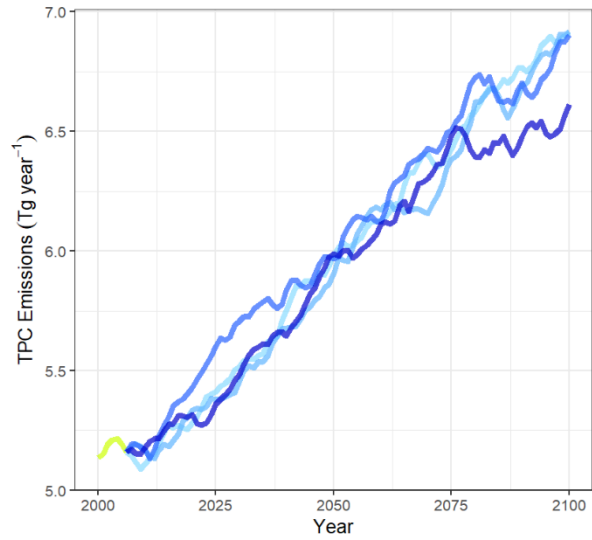
Scenario Historical RCP2.6 RCP4.5 RCP6.0 RCP8.5



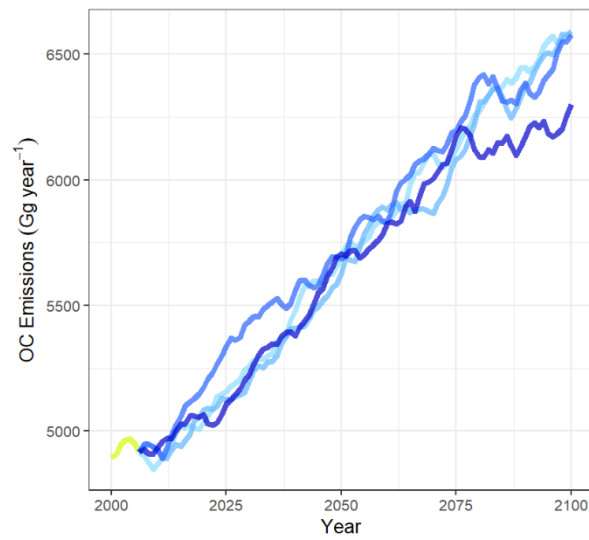
Scenario Historical RCP2.6 RCP4.5 RCP6.0 RCP8.5



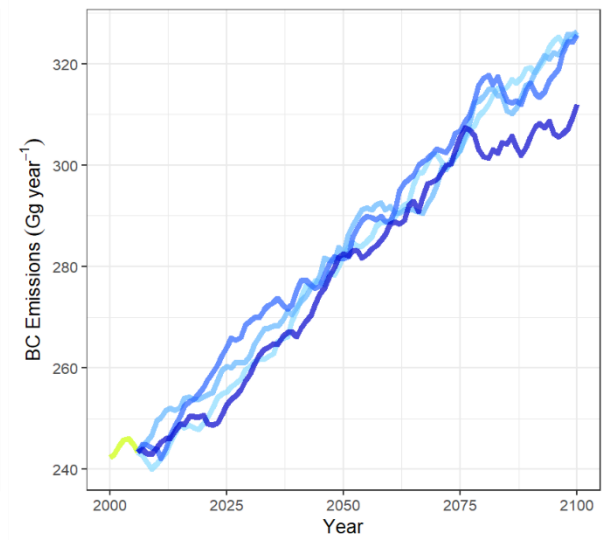
Scenario Historical RCP2.6 RCP4.5 RCP6.0 RCP8.5



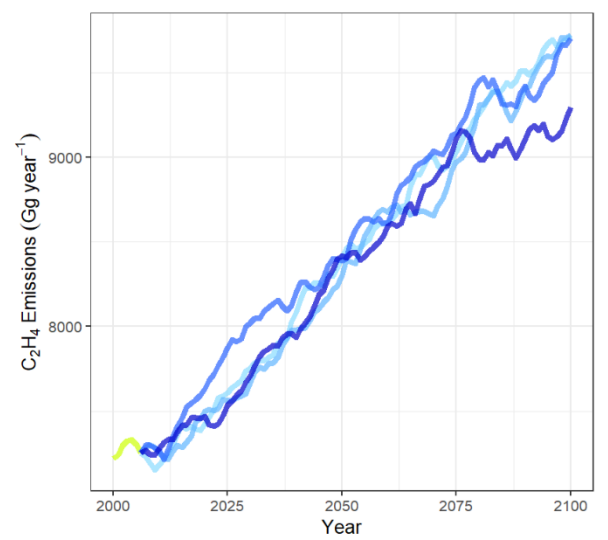
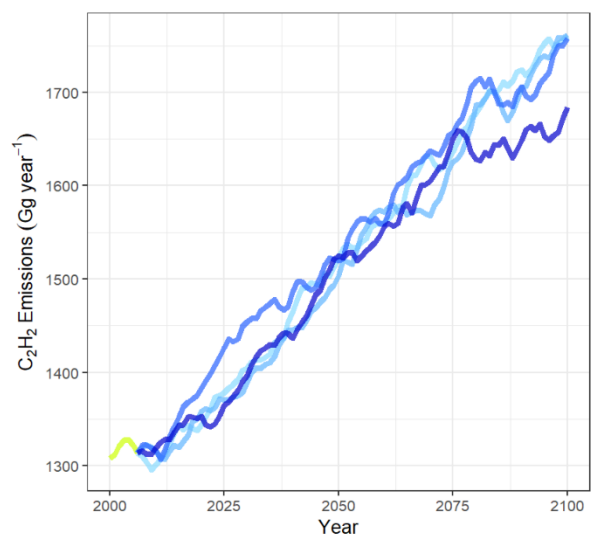
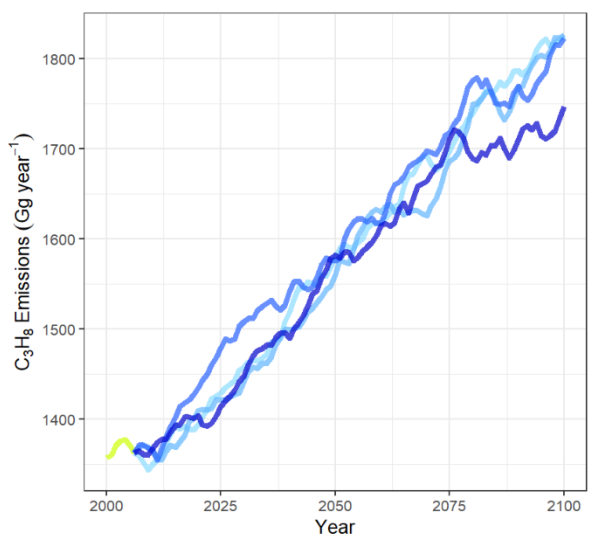
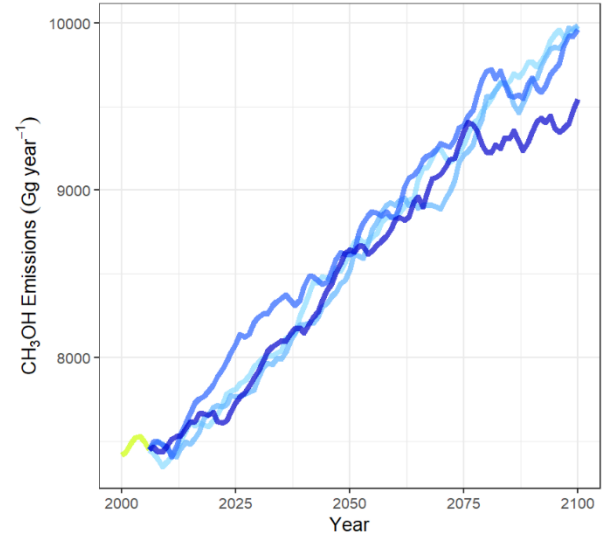
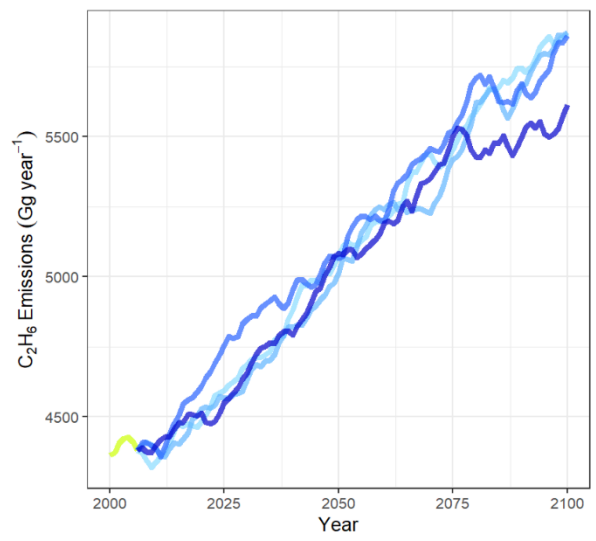
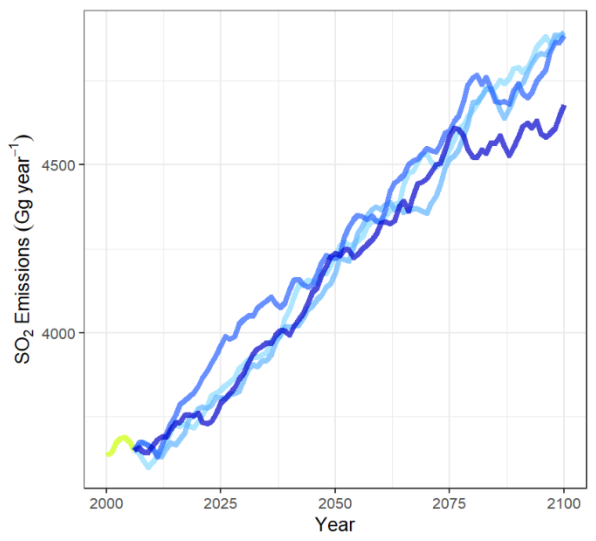
Scenario Historical RCP2.6 RCP4.5 RCP6.0 RCP8.5

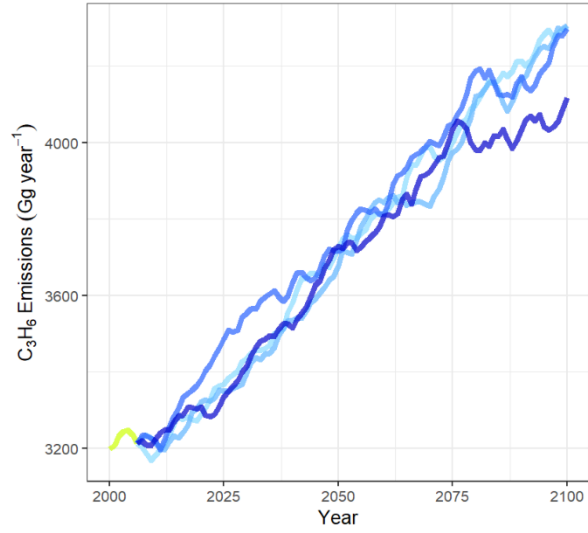


Scenario Historical RCP2.6 RCP4.5 RCP6.0 RCP8.5

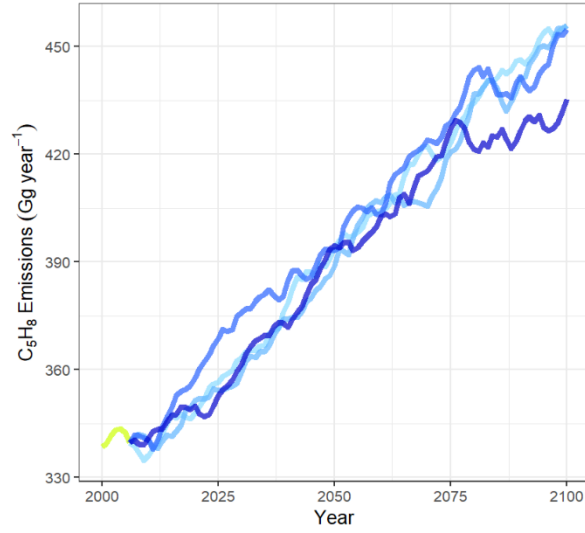


Scenario Historical RCP2.6 RCP4.5 RCP6.0 RCP8.5

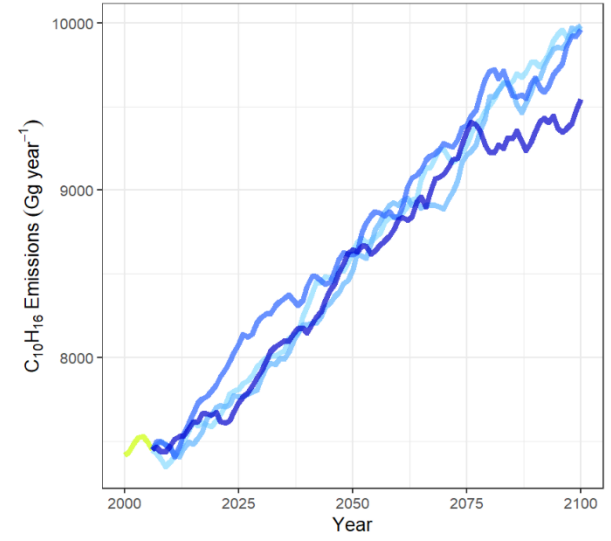




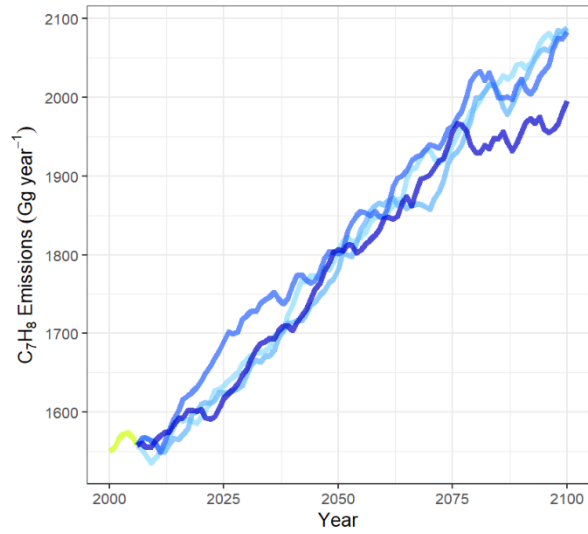
Scenario Historical RCP2.6 RCP4.5 RCP6.0 RCP8.5



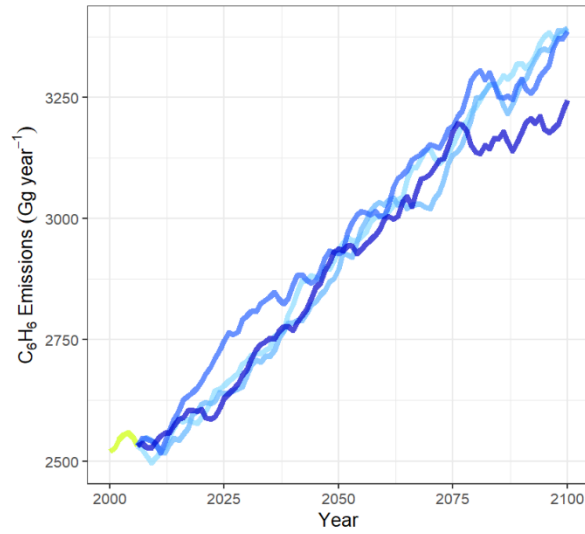
Scenario Historical RCP2.6 RCP4.5 RCP6.0 RCP8.5



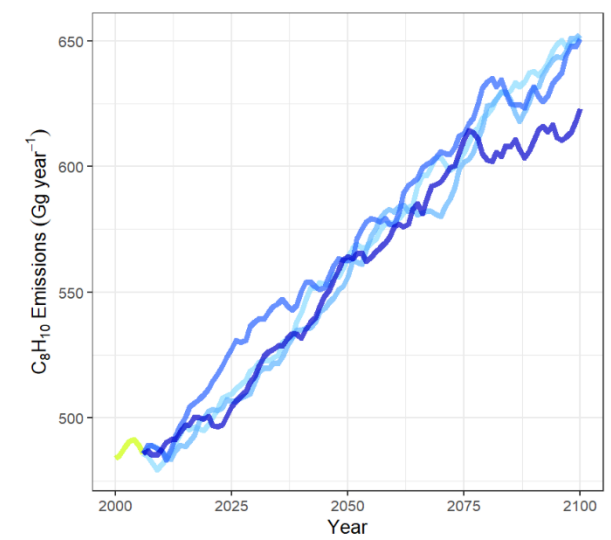
Scenario Historical RCP2.6 RCP4.5 RCP6.0 RCP8.5



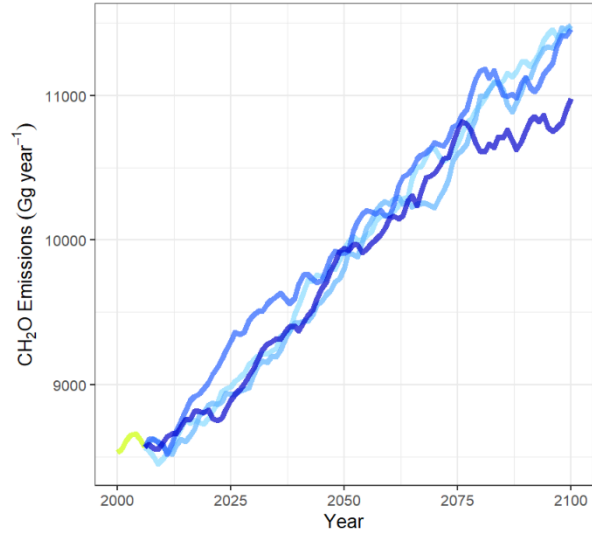
Scenario Historical RCP2.6 RCP4.5 RCP6.0 RCP8.5



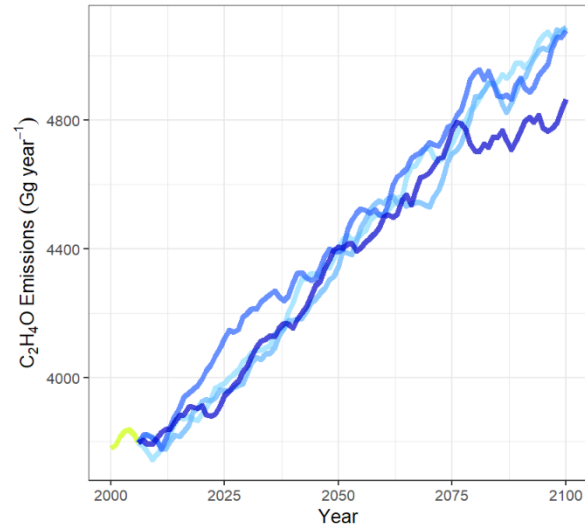
Scenario Historical RCP2.6 RCP4.5 RCP6.0 RCP8.5



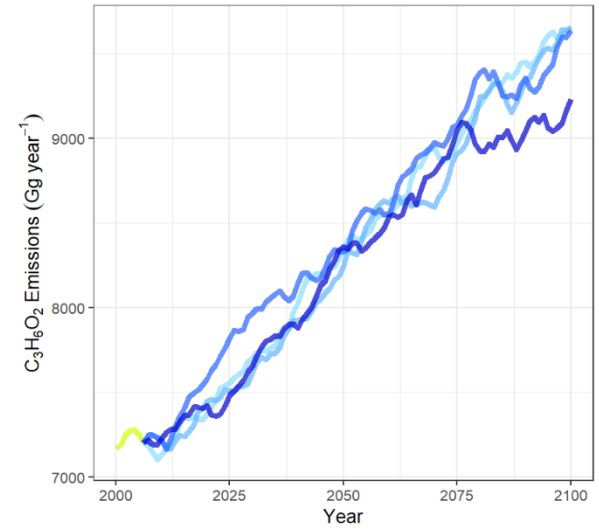
Scenario Historical RCP2.6 RCP4.5 RCP6.0 RCP8.5



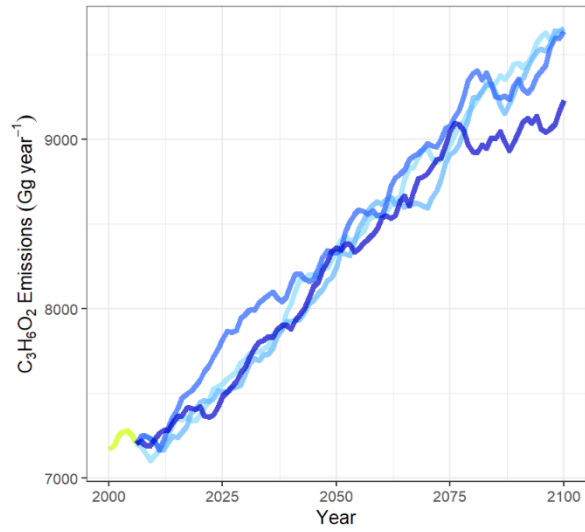
Scenario Historical RCP2.6 RCP4.5 RCP6.0 RCP8.5



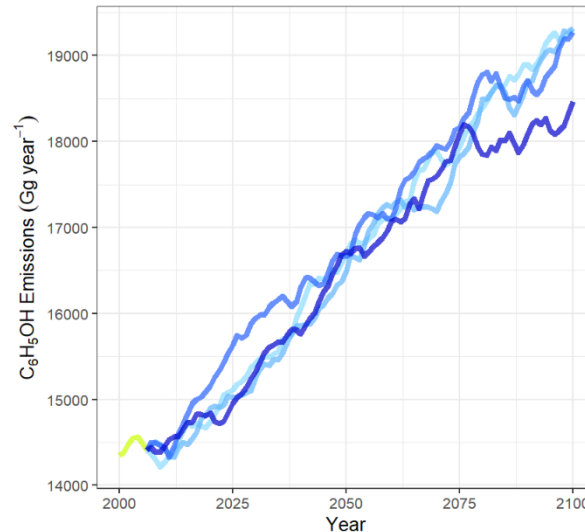
Scenario Historical RCP2.6 RCP4.5 RCP6.0 RCP8.5



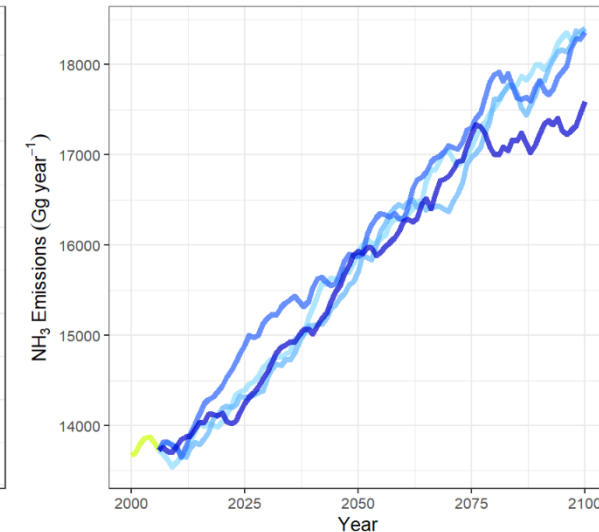
Scenario Historical RCP2.6 RCP4.5 RCP6.0 RCP8.5



Scenario Historical RCP2.6 RCP4.5 RCP6.0 RCP8.5



Scenario Historical RCP2.6 RCP4.5 RCP6.0 RCP8.5



Scenario Historical RCP2.6 RCP4.5 RCP6.0 RCP8.5

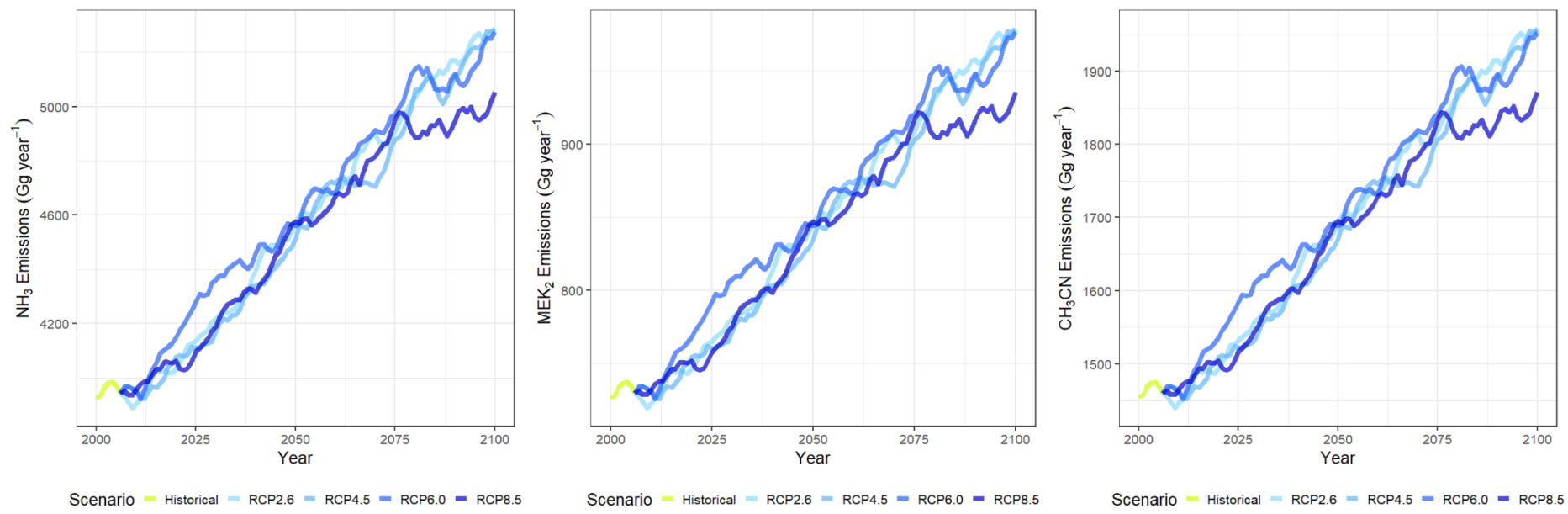


Figure S43. Projected annual emissions of 33 gaseous species from forest fires in Siberia (2000-2100)

Table S6. Projected emissions of 28 gaseous species from forest fires in Siberia from 2000 to 2100 \pm 2 standard deviation.

sp.	Year	2000 - 2020	2021 - 2040	2041 - 2060	2061 - 2080	2081 - 2100
Gg CH ₄ year ⁻¹	Historical	2493.47 \pm 15.23	NA	NA	NA	NA
	RCP8.5	2517.75 \pm 29.76	2640.33 \pm 67.50	2851.95 \pm 60.22	3038.45 \pm 64.50	3117.90 \pm 27.88
	RCP6.0	2532.65 \pm 48.92	2734.43 \pm 52.75	2890.50 \pm 55.16	3096.40 \pm 69.57	3232.36 \pm 42.66
	RCP4.5	2504.09 \pm 29.04	2636.79 \pm 54.37	2852.33 \pm 82.49	3022.48 \pm 68.91	3238.76 \pm 55.07
	RCP2.6	2500.19 \pm 33.52	2654.75 \pm 57.36	2875.34 \pm 50.33	3063.99 \pm 60.75	3259.20 \pm 45.08
Gg NMHC year ⁻¹	Historical	2591.25 \pm 15.83	NA	NA	NA	NA
	RCP8.5	2616.47 \pm 30.93	2743.87 \pm 70.16	2963.81 \pm 62.60	3157.60 \pm 67.03	3240.17 \pm 28.99
	RCP6.0	2631.97 \pm 50.86	2841.67 \pm 54.82	3003.87 \pm 57.35	3217.82 \pm 72.30	3359.12 \pm 44.34
	RCP4.5	2602.31 \pm 30.18	2740.20 \pm 56.50	2964.18 \pm 85.73	3141.01 \pm 71.61	3365.78 \pm 57.25
	RCP2.6	2598.25 \pm 34.84	2758.86 \pm 59.59	2988.11 \pm 52.29	3184.15 \pm 63.12	3387.01 \pm 46.84
Gg H ₂ year ⁻¹	Historical	811.60 \pm 4.98	NA	NA	NA	NA
	RCP8.5	819.49 \pm 9.69	859.41 \pm 21.97	928.27 \pm 19.59	988.98 \pm 21.00	1014.85 \pm 9.07
	RCP6.0	824.33 \pm 15.93	890.04 \pm 17.16	940.83 \pm 17.94	1007.85 \pm 22.65	1052.10 \pm 13.88
	RCP4.5	815.04 \pm 9.45	858.25 \pm 17.69	928.39 \pm 26.84	983.78 \pm 22.44	1054.18 \pm 17.92
	RCP2.6	813.77 \pm 10.91	864.08 \pm 18.67	935.89 \pm 16.38	997.29 \pm 19.78	1060.82 \pm 14.66
Gg NO _x year ⁻¹	Historical	826.23 \pm 5.06	NA	NA	NA	NA
	RCP8.5	834.29 \pm 9.86	874.93 \pm 22.39	945.06 \pm 19.97	1006.86 \pm 21.39	1033.19 \pm 9.22
	RCP6.0	839.24 \pm 16.22	906.12 \pm 17.48	957.83 \pm 18.28	1026.06 \pm 23.05	1071.11 \pm 14.15
	RCP4.5	829.77 \pm 9.63	873.76 \pm 18.01	945.18 \pm 27.34	1001.56 \pm 22.84	1073.24 \pm 18.26
	RCP2.6	828.49 \pm 11.11	879.71 \pm 19.01	952.81 \pm 16.68	1015.31 \pm 20.14	1080.00 \pm 14.95
Gg N ₂ O year ⁻¹	Historical	122.17 \pm 0.76	NA	NA	NA	NA
	RCP8.5	123.38 \pm 1.45	129.38 \pm 3.32	139.77 \pm 2.96	148.94 \pm 3.17	152.81 \pm 1.36
	RCP6.0	124.11 \pm 2.39	134.01 \pm 2.61	141.66 \pm 2.71	151.77 \pm 3.41	158.43 \pm 2.10
	RCP4.5	122.71 \pm 1.43	129.23 \pm 2.67	139.79 \pm 4.05	148.14 \pm 3.38	158.72 \pm 2.69
	RCP2.6	122.52 \pm 1.65	130.09 \pm 2.80	140.93 \pm 2.48	150.18 \pm 2.97	159.74 \pm 2.22

sp.	Year	2000 - 2020	2021 - 2040	2041 - 2060	2061 - 2080	2081 - 2100
Gg OC year ⁻¹	Historical	4938.03 ± 30.25	NA	NA	NA	NA
	RCP8.5	4986.12 ± 58.95	5228.90 ± 133.69	5647.99 ± 119.28	6017.33 ± 127.76	6174.67 ± 55.21
	RCP6.0	5015.62 ± 96.91	5415.27 ± 104.47	5724.37 ± 109.25	6132.08 ± 137.76	6401.33 ± 84.51
	RCP4.5	4959.11 ± 57.49	5221.89 ± 107.65	5648.72 ± 163.36	5985.69 ± 136.45	6414.01 ± 109.07
	RCP2.6	4951.38 ± 66.41	5257.44 ± 113.59	5694.32 ± 99.65	6067.91 ± 120.32	6454.48 ± 89.26
Gg BC year ⁻¹	Historical	244.45 ± 1.49	NA	NA	NA	NA
	RCP8.5	246.82 ± 2.91	258.84 ± 6.61	279.61 ± 5.90	297.87 ± 6.31	305.67 ± 2.73
	RCP6.0	248.27 ± 4.79	268.06 ± 5.17	283.39 ± 5.40	303.57 ± 6.82	316.89 ± 4.19
	RCP4.5	249.83 ± 3.90	261.82 ± 7.74	282.74 ± 11.37	293.47 ± 19.22	310.66 ± 23.28
	RCP2.6	245.09 ± 3.27	260.25 ± 5.62	281.87 ± 4.93	300.39 ± 5.97	319.51 ± 4.42
Gg SO ₂ year ⁻¹	Historical	366.68 ± 2.25	NA	NA	NA	NA
	RCP8.5	370.23 ± 4.38	388.26 ± 9.93	419.42 ± 8.86	446.82 ± 9.49	458.52 ± 4.11
	RCP6.0	372.43 ± 7.20	402.12 ± 7.75	425.06 ± 8.12	455.35 ± 10.23	475.33 ± 6.27
	RCP4.5	368.23 ± 4.27	387.77 ± 8.00	419.45 ± 12.13	444.48 ± 10.13	476.28 ± 8.09
	RCP2.6	367.67 ± 4.94	390.40 ± 8.44	422.82 ± 7.39	450.57 ± 8.94	479.29 ± 6.64
Gg C ₂ H ₆ year ⁻¹	Historical	440.02 ± 2.69	NA	NA	NA	NA
	RCP8.5	444.30 ± 5.26	465.93 ± 11.91	503.28 ± 10.62	536.19 ± 11.38	550.21 ± 4.92
	RCP6.0	446.91 ± 8.64	482.53 ± 9.30	510.09 ± 9.74	546.42 ± 12.27	570.40 ± 7.53
	RCP4.5	441.89 ± 5.13	465.31 ± 9.60	503.34 ± 14.56	533.37 ± 12.16	571.54 ± 9.73
	RCP2.6	441.19 ± 5.93	468.47 ± 10.13	507.41 ± 8.90	540.68 ± 10.74	575.14 ± 7.95
Gg CH ₃ OH year ⁻¹	Historical	748.03 ± 4.57	NA	NA	NA	NA
	RCP8.5	755.32 ± 8.93	792.10 ± 20.25	855.59 ± 18.08	911.53 ± 19.36	935.37 ± 8.38
	RCP6.0	759.79 ± 14.67	820.33 ± 15.83	867.15 ± 16.55	928.92 ± 20.88	969.70 ± 12.81
	RCP4.5	751.21 ± 8.72	791.03 ± 16.31	855.70 ± 24.75	906.75 ± 20.66	971.62 ± 16.52
	RCP2.6	750.05 ± 10.07	796.42 ± 17.21	862.59 ± 15.10	919.19 ± 18.22	977.75 ± 13.53

sp.	Year	2000 - 2020	2021 - 2040	2041 - 2060	2061 - 2080	2081 - 2100
Gg C ₃ H ₈ year ⁻¹	Historical	136.85 ± 0.83	NA	NA	NA	NA
	RCP8.5	138.18 ± 1.65	144.92 ± 3.71	156.54 ± 3.31	166.80 ± 3.54	171.15 ± 1.55
	RCP6.0	139.01 ± 2.68	150.10 ± 2.89	158.67 ± 3.03	169.98 ± 3.82	177.44 ± 2.34
	RCP4.5	137.45 ± 1.60	144.74 ± 2.97	156.58 ± 4.53	165.93 ± 3.79	177.79 ± 3.03
	RCP2.6	137.22 ± 1.84	145.71 ± 3.15	157.85 ± 2.77	168.21 ± 3.33	178.91 ± 2.47
Gg C ₂ H ₂ year ⁻¹	Historical	131.97 ± 0.81	NA	NA	NA	NA
	RCP8.5	133.24 ± 1.58	139.76 ± 3.59	150.95 ± 3.19	160.84 ± 3.40	165.03 ± 1.47
	RCP6.0	134.04 ± 2.60	144.74 ± 2.79	153.00 ± 2.92	163.90 ± 3.67	171.10 ± 2.25
	RCP4.5	132.53 ± 1.52	139.56 ± 2.87	150.99 ± 4.36	160.00 ± 3.64	171.45 ± 2.91
	RCP2.6	132.32 ± 1.78	140.52 ± 3.03	152.20 ± 2.66	162.19 ± 3.23	172.52 ± 2.40
Gg C ₂ H ₄ year ⁻¹	Historical	728.47 ± 4.46	NA	NA	NA	NA
	RCP8.5	735.55 ± 8.68	771.39 ± 19.72	833.22 ± 17.59	887.70 ± 18.83	910.92 ± 8.14
	RCP6.0	739.90 ± 14.28	798.88 ± 15.42	844.48 ± 16.13	904.63 ± 20.33	944.34 ± 12.47
	RCP4.5	731.57 ± 8.47	770.35 ± 15.88	833.33 ± 24.11	883.04 ± 20.14	946.23 ± 16.09
	RCP2.6	730.45 ± 9.78	775.60 ± 16.76	840.04 ± 14.69	895.17 ± 17.75	952.18 ± 13.17
Gg C ₃ H ₆ year ⁻¹	Historical	322.65 ± 1.98	NA	NA	NA	NA
	RCP8.5	325.79 ± 3.86	341.68 ± 8.73	369.07 ± 7.80	393.21 ± 8.34	403.48 ± 3.61
	RCP6.0	327.72 ± 6.34	353.84 ± 6.83	374.04 ± 7.14	400.70 ± 9.02	418.29 ± 5.53
	RCP4.5	324.03 ± 3.76	341.22 ± 7.04	369.13 ± 10.67	391.15 ± 8.91	419.12 ± 7.12
	RCP2.6	323.53 ± 4.35	343.54 ± 7.42	372.11 ± 6.51	396.51 ± 7.85	421.77 ± 5.83
Gg C ₅ H ₈ year ⁻¹	Historical	34.15 ± 0.21	NA	NA	NA	NA
	RCP8.5	34.45 ± 0.41	36.14 ± 0.94	39.04 ± 0.82	41.62 ± 0.89	42.68 ± 0.38
	RCP6.0	34.65 ± 0.68	37.44 ± 0.71	39.60 ± 0.76	42.42 ± 0.96	44.28 ± 0.59
	RCP4.5	34.27 ± 0.41	36.10 ± 0.76	39.06 ± 1.12	41.40 ± 0.96	44.38 ± 0.75
	RCP2.6	34.21 ± 0.48	36.34 ± 0.78	39.38 ± 0.71	41.98 ± 0.84	44.69 ± 0.62

sp.	Year	2000 - 2020	2021 - 2040	2041 - 2060	2061 - 2080	2081 - 2100
Gg C ₁₀ H ₁₆ year ⁻¹	Historical	748.03 ± 4.57	NA	NA	NA	NA
	RCP8.5	755.32 ± 8.93	792.10 ± 20.25	855.59 ± 18.08	911.53 ± 19.36	935.37 ± 8.38
	RCP6.0	759.79 ± 14.67	820.33 ± 15.83	867.15 ± 16.55	928.92 ± 20.88	969.70 ± 12.81
	RCP4.5	751.21 ± 8.72	791.03 ± 16.31	855.70 ± 24.75	906.75 ± 20.66	971.62 ± 16.52
	RCP2.6	750.05 ± 10.07	796.42 ± 17.21	862.59 ± 15.10	919.19 ± 18.22	977.75 ± 13.53
Gg C ₇ H ₈ year ⁻¹	Historical	156.42 ± 0.96	NA	NA	NA	NA
	RCP8.5	157.94 ± 1.86	165.64 ± 4.25	178.92 ± 3.80	190.63 ± 4.06	195.63 ± 1.75
	RCP6.0	158.87 ± 3.08	171.55 ± 3.31	181.33 ± 3.46	194.25 ± 4.37	202.80 ± 2.67
	RCP4.5	157.09 ± 1.81	165.43 ± 3.42	178.95 ± 5.18	189.63 ± 4.33	203.20 ± 3.47
	RCP2.6	156.83 ± 2.11	166.55 ± 3.60	180.39 ± 3.17	192.25 ± 3.80	204.48 ± 2.83
Gg C ₆ H ₆ year ⁻¹	Historical	254.23 ± 1.56	NA	NA	NA	NA
	RCP8.5	256.68 ± 3.03	269.19 ± 6.88	290.77 ± 6.14	309.78 ± 6.57	317.90 ± 2.85
	RCP6.0	258.21 ± 5.01	278.79 ± 5.37	294.71 ± 5.63	315.69 ± 7.10	329.57 ± 4.36
	RCP4.5	255.30 ± 2.97	268.82 ± 5.55	290.82 ± 8.42	308.16 ± 7.03	330.22 ± 5.61
	RCP2.6	254.89 ± 3.42	270.66 ± 5.86	293.15 ± 5.13	312.40 ± 6.19	332.31 ± 4.59
Gg C ₈ H ₁₀ year ⁻¹	Historical	48.81 ± 0.30	NA	NA	NA	NA
	RCP8.5	49.30 ± 0.59	51.70 ± 1.33	55.85 ± 1.19	59.52 ± 1.27	61.07 ± 0.54
	RCP6.0	49.59 ± 0.97	53.56 ± 1.04	56.63 ± 1.08	60.67 ± 1.36	63.33 ± 0.84
	RCP4.5	49.04 ± 0.57	51.64 ± 1.07	55.88 ± 1.63	59.22 ± 1.35	63.46 ± 1.08
	RCP2.6	48.96 ± 0.65	51.99 ± 1.13	56.33 ± 0.99	60.03 ± 1.19	63.85 ± 0.89
Gg CH ₂ O year ⁻¹	Historical	860.47 ± 5.29	NA	NA	NA	NA
	RCP8.5	868.86 ± 10.27	911.17 ± 23.31	984.20 ± 20.79	1048.56 ± 22.26	1075.97 ± 9.62
	RCP6.0	873.99 ± 16.87	943.63 ± 18.19	997.50 ± 19.03	1068.56 ± 24.00	1115.47 ± 14.74
	RCP4.5	864.15 ± 10.01	909.94 ± 18.77	984.32 ± 28.47	1043.05 ± 23.77	1117.69 ± 19.01

sp.	Year	2000 - 2020	2021 - 2040	2041 - 2060	2061 - 2080	2081 - 2100
	RCP2.6	862.80 ± 11.55	916.15 ± 19.79	992.27 ± 17.37	1057.38 ± 20.96	1124.73 ± 15.55
Gg C ₂ H ₄ O year ⁻¹	Historical	381.33 ± 2.34	NA	NA	NA	NA
	RCP8.5	385.05 ± 4.54	403.81 ± 10.33	436.19 ± 9.20	464.70 ± 9.85	476.84 ± 4.28
	RCP6.0	387.33 ± 7.47	418.18 ± 8.07	442.07 ± 8.46	473.57 ± 10.65	494.35 ± 6.54
	RCP4.5	382.96 ± 4.43	403.27 ± 8.31	436.23 ± 12.61	462.26 ± 10.55	495.33 ± 8.42
	RCP2.6	382.37 ± 5.12	406.01 ± 8.77	439.76 ± 7.70	468.60 ± 9.28	498.47 ± 6.90
Gg C ₃ H ₆ O year ⁻¹	Historical	728.47 ± 4.46	NA	NA	NA	NA
	RCP8.5	735.55 ± 8.68	771.39 ± 19.72	833.22 ± 17.59	887.70 ± 18.83	910.92 ± 8.14
	RCP6.0	739.90 ± 14.28	798.88 ± 15.42	844.48 ± 16.13	904.63 ± 20.33	944.34 ± 12.47
	RCP4.5	731.57 ± 8.47	770.35 ± 15.88	833.33 ± 24.11	883.04 ± 20.14	946.23 ± 16.09
	RCP2.6	730.45 ± 9.78	775.60 ± 16.76	840.04 ± 14.69	895.17 ± 17.75	952.18 ± 13.17
Gg C ₃ H ₆ O ₂ year ⁻¹	Historical	723.58 ± 4.44	NA	NA	NA	NA
	RCP8.5	730.63 ± 8.62	766.22 ± 19.60	827.62 ± 17.48	881.74 ± 18.72	904.80 ± 8.08
	RCP6.0	734.96 ± 14.19	793.51 ± 15.31	838.81 ± 16.01	898.56 ± 20.19	938.02 ± 12.38
	RCP4.5	726.66 ± 8.42	765.16 ± 15.79	827.72 ± 23.93	877.11 ± 19.99	939.87 ± 15.97
	RCP2.6	725.55 ± 9.74	770.38 ± 16.64	834.41 ± 14.61	889.16 ± 17.63	945.79 ± 13.09
Gg C ₆ H ₅ OH year ⁻¹	Historical	1447.18 ± 8.86	NA	NA	NA	NA
	RCP8.5	1043.78 ± 676.60	1532.42 ± 39.17	1655.24 ± 34.96	1763.49 ± 37.43	1809.60 ± 16.19
	RCP6.0	1049.94 ± 680.86	1587.04 ± 30.61	1677.63 ± 32.01	1797.12 ± 40.37	1876.04 ± 24.76
	RCP4.5	1038.10 ± 672.92	1530.38 ± 31.55	1655.46 ± 47.88	1754.23 ± 39.99	1879.75 ± 31.97
	RCP2.6	1036.50 ± 671.92	1540.80 ± 33.28	1668.84 ± 29.21	1778.32 ± 35.28	1891.61 ± 26.16
Gg NH ₃ year ⁻¹	Historical	1378.72 ± 8.47	NA	NA	NA	NA
	RCP8.5	1392.15 ± 16.45	1459.96 ± 37.33	1576.96 ± 33.31	1680.09 ± 35.67	1724.03 ± 15.42
	RCP6.0	1400.39 ± 27.06	1511.98 ± 29.15	1598.28 ± 30.51	1712.12 ± 38.45	1787.30 ± 23.59
	RCP4.5	1384.62 ± 16.06	1458.00 ± 30.05	1577.17 ± 45.62	1671.25 ± 38.11	1790.83 ± 30.45

sp.	Year	2000 - 2020	2021 - 2040	2041 - 2060	2061 - 2080	2081 - 2100
	RCP2.6	1382.46 ± 18.54	1467.91 ± 31.71	1589.90 ± 27.83	1694.20 ± 33.61	1802.13 ± 24.92
Gg HCN year ⁻¹	Historical	396.00 ± 2.43	NA	NA	NA	NA
	RCP8.5	399.86 ± 4.73	419.34 ± 10.74	452.95 ± 9.57	482.56 ± 10.25	495.19 ± 4.44
	RCP6.0	402.21 ± 7.77	434.28 ± 8.38	459.08 ± 8.77	491.78 ± 11.05	513.37 ± 6.76
	RCP4.5	397.69 ± 4.61	418.77 ± 8.66	453.02 ± 13.09	480.04 ± 10.94	514.39 ± 8.74
	RCP2.6	397.07 ± 5.32	421.63 ± 9.11	456.67 ± 7.99	486.65 ± 9.65	517.64 ± 7.16
Gg MEK ₂ year ⁻¹	Historical	73.26 ± 0.46	NA	NA	NA	NA
	RCP8.5	74.00 ± 0.88	77.61 ± 1.99	83.83 ± 1.77	89.34 ± 1.90	91.67 ± 0.82
	RCP6.0	74.43 ± 1.44	80.38 ± 1.55	84.97 ± 1.64	91.03 ± 2.05	95.03 ± 1.26
	RCP4.5	73.59 ± 0.85	77.49 ± 1.60	83.85 ± 2.43	88.86 ± 2.03	95.22 ± 1.62
	RCP2.6	73.47 ± 0.99	78.02 ± 1.69	84.52 ± 1.48	90.07 ± 1.79	95.82 ± 1.32
Gg CH ₃ CN year ⁻¹	Historical	146.65 ± 0.88	NA	NA	NA	NA
	RCP8.5	148.06 ± 1.75	155.28 ± 3.97	167.73 ± 3.55	178.71 ± 3.79	183.38 ± 1.64
	RCP6.0	148.94 ± 2.88	160.82 ± 3.11	170.00 ± 3.25	182.12 ± 4.08	190.13 ± 2.51
	RCP4.5	147.26 ± 1.70	155.08 ± 3.21	167.76 ± 4.85	177.77 ± 4.07	190.49 ± 3.24
	RCP2.6	147.03 ± 1.98	156.12 ± 3.37	169.13 ± 2.96	180.24 ± 3.59	191.70 ± 2.67

References

- Agee, J. K.: Fire Ecology of Pacific Northwest Forests, *Electron. Green J.*, 1, <https://doi.org/10.5070/g31710279>, 1997.
- Albini, F. A.: Rocky Mountain Research Station, USDA For. Serv., Intermt. For. Range Exp. Stn., Ogden, UT. Gen. Tech. Rep., 1–22, 1976.
- Andreae, M.: Emission of trace gases and aerosols from biomass burning. *Global Biogeochemical, At. Chem. Phys.*, 15 (4), 955–966, 2019.
- Andreae, M. O. and Merlet, P.: Emission of trace gases and aerosols from biomass burning, 15, 955–966, 2001.
- Archibald, S., Roy, D. P., van Wilgen, B. W., and Scholes, R. J.: What limits fire? An examination of drivers of burnt area in Southern Africa, *Glob. Chang. Biol.*, 15, 613–630, <https://doi.org/10.1111/j.1365-2486.2008.01754.x>, 2009.
- Byram, G. M.: Combustion of forest fuels, in: *Forest Fire Control and Use*, edited by: Davis, K. P., McGraw-Hill, New York, 61–89, <https://doi.org/10.2307/1932261>, 1959.
- Cecil, D. J.: LIS/OTD 0.5 Degree High Resolution Full Climatology (HRFC) V2.3.2015, <https://doi.org/http://dx.doi.org/10.5067/LIS/LIS-OTD/DATA302>, 2001.
- CIESIN: Gridded Population of the World, Version 4.11 (GPWv4): Population Count, Revision 11, <https://doi.org/https://doi.org/10.7927/H4JW8BX5>, 2018.
- Cochrane, M. A.: Fire science for rainforests, *Nature*, 421, 913–919, <https://doi.org/10.1038/nature01437>, 2003.
- Dickinson, M. B. and Johnson, E. A.: Fire Effects on Trees, in: *Forest Fires*, 477–525, <https://doi.org/10.1016/b978-012386660-8/50016-7>, 2001.
- Forestry Canada Fire Danger Group: Development of the Canadian Forest Fire Behavior Prediction System, https://cfs.nrcan.gc.ca/publications?id=10068%0Ahttps://www.frames.gov/documents/catalog/forestry_canada_fire_danger_group_1992.pdf, 1992.
- Hessilt, T. D., Werf, G. Van Der, Abatzoglou, J. T., and Scholten, R. C.: Future increases in lightning-ignited boreal fires from conjunct increases in dry fuels and lightning, *Proc. 23rd EGU Gen. Assem.*, 2021.
- Ivanova, G. A. and Ivanov, V. A.: Fire Regimes in Siberian Forests, *Int. For. Fire News*, 32, 67–69, 2005.
- Jones, P. W.: First- and second-order conservative remapping schemes for grids in spherical coordinates, *Mon. Weather Rev.*, 127, 2204–2210, [https://doi.org/10.1175/1520-0493\(1999\)127<2204:FASOCR>2.0.CO;2](https://doi.org/10.1175/1520-0493(1999)127<2204:FASOCR>2.0.CO;2), 1999.
- Kharuk, V. I., Mariya, L. D., Ilya, A. P., Sergei, T. I., and Kenneth, J. R.: Larch Forests of Middle Siberia: Long-Term Trends in Fire Return Intervals, *Reg. Environ. Chang.*, 16, 2389–2397, <https://doi.org/doi:10.1007/s10113-016-0964-9>, 2016.
- Kharuk, V. I., Dvinskaya, M. L., Im, S. T., Golyukov, A. S., and Smith, K. T.: Wildfires in the Siberian Arctic, *Fire*, 5, 1–16, <https://doi.org/10.3390/fire5040106>, 2022.
- Knorr, W., Kaminski, T., Arneth, A., and Weber, U.: Impact of human population density on fire frequency at the global scale, *Biogeosciences*, 11, 1085–1102, <https://doi.org/10.5194/bg-11-1085-2014>, 2014.
- Latham, D. and Schlieter, J.: Ignition probabilities of wildland fuels based on simulated lightning discharges, *United States Dep. Agric. For. Serv.*, 16, 1989.
- Latham, D. and Williams, E.: Lightning and Forest Fires, *Mon. Weather Rev.*, 51, 566–567, [https://doi.org/10.1175/1520-0493\(1923\)51<566:laffic>2.0.co;2](https://doi.org/10.1175/1520-0493(1923)51<566:laffic>2.0.co;2), 2001.
- Peterson, D. L. and Ryan, K. C.: Modeling postfire conifer mortality for long-range planning, *Environ. Manage.*, 10, 797–808, <https://doi.org/10.1007/BF01867732>, 1986.
- Pyne, S. J., Andrews, P. L., and Laren, R. D.: *Introduction to Wildland Fire*, 1996.
- Romps, D. M., Seeley, J. T., Vollaro, D., and Molinari, J.: Projected increase in lightning strikes in the united states due to global warming, *Science (80-.)*, 346, 851–854, <https://doi.org/10.1126/science.1259100>, 2014.

- Rothermell, R. C.: A Mathematical Model for Predicting Fire Spread, United States Dep. Agric. For. Serv. Res. Pap., 46, 1972.
- Running, S. W., Nemani, R. R., and Hungerford, R. D.: Extrapolation of synoptic meteorological data in mountainous terrain and its use for simulating forest evapotranspiration and photosynthesis, *Can. J. For. Res.*, <https://doi.org/doi.org/10.1139/x87-081>, 1987.
- Sato, H., Itoh, A., and Kohyama, T.: SEIB-DGVM: A new Dynamic Global Vegetation Model using a spatially explicit individual-based approach, *Ecol. Modell.*, 200, 279–307, <https://doi.org/10.1016/j.ecolmodel.2006.09.006>, 2007.
- Schulzweida, U.: CDO User Guide, <https://doi.org/10.5281/zenodo.3539275>, 2019.
- Sofronov, M. A., Volokitina, A. V., and Shvidenko, A. Z.: Wildland fires in the north of Central Siberia, *Commonw. For. Rev.*, 77, 124–127, 1998.
- Thonicke, K., Venevsky, S., and Sitch, S.: The role of fire disturbance for global vegetation dynamics: coupling fire into a Dynamic Global Vegetation Model, *Glob. Ecol. Biogeogr.*, 10, 661–677, 2001.
- Thonicke, K., Spessa, A., Prentice, I. C., Harrison, S. P., Dong, L., and Carmona-Moreno, C.: The influence of vegetation, fire spread and fire behaviour on biomass burning and trace gas emissions: Results from a process-based model, *Biogeosciences*, 7, 1991–2011, <https://doi.org/10.5194/bg-7-1991-2010>, 2010.
- Venevsky, S., Thonicke, K., Sitch, S., and Cramer, W.: Simulating fire regimes in human-dominated ecosystems: Iberian Peninsula case study, *Glob. Chang. Biol.*, 8, 984–998, <https://doi.org/10.1046/j.1365-2486.2002.00528.x>, 2002.
- Viegas, D. X., Viegas, T. S. P., and Ferreira, D.: Moisture content of fine forest fuels and fire occurrence in central Portugal, *Int. J. Wildl. Fire*, 2, 69–86, <https://doi.org/10.1071/WF9920069>, 1992.
- Williams, R. J., Gill, A. M., and Moore, P. H. R.: Seasonal changes in fire behaviour in a tropical savanna in Northern Australia, *Int. J. Wildl. Fire*, 8, 227–239, <https://doi.org/10.1071/WF9980227>, 1998.
- Wilson, R. A.: A Reexamination of Fire Spread in Free-Burning Porous Fuel Beds, United States Dep. Agric. For. Serv., 1982.
- Xu, W., Scholten, R. C., Hessilt, T. D., Liu, Y., and Veraverbeke, S.: Overwintering fires rising in eastern Siberia, *Environ. Res. Lett.*, 17, <https://doi.org/10.1088/1748-9326/ac59aa>, 2022.